Classification des IRM par les descripteurs de contenu : application au diagnostic précoce de la maladie d'Alzheimer

Olfa Ben Ahmed

THÈSE EN COTUTELLE PRÉSENTÉE

POUR OBTENIR LE GRADE DE DOCTEUR DE

L'UNIVERSITÉ DE BORDEAUX

ET DE L'UNIVERSITÉ DE SFAX

ÉCOLE DOCTORALE DE MATHÉMATIQUES ET INFORMATIQUE UBX

ÉCOLE DOCTORALE DE L'ÉCOLE NATIONALE D'INGÉNIEURS DE SFAX

SPÉCIALITÉ INFORMATIQUE

Par Olfa BEN AHMED

Features-based MRI brain classification with domain knowledge: Application to Alzheimer's disease diagnosis

Sous la direction de Jenny BENOIS-PINEAU
Michèle ALLARD
et de Chokri BEN AMAR

Soutenue le 14-01-2015 au Laboratoire Bordelais de Recherche en Informatique (LaBRI)

Membres de jury :

M. MÜLLER, Henning	Professeur, Haute École Spécialisée de Suisse occidentale	Président
M. AMIRI, Hamid	Professeur, ENIT Université de Tunis	Rapporteur
M. QUELLEC, Gwénolé	Chargé de recherche,CHU Morvan, Brest	Examinateur
Mme. BENOIS-PINEAU,	Professeur, Université de Bordeaux	Directrice de thèse
M. BEN AMAR, Chokri	Professeur, ENIS Université de Sfax	Co-directeur de thèse
Mme. ALLARD, Michelle	Professeur, Université de Bordeaux	Co-directrice de thèse
Mme. CATHELINE, Gwénaëlle	Maître de conférences, Université de Bordeaux	Invitée

Dédicace

À mes parents...

Tous les mots ne sauraient exprimer ma gratitude et ma reconnaissance pour vos sacrifices, mon amour éternel et ma considération pour les sacrifices que vous avez consenti pour mon instruction et mon bien être.

À mes deux frères et à ma soeur...
Je vous souhaite tous un avenir plein de succés.

À tous ceux que j'aime et qui se reconnaitront...

Je dédie cette thèse...

Olfa

Remerciements

En premier lieu, je souhaite remercier Madame **Jenny Benois-Pineau** ma directrice de thèse pour tout ce qu'elle m'a appris, conseillé, enseigné, soutenu, coaché, et pour tout le temps qu'elle m'a accordé. Je présente mes remerciements et ma gratitude aussi à mon co-directeur de thèse Monsieur **Chokri Ben Amar** pour la confiance qui m'a accordé pour travailler sur ce sujet, pour son support et son soutient. J'adresse mes sincéres remerciements à Madame **Michèle Allard**, professeur à l'université de Bordeaux, responsable d'Equipe Neuroimagerie et Cognition humaine de Institut de Neurosciences Cognitives et intégratives d'Aquitaine et co-directeirce de la présente thèse pour ses nombreux conseils et riches discussions, pour son temps et son accueil. Merci aussi au Docteur **Gwénaëlle Catheline** maïtre de conférences à l'université de Bordeaux pour sa gentilesse et son aide précieuse. Je suis trés honorée de remercier mon jury de thèse et je tiens à remercier Monsieur **Henning Müller**, professeur de Haute École Spécialisée de Suisse occidentale, pour l'honneur qu'il m'a fait en acceptant d' être président de mon jury de thèse, pour les suggestions et les remarques judicieuses quil ma indiquées, Monsieur **Hamid Amiri**, professeur à l'université de Tunis pour sa participation à mon jury de thèse en qualité de rapporteur et pour toutes les remarques intéressantes qu'il m'a donné. Je tiens également à exprimer ma reconnaissance à Monsieur **Gwénolé Quellec** pour avoir accepté de juger mon travail en tant qu'examinateur. Merci à l'ensemble des membres du **LaBRI** pour leur accueil. Je remercie également le personnel administratif du laboratoire pour son efficacité et sa bonne humeur. Merci à tout mes collégues et amis du LaBRI. Merci à tout ceux qui étaient à coté de moi durant ces trois ans de cette thèse.

Abstract

Content-Based Visual Information Retrieval and Classification on Magnetic Resonance Imaging is penetrating the universe of IT tools supporting clinical decision making. A clinician can take profit from retrieving subjects' scans with similar patterns. In this thesis, we use the visual indexing framework and pattern recognition analysis based on structural MRI and Tensor Diffusion Imaging data to discriminate three categories of subjects: Normal Controls (NC), Mild Cognitive Impairment (MCI) and Alzheimer's Disease (AD). The approach extracts visual features from the most involved areas in the disease: Hippocampus and Posterior Cingulate Cortex (PCC). Hence, we represent signal variations (atrophy) inside the Region of Interest anatomy by a set of local features and we build a disease-related signature using an atlas based parcellation of the brain scan. The extracted features are quantized using the Bag-of-Visual-Words approach to build one signature by brain/ROI (subject). This yields a transformation of a full MRI brain into a compact disease-related signature. Several schemes of information fusion are applied to enhance the diagnosis performance. The proposed approach is less time-consuming compared to the state of the arts Volumetric methods, computer-based and does not require the intervention of an expert during the classification/retrieval phase.

Résumé

L'augmentation de la durée de vie dans les pays développés a été accompagnée par une augmentation sans précédent des cas des pathologies neuro-dégénératives liées è l'âge. La maladie d'Alzheimer (MA) est le type le plus fréquent de démence. Selon l'Association "Alzheimer Disease International" [1], il y a approximativement 36 millions de personnes atteintes par la MA dans le tout monde et selon les estimations ce nombre devrait tripler pour atteindre 115 millions en 2050. L'impact économique mondial de la maladie dAlzheimer pesait 600 milliards de dollars en 2010. Les conséquences socio économiques de cet accroissement sont lourdes ce qui rend le diagnostic précoce de la MA une urgence de santé publique. En effet, l'identification des marqueurs morphologiques présents dans les stades initiaux de la MA devraient aider au diagnostic précoce, et donc à une prise en charge mieux adaptée des patients.

Plusieurs méthodes et techniques ont été proposés dans ce cadre pour l'étude de la morphologie de structure de cerveau humain à travers l'Imagerie cérébrale par Résonnance Magnétique (IRM). On peut distinguer deux grandes familles de méthodes. Premièrement, les méthodes d'analyse par région d'intérêt (ROI) (volumétrique), ces méthodes extraient une ROI et étudient sa variation de volume. Cependant, elles présentent certaines limites dans la mesure où la délimitation est coûteuse en temps et dépend de l'observateur. Le deuxième groupe est le groupe des méthodes voxéliques qui s'intéressent à la détection des différences significatives au niveau de la matière grise entre deux groupes de sujets par des tests voxel à voxel. Toutefois, ces dernières permettent seulement une localisation de l'atrophie mais

[1] http://www.alz.org/

aucune appréciation visuelle ou quantification, il est donc difficile d'avoir un indice réflétant le degré d'atrophie d'un patient donné. Les méthodes traditionnelles d'analyse des IRM ont été souvent développées dans l'optique d'étude des groupes, leurs intérêt pour un diagnostic individuel reste limité et leurs applications cliniques restent encore inadaptées. En effet, ces méthodes sont loin d' être capables à émuler le processus de diagnostic fait par le médecin. En réalité, le clinicien analyse l'IRM du patient et essai de quantifier visuellement l'atrophie. Il est très évident que le processus de diagnostic médical repose sur la capacité de médecin d'apprendre des cas similaires déjà vus d'une part et sur son aptitude de détecter et de caractériser des cibles pathologiques (interpréter visuellement les altérations spécifiques) d'autre part. En effet, le médecin fait souvent appel à sa mémoire d'expériences passées dans l'exercice, pour chercher une ressemblance entre des anciennes images et la nouvelle. Une telle ressemblance, si elle existe, devrait aider énormément dans la résolution du nouveau problème en main. Aussi, l'interprétation visuelle des motifs associés aux atrophies fait appel d'une façon explicite aux techniques de reconnaissance des formes et d'apprentissage qui consistent à déterminer selon un citère de similarité visuelle à quelle classe de sujets connue le nouveau cas peut être associé ou bien quelle est la liste des images qui sont lui similaires?

Les outils méthodologiques en indexation et recherche des images par le contenu sont déjà assez matures et ce domaine s'ouvre vers les applications médicales. Dans cette thèse, nous nous intéressons à l'indexation visuelle, à la recherche et à la classification des images cérébrales IRM par le contenu pour l'aide au diagnostic précoce de la maladie d'Alzheimer. L'idée principale est de donner au clinicien des informations sur les images ayant des caractéristiques visuelles similaires. À base de ces informations, le médecin se rend capable de prendre la décision à propos de la maladie dans son stade précoce. Trois catégories de sujets sont à distinguer : sujets sains (NC), sujets avec troubles cognitifs légers (MCI) et sujets atteints par la maladie d'Alzheimer (AD). Dans ce travail, nous proposons des solutions pour l'aide au diagnostic de la MA basées sur une quantifications l'atrophie cérébrale sous forme d'une signature visuelle spécifique à la MA. Les connaissances sont représentées d'une façon étroitement lié à la méthode de raisonnement de médecin pour un diagnostic individuel. Nous nous sommes basés sur les outils d'indexation par le contenu couplés avec les connaissances de domaine en acquisition des images IRM et en diagnostic de la MA. Pour

rendre cette signature spécifique à la maladie dAlzheimer nous avons adopté un ensemble de méthodologies:

Nous nous sommes concentrés uniquement sur la description fine des régions qui sont impliquées dans la maladie d'Alzheimer et qui causent des changements particuliers dans la structure de cerveau. En se basant sur des informations fournis par nos partenaires de l'INCIA, nous étudions deux zones de cerveau : l'hippocampe : région cérébrale impliquée dans la mémorisation, et le Cortex Cingulaire Postérieur (CCP) qui correspond à la zone de la mémoire autobiographique. Ces régions sont extraites en utilisant un atlas normalisé adopté à notre problématique.

Pour extraire l'information visuelle, nous avons opté à une approche 2D pour capter le spectre complet et local de l'atrophie. Nous avons appliqué des descripteurs de contenu locaux comme (SIFT, SURF et Fonctions Harmoniques Circulaires de Laguerre-Gauss (CHFs)) pour représenter la variation de signal dans une région d'intérêt sur les images IRM pour détecter les changements de la structure de cerveau dans le cas de la MA. L'utilisation des CHFs est une nouvelle technique pour la construction des descripteurs représentatifs distincts. L'algorithme effectue une analyse multi-résolution de l'image dans le domaine transformé par Laguerre Gauss et collecte dans un descripteur local les coefficients transformés dans plusieurs échelles.

Les caractéristiques extraites de chaque région sont ensuite quantifiées en utilisant l'approche Sac de mots visuels typique pour l'indexation visuelle. Cela donne une transformation d'une image ou d'une ROI du cerveau en une signature, un histogramme des caractéristiques quantifiées. Afin de réduire la dimension de la signature, nous avons utilisé la technique de PCA.

Dans ces travaux, nous nous sommes aussi intéressés à la fusion d'information issue de différents marqueurs extraits des IRM. Des stratégies de fusion ont été proposées pour renforcer les décisions à savoir une fusion tardive et une fusion précoce. En premier lieu, nous avons appliqué une fusion tardive pour fusionner les résultats de classification issue de l'utilisation de la structure de l'hippocampe et le volume de Liquide Cérébro-spinal (LCS) qui règne dans cette région. En effet, en se basant sur les connaissances de domaine, dans un stade précoce de la MA, l'hippocampe se rétrécit à cause de la dégénération des cellules et le LCS,

qui est un substance liquide dans la quelle baigne le cerveau, remplie le volume manquant. Dans un second lieu, nous avons appliqué une fusion précoce des vecteurs caractéristiques extraits des régions de l'hippocampe et du Cortex Circulaire Postérieur. En effet, au stade précoce, la maladie touche la région de l'hippocampe qui subit une perte massive de neurones. Au stade plus avancé, le CCP voit son métabolisme diminué et cet hypo-métabolisme serait prédictif d'une conversion rapide vers AD et donc il permettrait de détecter les cas MCI.

Aussi, nous avons aussi utilisé les cartes des diffusion (MD) de la modalité Imagerie à Tenseur de Diffusion (DTI) pour distinguer entre AD, NC et MCI. Nous avons appliqué le classifieur SVM avec différents noyaux pour classer les groupes.

Les méthodes proposées sont appliquées dans un premier temps sur des ensembles des sujets de la base de cas de maladie d'Alzheimer : la base ADNI. Et puis sur une cohorte réelle des sujets de groupe "Bordeaux-"City". Les méthodes proposées sont automatiques (sans la moindre intervention de clinicien), ne nécessitent pas une étape de segmentation coûteuse et fastidieuse grâce à l'utilisation d'un Atlas normalisé. Les résultats obtenus montrent que la description de contenu des régions de cerveau impliquées dans la MA permettent une bonne discrimination entre des patients AD, des sujets sains et des sujets MCI et donc peuvent être utilisés comme un outil potentiel d'aide au diagnostic de cette pathologie. En plus, les descripteurs CHFs donnent de meilleurs résultats par rapport aux descripteurs SIFT qui représente un benchmark. Aussi, la modalité DTI, qui est à nos connaissance, n'a jamais été question de recherche dans le cadre de recherche ou classification par le contenu pour le diagnostic d'Alzheimer, a donné des bons résultats pour classifier les sujets sains des sujets AD ou MCI. Les résultats obtenus apportent une amélioration par rapport aux méthodes volumétriques en termes de précision de classification et de temps de traitement.

Contents

List of Tables

List of Figures

Acronyms

AAL Automated Anatomical Labeling.

AD Alzheimer's disease.

ADNI Alzheimer's Disease Neuroimaging Initiative.

BOF Bag Of Features.

BoVW Bag Of Visual Word.

CAD Computer-Aided Diagnosis.

CBIR Content-based Image Retrieval.

CBVIR Content Based Visual Image Retrieval.

CHFs Circular Harmonic Functions.

CSF Cerebrospinal Fluid.

DBM Deformation-Based Morphometry.

DoG Difference Of Gaussian.

DTI Diffusion Tensor Imaging.

FA Fractional Anisotropy.

FBM Feature Based Morphometry.

FN False Negatives.

FP False Positives.

GL CH Laguerre-Gauss Circular Harmonic.

GM Gray Matter.

Hpc Hippocampus.

LBP Local Binary Pattern.

LOOCV Leave One Out Cross Validation.

MCI Mild Cognitive Impairment.

MD Means Diffusivity.

MMSE The Mini-Mental State Examination.

MNI Montreal Neurological Institute.

MRI Magnitique Resonance Imaging.

NC Normal Control.

NMR Nuclear Magnetic Resonance.

OBM Object-Based Morphometry.

PCC Posterior Cingulate Cortex.

PET Positron Emission Tomography.

ROI Region of Interest.

SIFT Scale Invariant Feature Transform.

sMRI structural Magnetic Resonance Imaging.

SPECT Single-Photon Emission Computerized Tomography.

SURF Speed Up Robust Feature.

SVM Support Vector Machines.

TN True Negatives.

TP True Positives.

VBM Voxel Based Morphometry.

WM White Matter.

Glossary

$I(x, y)$ A 2D image.

K Vocabulary size.

$L_n^\alpha(x)$ Laguerre polynomials.

$S(x, y)$ A slice S from an MRI.

$\Psi_n^\alpha(x)$ Laguerre functions.

$\equiv$ The modulo operator.

$f_{n,i}^s$ Feature i in the slice n of the projection p.

voxel Volume element; the element of 3D space corresponding to a pixel, for a given slice thickness.

Main Introduction

Contents

0.1 Motivation

0.1.1 Clinical Motivation

Alzheimer's disease

With the aging of population in developed countries, more people will be affected by dementia. Alzheimer's disease (AD) is one of the most frequent form of dementia. It is a progressive neurodegenerative disease, characterized by severe deterioration in cognitive function and by memory loss. Nowadays, AD represents a major public health problem and its early detection is very important to achieve delay in the disease progression. Medically speaking, Alzheimer's disease results from the accumulation of a protein called beta-amyloid in healthy neurons. This accumulation lead to the disintegration of microtubules in brain cells (Greenfield et al., 1997). Consequently, neurons become weaker, lose their ability to communicate efficiently with each other and finish by dieing. Thus, this neuronal death could contribute to loss of brain cells. Figure 1 illustrates the neurodegeneration process. Eventually, cells degeneration spreads to the hippocampus, which is a brain area involved in memory forming. As more neurons die, entire areas of the brain shrink. This leads to cognitive function problems which are symptoms of AD. In more advanced stage, damages become widespread and brain undergoes significant shrinkage (complete brain failure).

There are three clinical phases (stages) of AD:

- Preclinical AD:

  About half of the people in this phase do not report cognitive troubles some years before diagnosis, because cells degenerations associated with AD begin years even decades before subjects first show clinical symptoms. Indeed, biological changes are under way in the body before symptoms of disease appear. It is challenging to quantify patterns of structural change in the early stages of AD or during clinically normal stages. Thus, an accurate diagnosis of the disease in the clinical phase is not yet possible.

- Mild Cognitive Impairment (MCI): Most patients go through the transitional stage called Mild Cognitive Impairment before they lapse into AD. In this stage, subject may show memory problems long before he gets an Alzheimer's diagnosis. Disease in

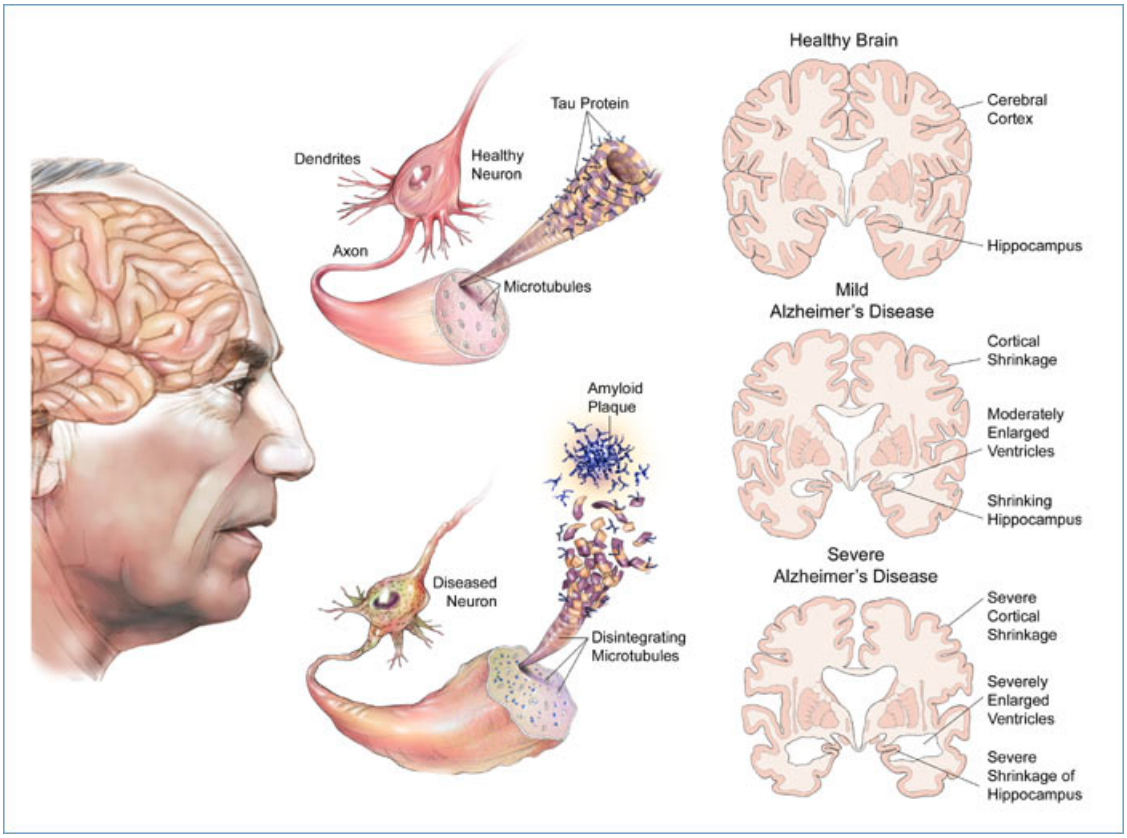

Figure 1: Cells degeneration process and brain shrinkage in the case of Alzheimer's disease dementia: spatio-temporal progression of the disease (By Chess Coach Will Stewart (USCF 2256, FIDE 2234))

this phase is not severe enough to disrupt a person's life. MCI is a challenging and confused group because in this phase the subject is not yet considered to have AD. From Figure 2, we can see that lines between MCI and normal age-related memory loss overlap, as are the lines between MCI and AD. Despite its large heterogeneity, MCI remains a group of interest in the study of early-stage AD and current research studies are focusing on proposing methods to predict conversion or not of MCI cases.

- Clinically Diagnosed AD:

  The late stage of Alzheimer's disease may also be called "severe". Subjects in this stage show decreased mental ability, total loss of cognitive function and finally this causes death.

Today, approximately 36 million persons are living with Alzheimer's disease worldwide

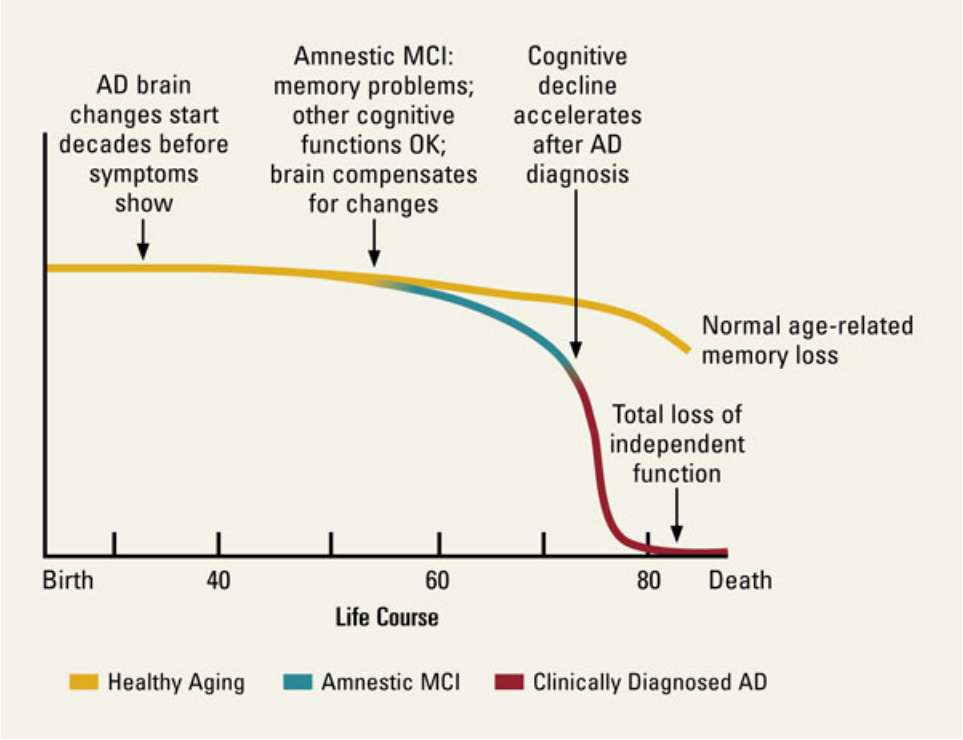

Figure 2: Clinical phases of Alzheimer's disease (Rodgers and on Aging., 2002)

and this number is expected to double increasing to 66 million by 2030 and even to triple to be 115 million by 2050 (Hebert et al., 2013). Indeed, every 67 seconds someone in the world develops Alzheimer's disease. The global estimated cost of dementia worldwide is US 600 billion dollars (380 billion €). For instance, in United States, there is an estimated 5.2 million persons of all ages have Alzheimer's disease by 2014. This includes an estimated 5 million people aged 65 and older, and approximately 200,000 individuals under age 65 who have younger-onset Alzheimer's (Alzheimer's Association, 2014). This number will dramatically increase in the next 40 years unless preventive measures are developed. Actually, there's no cure yet for AD but the effort to early AD diagnosis continues with great fervor. An early diagnosis of AD will allow patients to benefit from new treatments that may slow down neurodegeneration.

Recent advances in neuroimaging instruments show substantial improvement of image quality and acquisition speed. This increased the use of medical imaging considerably for AD diagnosis. Up to day, Magnitique Resonance Imaging (MRI) is the most used tool for

brain imaging in vivo for the assessment of AD. Such popularity comes from its good contrast of soft tissues and high spatial resolution which allow to capture the distribution of anatomical changes in brain structure. Toward this goal, there is still a need to find the best ways to extract and quantify pathological structural alterations from MRI. Traditional voxel-wise or volumetric methods are the gold standards methods for MRI analysis but these are still far from emulating the clinician diagnosis process. The shortcoming of such methods is that every *voxel* in the image is analyzed individually. Usually, the clinician identifies neurodegenerative diseases in MRI scans by looking for a disease specific pattern of neurodegeneration in the brain. This suggests that the decision relevant information is comprised in patterns and not only in single voxels. In addition, volumetric methods require a Region of Interest (ROI) segmentation which is time-consuming and user-depending. Actually, Alzheimer's disease may not affect only a single ROI, but several structures localized far away from each others. Then, the pattern of atrophy is difficult to quantify by those standard methods Therefore, the visual analysis of medical images could be a time consuming and fastidious task that demands a highly trained clinician. In addition, those proposed methods are interested in the group level diagnosis contrasting a group of patients versus a group of normal subjects. They have limited clinical value for individual diagnosis. Recently, a new trend towards disease-related pattern quantification for individual AD diagnosis has appeared, representing a fundamental shift of the research paradigm. Therefore, in this thesis, we investigate the computer vision tools and pattern recognition techniques to do the automatic individual diagnosis of Alzheimer's disease subjects without the need to a fastidious segmentation step.

0.1.2 Computer vision for medical imaging diagnosis

Due to an enormous increase of the diversity and of the volume of biomedical image collections and the large range of image modalities getting available nowadays, there is a need for providing automated tools to index and manage medical information. Computer vision field attracts greater interest from various research communities in medical imaging management. Many powerful computer vision tools (such as machine learning, pattern classification and image segmentation...) find extensive applications in the field of Computer-Aided Diagnosis (CAD) as it helps to bring much needed quantitative information not easily available by

trained clinicians. This allows for better diagnosis and treatment of diseases.

Recently, indexing and classification methods for Content Based Visual Image Retrieval (CBVIR) have been penetrating the universe of medical image analysis (Müller et al., 2004; Müller and Deserno, 2011). This is a normal "knowledge diffusion" process, when methodologies developed for multimedia mining penetrate a new application area. The latter brings its own specificity requiring an adjustment of methodologies on the basis of domain knowledge. Content-based Image Retrieval (CBIR) is the application of computer vision techniques to better human image content understanding and to index images with minimal human intervention.

Fully automatic normal and diseased human brain recognition from MRI is of great importance for research and clinical studies specially in Alzheimer's disease diagnosis application. For this aim, advances in computer vision and evolution of medical imaging techniques allow together for studying structural changes in human brain and their relationship with clinical diagnosis of AD. Medical information from structural Magnetic Resonance Imaging (sMRI) and Diffusion Tensor Imaging (DTI) are used for detecting structural abnormalities of the human brain and tracking the evolution of brain atrophy which is considered as a marker of AD process. Often, clinical diagnosis is based on a classification of medical images according to the anatomy of specific ROI known to be involved in the disease rather than the entire brain structure. Sometimes the distinguishing features that would indicate a particular classification are difficult to recognize even by a trained expert. The application of content-based indexing, classification and retrieval techniques in CAD has obtained increasing research interest by using the visual appearance of MRI tissues. The diagnosis here is based on classification of local individual pattern. Feature vectors extracted describing low level features in an image, is a basis of similarity measurement in a retrieval/classification procedure. Computer vision deals in general with information extraction from images. A variety of visual features, such as texture, shape and spatial relationships, which have been used in other domains, have been adopted in the medical domain with little alteration.

0.2 Thesis objectives

Brain anatomical difference in AD subjects at the group level has been well studied, but the pattern classification of MRI scans across individuals still remains less developed. The main challenge here lies first in the identification of features which provide the most reliable information about the particular disease (so-called disease signature). Moreover, symptoms of the disease can vary between individuals, in this case individual scan's patterns need to be taken into consideration and thus build a distinctive signature of disease-related atrophy per subject. In reality, pathology bearing regions tends to be highly localized. On the other hand, MR image is a collection of voxels characterized by spatial distribution and gray level intensities. Here, structure-based features may reflect the image information by describing the organizational pattern of these voxels. The extensive research on retrieval and classification in the domain of multimedia attempts to investigate the discriminative power of local features within brain regions that are sensitive to AD. Hence, the current research intends to discriminate between the normal and diseased brain using local features. We propose features-based methods to detect Alzheimer's disease at an early stage from structural MR images and Tensor-Diffusion Imaging modalities. We develop both content-based retrieval framework and Content-based classification framework for CAD using domain knowledge in AD. The main idea consists in refuting the hypothesis that morphological atrophies appear at the same voxel location for all subjects and thus automatically build distinctive signature of disease-related atrophy per subject. We use machine learning to do binary classification between AD versus NC, NC versus MCI and MCI versus AD and visual similarity retrieval methods to find similar cases to help diagnosis process. As explained in the last sections, the MCI group is very heterogeneous and it overlaps with AD and NC groups. We focus on the MCI/AD recognition task. We use local visual feature, such as the Circular Harmonic Functions (CHFs) descriptors, Scale Invariant Feature Transform (SIFT) and Speed Up Robust Feature (SURF).

Hence, we address the following research questions in this work:

- We aim to disseminate the knowledge of the CBIR approaches to AD diagnosis.
- Can visual features-based methods replace the fastidious ROI segmentation for effective

and efficient AD diagnosis ? and what is the performance in comparison with volumetric approaches?

- According to the domain knowledge in AD diagnosis, what anatomical patterns are characteristic of AD, NC or MCI brains ? How can one interpret the neurodegeneration pattern visually in MRI ? How can we represent the observed disease-related pattern ?
- Test the suitability of visual features to describe structural MRI and Tensor diffusion derived images.
- Can early or late fusion of different structural features improve the classification/retrieval results between MCI and AD cases ?
- Is the proposed approach comparable, in terms of performance, with existing volumetric approaches?

0.3 Contributions

The current thesis presents a multidisciplinary research efforts to investigate the emerging computer vision tools to the AD diagnosis. We design a pattern recognition approach in the paradigm of CBVIR to help early diagnosis of Alzheimer's disease from structural MRI and DTI. Indeed, we characterize brain abnormalities in terms of intra-ROI local patterns using consistent neuroanatomical features for the disease.

The major contributions can be summarized as flows:

- We refer to the domain knowledge in AD diagnosis to emulate the clinician diagnosis process. Hence, inspiring from the clinician's vision about the brain atrophy, we build distinctive and specific disease-related signature to discriminate between AD, NC and MCI brains. The extracted features are incorporated in a CAD system to assist clinicians on decision making tasks.
- We extract distinctive local and visual signatures of AD-related atrophy using an atlas-based approach without the need to a traditional tedious ROI segmentation. This help capturing different signals from a number of different tissues inside the ROI it self.

- We separate AD/MCI patients from NC using 2D MR images inside 3D MRI brain volumes and at the pattern level inside the traditional voxel level analysis.

- We represent signal variations inside the ROI anatomy by a set of local features. Here, we employ a multi resolution approach based on the Circular Harmonic Functions (CHFs), which is suitable for extracting the most relevant image features and even small and localized pattern. Extracted features are leveraged to distinguish normal from abnormal local ROI tissue.

- We use the domain knowledge of the acquired MRI and Alzheimer 's disease characteristics to extract appropriate features from the most involved ROIs in AD: hippocampus Hippocampus (Hpc) and Posterior Cingulate Cortex (PCC).

- We propose an early fusion of visual signatures from two selected characteristic regions, Hpc and PCC to improve discrimination power. We apply this approach not only to discriminate between AD and NC, but also to recognize the more challenging class of subjects (MCI) as well.

- Referring to the domain knowledge in hippocampus ROI shrinkage, we propose a late fusion of hippocampal visual features-based classifiers for Alzheimer's disease diagnosis. Here, the probabilistic outputs of classifies on both local features and the amount of Cerebrospinal Fluid (CSF) are fused to perform the final classification of the MRI scans.

- We present each brain scan by one global signature using the Bag Of Visual Word (BoVW) approach. To integrate atrophy information from different projections (sagital, axial and coronal), we propose to construct a separate codebook for MRI scans with each projection. Then, each image can be represented as a concatenation of histograms, each containing words from the corresponding projections.

- To test the effectiveness of our proposed disease-related signature, we design both Content-based retrieval and binary classification systems for CAD of AD. For classification purposes, we use the well-studied and efficient tool Support Vector Machines

(SVM). We applied the method on subset from the ADNI dataset and then on a small group of a French dataset of AD subjects, "Bordeaux-3City" dataset.

- Referring to the domain knowledge: when a brain is affected by Alzheimer's disease, hippocampus ROI undergoes a cells degeneration and then water molecules become less hindered because of loss of barriers for diffusion motion. In this case, we hypothesize that the fast diffusion of water on the hippocampal area results in brighter pixels on the MD maps. We extract visual features from MD maps and we build signatures to distinguish between an affected or a healthy hippocampus for AD CAD. The present research is the first attempt (in our best knowledge) to apply a CBIR techniques on the DTI modality for AD diagnosis. We means Diffusion maps.

0.4 Thesis outline

The organization of the rest of this thesis is as follows:

Chapter 1 This chapter introduces theories and concepts related to structural MRI and Tensor Diffusion imaging modalities. It presents the principals biomarkers for AD disease as well as the state-of-the-arts Alzheimer's disease diagnosis methods (for both DTI and sMRI modalities).

Chapter 2 We start in Chapter 2 by introducing the CBIR paradigm. Then, we present the concept of CBIR-based CAD system. Next, we review some recent research features-based methods for Alzheimer's disease diagnosis in the literature. The end of this chapter presents a review of the pattern recognition methods used for Alzheimer's disease patient discriminating. This chapter presents the mathematical background of the machine learning methods used in this thesis.

Chapter 3 The brain/ROI anatomy changes can be represented as a set of local features extracted from an MR images. Those features illustrate the presence or absence of atrophy in the specific tissue overlapping with atlas parcels. This chapter presents materials

and methods of the current work. Indeed, we generally present and explain our methodology in generating Alzheimer's disease-related signature using a local feature extraction method. First, we present the MRI preprocessing pipeline. Then, we describe the process of images signature construction. Hence, we describe the used methods such as the Bag of word approach (BoW) and Circulars Harmonic Functions (CHFs). We present the Atlas-based approach for ROI extraction. Materials are given in the end of chapter, we present the data used in the current research.

Chapter 4 It presents an application of the methodology described in chapter 3 but with more specific details referred to the domain knowledge in Alzheimer's disease diagnosis. Thus, it specifically address binary classification tasks (AD versus NC), (MCI versus NC) and (AD versus MCI). The modality used in this chapter is the Structural MRI. Visual features from the hippocampal region are extracted to emphasize the difference or similarity of subjects with respect to AD. Two kinds of features are extracted: visual local descriptors using SIFT, SURF and CHFs and the amount of CSF pixels in the hippocampal area. The proposed final classification is based on a late fusion scheme, where the probabilistic outputs of classifies on both local features of the hippocampus ROI and the amount of CSF. This approach has been applied on the baseline MR images of 218 subjects from the Alzheimer's Disease Neuroimaging Initiative (ADNI) database and then on the MRI subset "Bordeaux-3City" described in Chapter 3.

Chapter 5 In chapter 5, we use the visual indexing framework and pattern recognition on structural MRI data to discriminate between Normal Controls (NC), Mild Cognitive Impairment (MCI) and Alzheimer's Disease (AD). We use the Circular Harmonic Functions (CHFs) to extract local features from the hippocampus and Posterior Cingulate Cortex (PCC) ROIs. Tow schemes of CAD diagnosis are tested. First, a similarity retrieval approach is applied to retrieve the most similar cases. And then we propose a binary subjects classification framework with the same signatures. The fusion of features from both regions improves retrieval/classification results. Obtained results are promising and indicate that the combination of hippocampus and PCC atrophy captured by specific CHF features gives a good indicator to the diagnosis. The method is automatic less time consuming then volumetric

methods since it does not require a segmentation of ROI.

Chapter 6 This chapter presents an approach based on the comparison of visual features extracted from the hippocampal area on other modality (Tensor Diffusion Imaging) to help AD diagnosis. We stilluse the Circular Harmonic Functions (CHFs) to extract content from the Diffusion Tensor-derived map: Mean Diffusivity (MD). In this chapter, disease-related signature is illustrated by the motion of molecules water on the hippocampus ROI. First, we propose a CBIR method to retrieve similar scans. Then, we design a classification framework based on CHFs features and the Bag of Visual Words approach to classify between subjects. The DTI modality is a recent modalities and the present research is the first attempt (in our best knowledge) to apply features-based approaches on this modality for AD diagnosis.

Chapter 1

Alzheimer's disease detection with MRI: Background and literature review

Contents

1.1 Introduction

Neuroimaging is a well established technique in the medical examination routine providing a way for clinicians to analyze the structural and functional changes in the brain associated with the development of Alzheimer's disease in vivo. Commonly used neuro-image techniques include anatomical/Structural Magnetic Resonance Imaging MRI, Positron Emission Tomography (PET), Diffusion Tensor Imaging DTI and Single-Photon Emission Computerized Tomography (SPECT). MRI provides contrast images where different tissues are distinguished. It should be noted that the current work will focus on information extraction from sMRI and DTI modalities. Hence, in this chapter, we will first introduce the basic theory and concept of sMRI and DTI, then we will briefly describe their widely used measures of brain atrophy and finally, we will present a short survey of the (DTI/sMRI)-based methods for Alzheimer's disease diagnosis.

1.2 Magnetic Resonance Imaging Theory

Magnetic Resonance Imaging was mainly developed around 1980. MRI is based on the phenomenon of Nuclear Magnetic Resonance (NMR), which leaded to several Nobel prizes (Geva, 2006). MRI has presented itself as a powerful imaging technique as a way of visualizing detailed structures in-vivo. It is based on magnetic manipulation of protons to acquire images without ionizing radiation. In fact, in an MRI scanner, the patient is placed in a strong magnetic field. This magnetic field causes the hydrogen atoms (protons in the water molecules) in the patient's body to align either in parallel or anti-parallel to the field. Figure 1.1 shows the major components of the Magnetic Resonance Imaging system.

The radio-frequency coils in the machine emit radio-frequency (RF) pulses causing the proton to spin on its own axis. When the RF pulse is turned off, the protons go back to being aligned with static the static magnetic field and send electromagnetic energy back to the radio-frequency coils. This magnetic resonance signal is used to produce the 3 Dimensional grey-scale image. The rates of the proton spin relaxation can be in different, depending on the tissue type they are located in. This is how we are able to distinguish between brain tissues such as gray and white matter differences in an MR image.

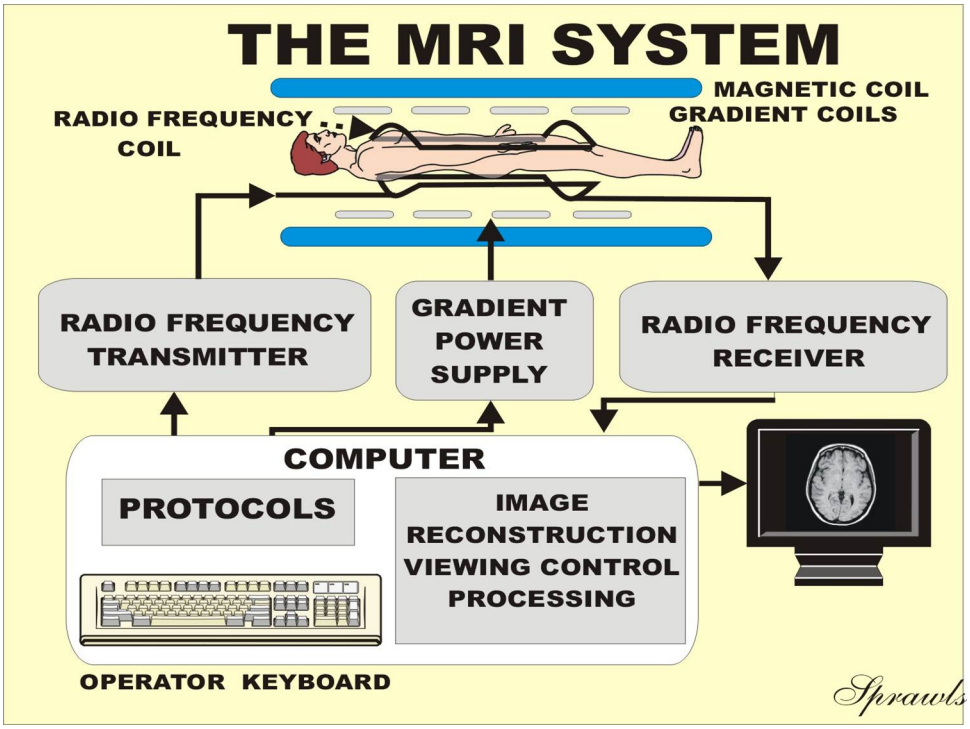

Figure 1.1: Components of the Magnetic Resonance Imaging System (Heggie, 2001).

More details about MRI can be found in (E. Mark Haacke, 1999).

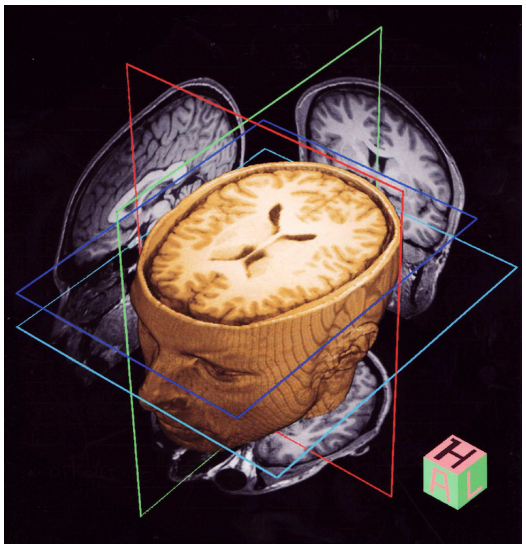

Figure 1.2: T1 (anatomical) image taken of Tim's brain by the MRC CBU (http://www.euroscientist.com/the-research-subject)

During the last decade, brain MRI has been widely used in clinical practice for diagnosis

(Rovira et al., 2009) because of its excellent soft-tissue contrast. Moreover, MRI is a safe and painless technique that uses electromagnetic waves to produce pictures which means that there is no exposure to radiation such as in Computed Tomography (CT) or X-rays scans. Therefore, MRI machines collect three-dimensional images. This allows us to represent the brain in axial, sagittal and coronal views at the same time (see Figure 1.2) which provide better localization of a lesion in the 3D space of the brain and allow structures involved by the tumor or dementia to be more clearly delineated. Hence, in this thesis we focus on human brain MRI features extraction with the aim of Alzheimer's disease diagnosis.

1.2.1 Structural MRI (sMRI)

Structural Magnetic Resonance Imaging (sMRI) is a non-invasive technique for examining the physical structure of the brain. It is the most commonly used imaging technique among others (PET, SPECT, DTI...). sMRI provides good tissue contrast enabling the detection of structural brain changes such as tumors or affected tissues. sMRI provides information to qualitatively and quantitatively describe the shape, size, and integrity of gray and white matter structures in the brain (E. Mark Haacke, 1999).

There are different types of structural images that may be collected by the MRI machines. The image type do not depend on the scanner itself but it is determined by the pattern of radio-frequency pulses. Tow basic parameters of MRI acquisition are involved:

- Repetition Time **RT**: is the time between successive Radio frequency RF pulses also called relaxation time.
- The Echo Time **TE**: represents the time between the start of the Radio frequency **RF** pulse and the maximum in the signal.

Two relaxation times for protons are commonly used known as **T1** and **T2** described below:

In clinical practice:

- TE is always shorter than TR

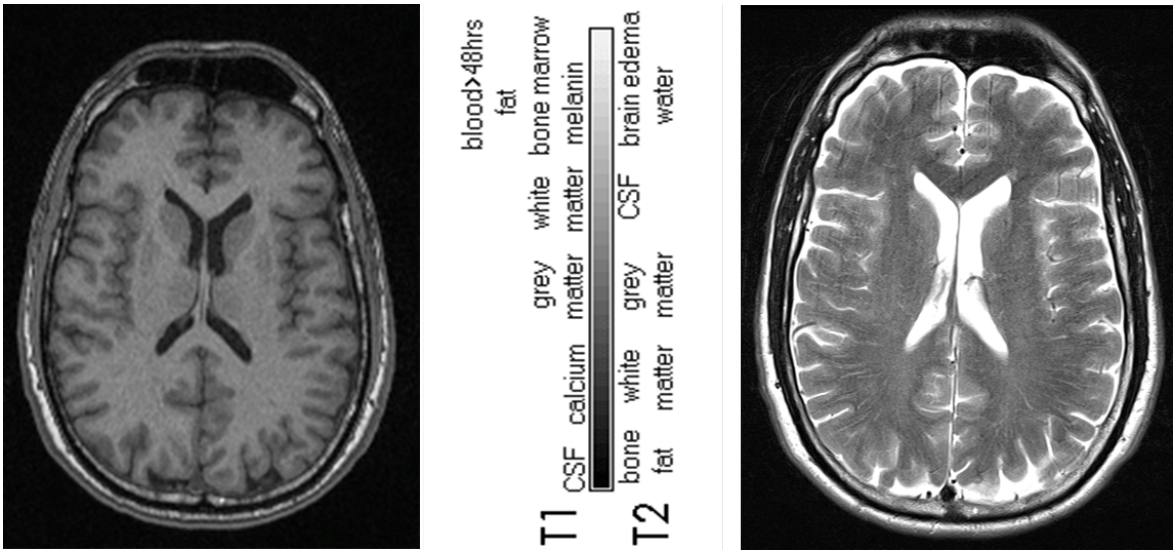

Figure 1.3: Axial slices of **T1-weighted** (left) and **T2-weighted** (right) images and grey map distribution of brain tissue (in the middle).

- A short TR = value approximately equal to the average T1 value, usually lower than 500 ms
- A long TR = 3 times the short TR, usually greater than 1500 ms
- A short TE is usually lower than 30 ms
- A long TE = 3 times the short TE, usually greater than 90 ms

T1-weighted images The T1-Weighted MRI is the standard imaging obtained with short **TE** and short **TR** ($TR < 1000\,ms$, $TE < 30\,ms$). In T1-weighted brain MRI, the Gray Matter (GM) is seen as a dark gray area, the White Matter (WM) is light gray and the Cerebrospinal Fluid (CSF) is black. Structural T1-weighted images are the most used in research studies because they allows an accurate differentiation of brain structure This is also the image type that functional MRI data are overlaid on.

T2-weighted images The T2-Weighted MRI is built with long **TE** and long **TR** ($TR > 2000\,ms$, $TE > 80\,ms$). In T2-weighted images of the brain, CSF is bright, GM is light gray, and WM is dark gray. This type of images is collected mostly for medical purposes,

since MRI contrast allows clinicians to see abnormalities within the ventricles and cerebral cortex better than on T1-weighted images.

However, radiologists used both T1- and T2-weighted images for medical diagnosis. T2-weighted images are sometimes collected for research purposes and they are often not as useful for analysis because the GM and WM boundaries are not as clearly defined as in T1-weighted images. MR-based brain morphometry is usually performed on the basis of T1-weighted imaging data (van der Kouwe et al., 2008). Hence, in the current research we consider the use of T1-weighted brain MRI.

The picture of Figure 1.3 shows an axial T2-weighted image, on the right, and a T1-weighted image at the same slice level on the left. As, it is shown in the left, in the axial slice of the T1-weighted image, grey matter is lightly colored, while white matter appears darker. In the right, the axial slice of the T2-weighted image, CSF has a higher signal intensity than tissue and therefore appear bright.

1.2.2 Diffusion Tensor Imaging (DTI)

Diffusion Tensor Imaging is relatively a new Magnetic Resonance technique (Basser and Pierpaoli, 1996).

DTI concept

DTI yields quantitative measures for tissue microstructures by measuring the diffusion information of water molecules (Bihan, 2003). Random motion of water molecules, can be quantified and reflects intrinsic features of microstructural brain tissue in vivo which just a few years ago would have been considered impossible. Indeed, diffusion signals capture microstructural properties of brain tissue that cannot otherwise be captured on traditional anatomical MRI. Actually, the quantitative information about brain ultrastructure is given by quantifying isotropic and anisotropic water diffusion. The diffusion ellipsoids and tensors for isotropic unrestricted diffusion, isotropic restricted diffusion, and anisotropic restricted diffusion are shown in Figure 1.4.

In fact, in an unrestricted environment such as the ventricles, large spaces deep in the brain, which offer limited constraints, water molecules move randomly in every direction. The

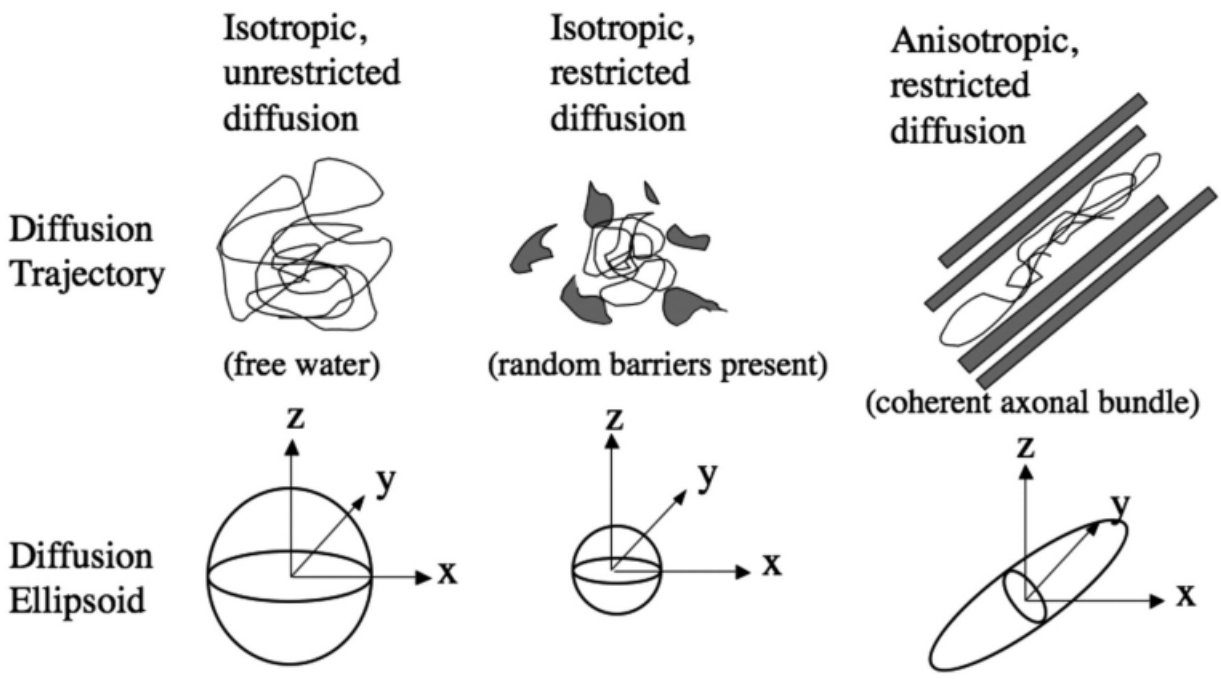

Figure 1.4: Isotropic and anisotropic diffusion. In the isotropic case, the diffusion is similar in all directions. However, when the field is anisotropic, the diffusion is larger in one direction than the other (Mukherjee et al., 2008)

.

random motion is described as isotropic. By contrast, water molecules diffuse preferentially in one direction over another in a constrained environment. This movement is called anisotropic. An example of such an anisotropic environment is within the white-matter fibers which are constrained by the presence of axons that limit molecular movement in some directions. Those measurements are presented by tow mainly used qualitative DTI-derived images, the Means Diffusivity (MD) and the Fractional Anisotropy (FA). MD represents the magnitude of water diffusion and FA reflects the degree of anisotropy. They are estimated from the DTI data following the procedure expanded in the next section. The measurement of signal loss or attenuation is a function of the diffusivity in a chosen direction as shown below:

$$S = S_0 \exp(-bD) \;\; where \;\; b = -\gamma^2 G^2 \delta^2 \left(\Delta - \frac{\delta}{3}\right) \tag{1.1}$$

Where S_0 is the signal intensity without the diffusion weighting, S is the signal with

the gradient, γ is the gyromagnetic ratio, G is the strength of the gradient pulse, δ is the duration of the pulse, Δ is the time between the two pulses, and finally D is the estimated diffusivity or apparent diffusion coefficient (ADC) (Lebihan and Breton, 1985). The degree to which the pulse sequence is sensitive to diffusion is expressed through the "b-value" given in equation 1.1

Quantitative diffusion measurements

In DTI, diffusion property is quantified by fitting the measured water diffusion to a simple tensor model with a 3*3 symmetric matrix :

$$D = \begin{pmatrix} D_{xx} & D_{xy} & D_{xz} \\ D_{yx} & D_{yy} & D_{yz} \\ D_{zx} & D_{zy} & D_{zz} \end{pmatrix} \tag{1.2}$$

D describes the covariance of diffusion displacements in 3D normalized by the diffusion time. The diagonal elements D_{xx}, D_{yy} and D_{zz} are the diffusion variances along the x, y and z axes, and the off-diagonal elements are the covariance terms and are symmetric about the diagonal ($D_{xz} = D_{zx}$). The diagonalization of this matrix yields three eigenvalues (λ_1, λ_2, and λ_3) that describe the three-dimensional diffusion properties of water within tissues and three eigenvectors, (v_1, v_2, and v_3), describing the extent and the orientation of anisotropy.

A tensor may be represented by an ellipse visually around the center of the voxel (see the bottom of Figure1.4). The shape of the ellipse varies with the size of anisotropy. In the open water (eg cerebrospinal fluid CSF) the replacement of water molecules is random. In this case, the ellipse becomes a sphere. In the white matter, the ellipse is elongated in the direction of the fibers, the more it is elongated the more the anisotropy will be important Figure 1.5.

A tensor is computed in each pixel and then several contrasts can be generated such as the Mean Diffusivity (MD) and the fractional anisotropy (FA). First, the mean diffusivity is the average of three eigenvalues (Equation 1.3) , indicating the magnitude of overall water

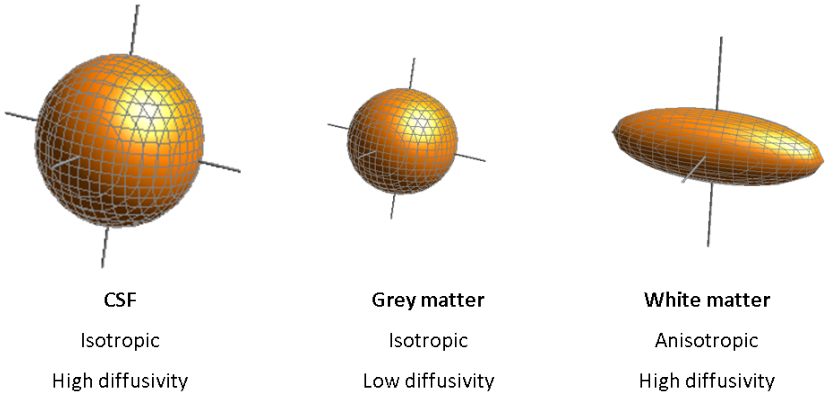

Figure 1.5: Example of diffusivity on CSF, GM and WM tissues

diffusion in each pixel. Second, the fractional anisotropy is the degree of diffusion anisotropy (Equation 1.4).

$$MD = (\lambda_1 + \lambda_2 + \lambda_3)/3 \tag{1.3}$$

$$FA = \sqrt{\frac{1}{2}}.\frac{\sqrt{(\lambda_1 - \lambda_2)^2(\lambda_1 - \lambda_3)^2(\lambda_2 - \lambda_3)^2}}{\sqrt{(\lambda_1^2 + \lambda_2^2 + \lambda_3^2)}} \tag{1.4}$$

FA ranges from 0 (isotropic diffusion) to 1 (diffusion exclusively along one direction). If diffusion is isotropic ($\lambda_1 = \lambda_2 = \lambda_3$), this measure becomes 0. An FA value close to 1 indicates a high diffusion anisotropy.

In addition to these scalar measures, a very common method in DTI is to display tensor orientation, described by the major eigenvector direction, as RGB color maps. In Figure 1.6, the RGB map is compared with the DTI-derived maps. In the latter, the white matter area looks homogeneous. However, the color-coded orientation map contains various colors in the white matter area. For diffusion tensors with high anisotropy, the major eigenvector direction is generally parallel to the direction of WM tract, and the RGB color map is used to indicate the major eigenvector orientation. Red color indicates that the fibers at that voxel are running in the left-right direction, blue indicates the inferior-superior direction (down-up), and green means they are running in the anterior-posterior direction (front-back).

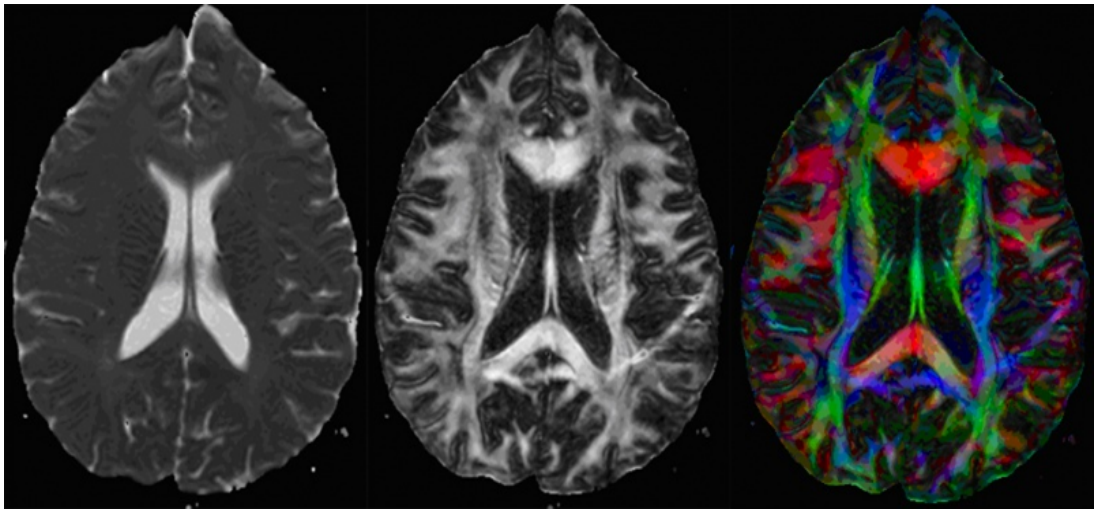

Figure 1.6: Quantitative maps of DTI measurements. Left to right: the mean diffusivity (MD; CSF appearing hyperintense), fractional anisotropy (FA; hyperintense in white matter), the major eigenvector direction indicated by RGB color map.

Consequently, with this respect, DTI could be a diagnostic tool that quantifies the degree of tissue atrophy and thus could be a good biomarker for disease diagnosis in particular for Alzheimer's disease diagnosis. In this thesis we will focus on the use of the MD maps to classify subject with and without AD.

Both structural MRI and DTI measures promise to aid diagnosis and treatment monitoring of MCI and AD by quantifying patterns of structural brain atrophy. Here, several sMRI and DTI biomarkers are involved and a variety of methodologies and techniques are proposed to analyze brain tissue and to detect abnormalities. This will be detailed in the next section.

1.3 Alzheimer's disease diagnosis using sMRI

1.3.1 MRI and its ability to capture visual brain atrophy in AD

In the past decade, anatomical magnetic resonance imaging has been increasingly used to help clinicians in Alzheimer's diseases diagnosis (DeKosky and Marek, 2003) because it is widely available, and very sensitive to the atrophy that occurs with AD. Moreover, structural MRI provides high resolution images of brain tissue, it is thus possible to measure cortical thickness and volumes of different regions.

From a practical point of view, an observer with some experience may well be able to identify the more atrophic medial temporal lobe areas in figure. Looking at the same scans from the feature extraction perspective, it becomes evident that there are substantial differences between both scans, (e.g. regarding brightness, anatomy of the ventricles or differences in brain structures) that are unrelated to the diagnostic problem. Generally, the pattern of cell neurodegeneration seen using anatomical MRI is presented by (Braak and Braak, 1998) and several brain areas may be sensitive biomarkers for AD. The most interesting ones are cited below:

MRI cortical thickness shrivels up It has been reported that AD patients show evidence of cortical atrophy, in comparison with normal subject (Arnold et al.; Brun and Gustafson, 1976). The cerebral cortex shrink (atrophy) in multiple regions as the disease advances, damaging areas involved in thinking, planning and remembering.

Hippocampus volume loss Rates of whole-brain and hippocampal atrophy are sensitive markers of neurodegeneration, and are increasingly used as outcome measures in AD diagnosis (Pelletier et al., 2013). The hippocampus is an area of the cortex that plays a key role in formation of new memories. Several studies show that the hippocampus, and the entorhinal cortex are the most vulnerable Regions of Interest (ROIs) with respect to AD pathology (Braak and Braak, 1998). High rates of hippocampal atrophy compared with cognitively normal persons have been measured using MRI in both AD and MCI patients (Van de Pol et al., 2007; Schuff et al., 2009). In (Wang et al., 2003; Scher et al., 2007), the authors demonstrate that hippocampal volume loss distinguish very mild AD from healthy aging.

Ventricles enlargement The Ventricles -chambers fluid-filled spaces within the brain- are noticeably enlarged. Accordingly to (Schott et al., 2005) and (Bradley et al., 2002), an increased rates of ventricular expansion and whole-brain atrophy were seen in AD compared with control subjects. Many studies have shown a correlation between the enlargement of ventricles and the progression of AD. Recently, in (Nestor et al., 2008), the authors show that Ventricular enlargement represents a marker of disease progression in subjects with MCI and

subjects with AD.

Cerebrospinal fluid (CSF) biomarkers CSF fluid replaces brain tissue which is lost due to neuronal cell degeneration or the loss of volume of some region. Consequently an increased amount of CSF fluid has been advocated as diagnostic measures for diagnosing or excluding AD in several studies (Blennow et al., 2010).

Figure 1.7 shows typical MRI scans of an older cognitively normal Normal Control (NC) subject, an amnestic mild cognitive impairment (aMCI) subject, and an Alzheimer's disease AD subject From the ADNI dataset. As it can been seen in the figures, there is an increasing medial temporal atrophy, MRI cortical thickness shrivels up, a loss of hippocampus volume (C) and ventricular, enlargement (B) in AD when compared with NC . In the case of AD, the volume losses appeared together with an increase of CSF, illustrated by dark area in the degenerated area.

In Figures 1.10 and 1.11, we illustrate the same phenomena on the images taken from the ADNI dataset witch is the main experimental dataset in the current work. They show respectively representative T1-weighted intensity histograms for healthy and Alzheimer's disease (AD) patient selected from the ADNI dataset. The units of the y-axis correspond to the number of voxels, and the units of the x-axis are the intensity values. The histograms allow us to see where peaks of intensity occur or disappear. The observed variability in the shape of the histograms is due to varying tissue proportions across the MRIs. For example, the NC brain contains relatively small amount of CSF and hence the lowest intensity peak is practically missing from its histogram. The proportion of CSF is increased in AD due to the enlargement of ventricles, leading to reappearance of the lowest intensity peak. This brain, however, contains only a small amount of gray matter (GM), thus decreasing the middle peak of the image histogram. In addition, the AD histogram has large CSF amount compartments compared to that seen in the normal histogram. Additionally, in the diseased brain, the contrast between gray and white matter is considerably reduced, and the two histograms peaks have merged.

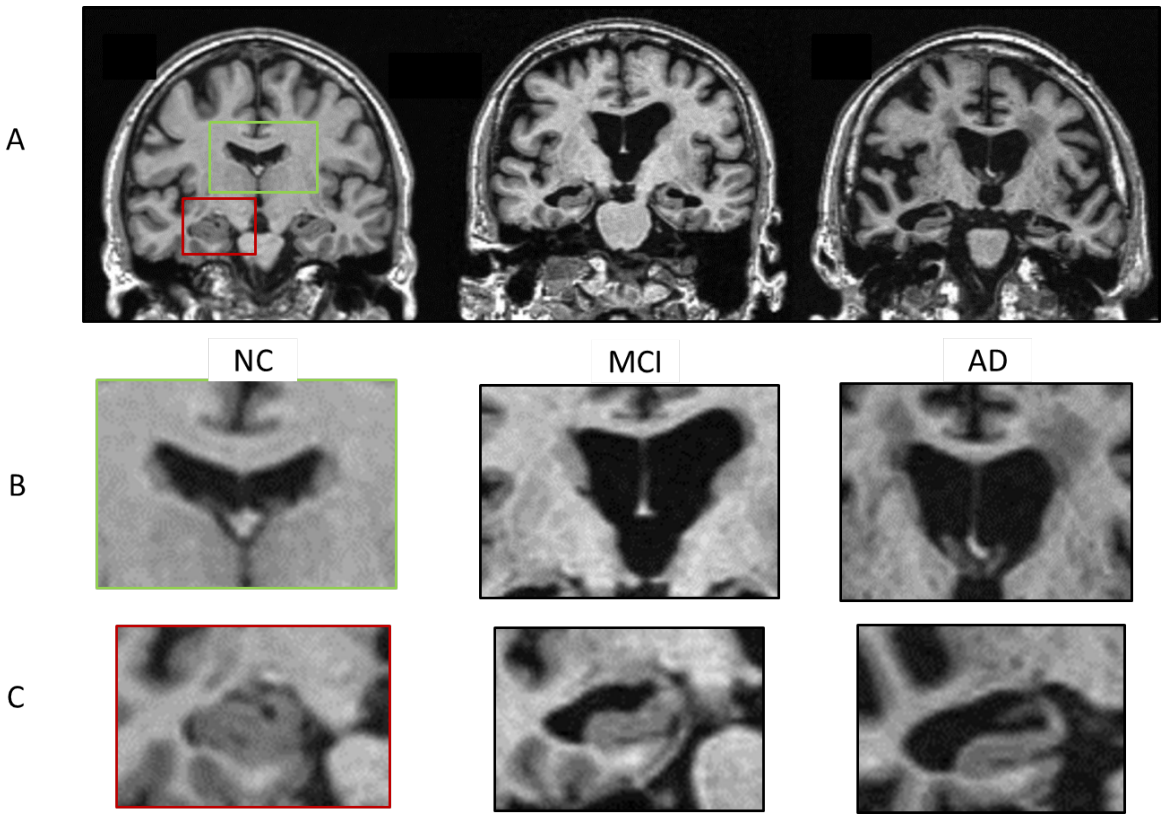

Figure 1.7: A: T1-weigthed MRI scans(1.5 Tesla) of an older cognitively normal (CN) subject, a Mild Cognitive Impairment (MCI) subject, and an Alzheimer's disease (AD) subject in tree cases (NC ,MCI and AD) B: Lateral Ventricles enlargement (Green). C : Progressive atrophy of Hippocampus structure (Red).

1.3.2 AD diagnosis methods

Computer Aided Diagnosis (CAD) tools based on medical imaging are a very valuable help for clinicians in the AD diagnosis. They can offer meaningful comparison between normal and diseased persons by analyzing, detecting and quantifying the brain abnormalities. The effectiveness of MRI as a valuable diagnostic technique in neurological diseases has been widely proved, usually on the T1-weighted imaging data. Such popularity comes from the obtained good contrast between soft tissues, giving the possibility of identifying the distribution of changes in neuroanatomical structures, such as estimates of damaged tissue or atrophy rates. During the last decade, various works in AD diagnosis have been reported. A thorough review of all these studies is beyond the scope of this section.

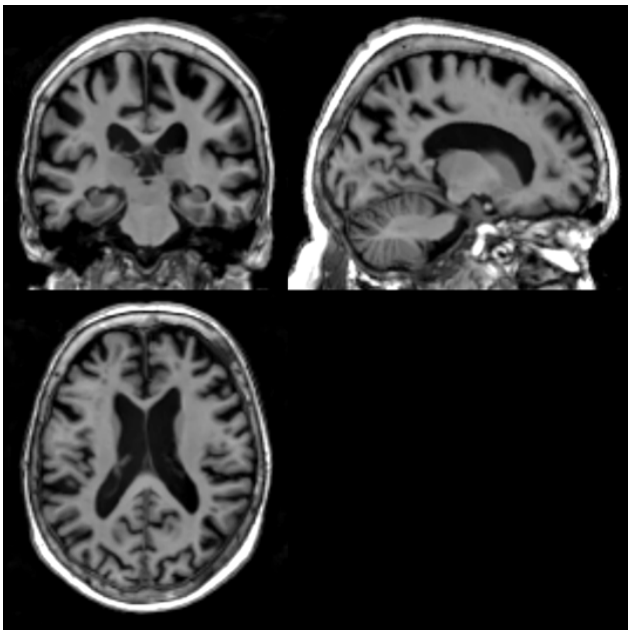

Figure 1.8: Structural MRI of the 136-S0299 AD subject from the ADNI dataset

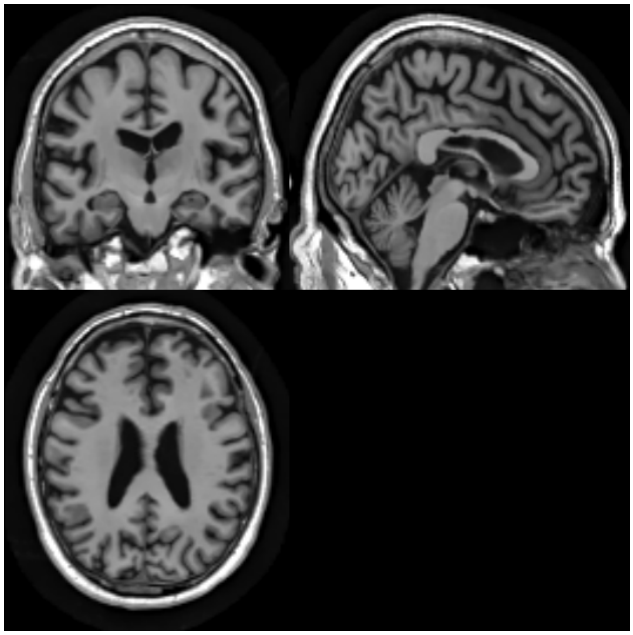

Figure 1.9: Structural MRI the 007-S1206 NC subject from the ADNI dataset

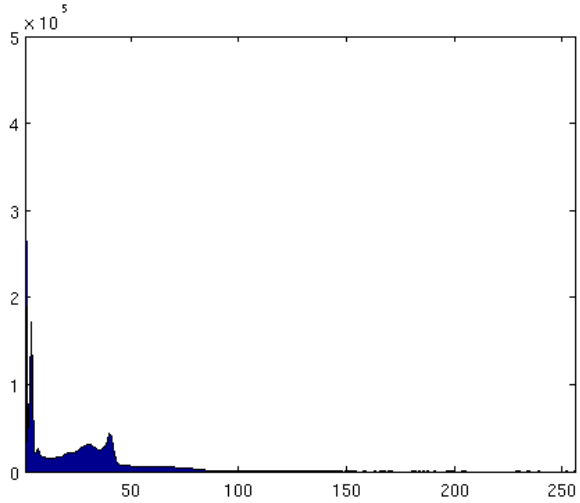

Figure 1.10: Structural MRI of the 136-S0299 AD subject from the ADNI dataset

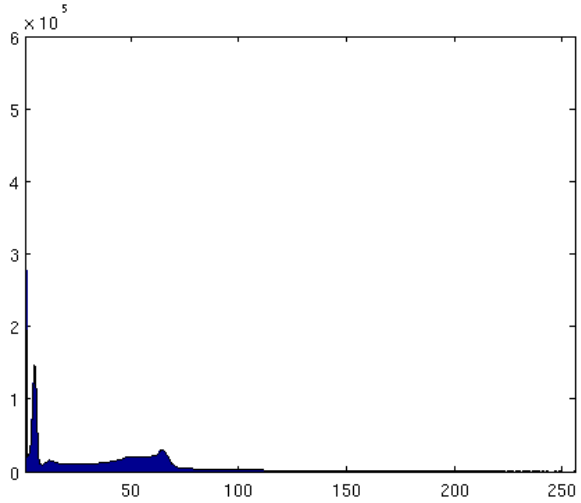

Figure 1.11: Structural MRI the 007-S1206 NC subject from the ADNI dataset

Quantitative Region of Interest methods/Volumetric approaches

Volumetric methods are quantitative and have been used to extract three-dimensional (3D) measurements of specified brain structures on MRI scans. The 3D nature of volumetric approaches let them exploit complete spatial information of the scans.

Recently, a variety of ROI-based volumetric methods have been proposed to demonstrate significant differences in volumes of specific Regions of interest (ROI) across population in the aim of AD diagnosis (Chetelat and Baron, 2003; Tapiola et al., 2008; Convit et al., 1997, 2000; Querbes et al., 2009; Coupé et al., 2012). Indeed, such volumetric measurements, require the segmentation of these ROI from the MR images, most often manually. Furthermore, a priori assumptions about the expectedly affected brain structures is needed to select the appropriate ROI.

Manual segmentation Tracing and quantifying the volume of medial temporal lobe structures (for example, the hippocampus or entorhinal cortex) or posterior cingulate have been used in Alzheimer's disease diagnosis and provide an efficient quantification of tissue atrophy. However, manual measurements are tedious and time-consuming .

Automated and semi-automated techniques Although other automatic or semi automatic methods of ROIs segmentation have been developed over the past decade. In the recent past, methods have been proposed to automatically parcellate GM volumes, hippocampus or cortical surfaces into ROIs. Those automated and semi-automated methods are useful for large-scale studies because they do not require a significant manual intervention.

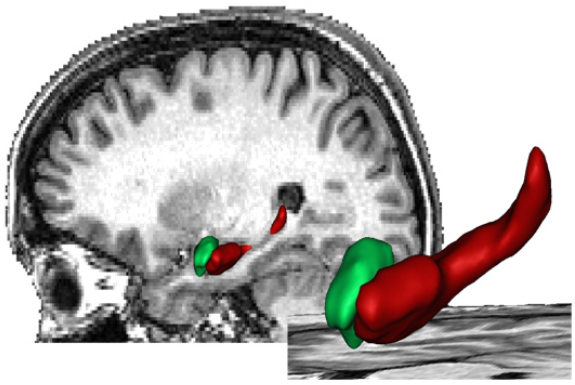

Figure 1.12: SACHA: automatic segmentation of the hippocampus and the amygdala from MRI (Chupin et al., 2009b)

Volumetric Analysis Several studies based on structural MRI volumetric measurements of specific ROIs, have demonstrated significant results in discriminating AD patients from

normal controls. Several works have been proposed that use the hippocampal volume (Colliot et al., 2008; Chupin et al., 2009b; Klöppel et al., 2008). The volume of the Entorhinal cortex or the lateral ventricle have been also considered for the same propose. In the AD-related research, the volumetric analysis of hippocampus is the most extensive study. Several automatic hippocampus segmentation approaches have been proposed (Chupin et al., 2009a; Colliot et al., 2008; Chupin et al., 2009b), those methods show significant variability in the measurement of atrophy rates due to differences in the detection of the hippocampal boundaries. On the other hand, manual segmentation of the hippocampus by experienced radiologists suffer from inter-rater variability. Volumetric methods present an advantage which consists in the fact that the measurements describe a known anatomic structure that (in the case of the hippocampus) is closely related to the pathological symptoms of the disease.

Shape Analysis However, volumetric analysis can identify hippocampal atrophy in MCI, but may not localize the local structural changes. In the contrary, shape analysis has the potential to provide important information beyond simple volume measurements. It may characterize abnormalities in the absence of volume differences and localize the region of statistically significant structural changes. One notable 3D shape analysis approach explore spherical harmonics (SPHARM) coefficients. In (Gerardin et al., 2009; Gutman et al., 2009), the authors characterize the shape of the hippocampus as a series of parameters illustrated by spherical harmonics. It means that they consider the geometrical information of the hippocampus, rather than the intensity or the volume. Some recent works showed that shape measures reveal new information in addition to size or volumetric differences, which might assist in the understanding of structural differences due to neuroanatomical diseases. For instance, (Yang et al., 2010) combines volume features and shape features to classify AD from NC using neural network (ANN) classifier.

Traditional ROI-based methods give global differences in structure and it is not easy to obtain information on specific localized structural changes. In addition, the disadvantage of using a single region of interest to boost 3D information as a disease marker is that it is spatially limited and does not explore all of the available information in a 3D Image. Finally, Those approaches need a priori definition of regions of interest. This can be avoided by the

application of recently developed Morphometric analysis.

Morphometric methods

Aside from volumetric approaches, morphometric methods have gained great interest because they first help to detect structural changes in MRIs and second, do not depend on the clinician abilities. Morphometric methods are voxel-based approaches which where specifically implemented for various imaging modalities such as T1-weighted MRI or diffusion tensor imaging (DTI). In such methods, brain images are first non-linearly registered to a common template, and then univariate statistical tests are performed in each voxel to detect significant group differences. The results are probability maps often referred to as "concentration map" of the three brain tissues (cerebrospinal fluid, white and gray matter). Indeed, the brain tissue are obtained from the fuzzy segmentation step performed prior to the non-linear registration to the template.

However, morphometric methods are not restricted to analysis of voxels from the entire brain, but can be applied to specific regions also. The idea consists in grouping neighboring voxels into anatomical regions using an anatomical atlas (Ye et al., 2008). For instance in (Magnin et al., 2009; Lao et al., 2004), probability maps are divided into 116 regions of interest using the Automatic Anatomical Labeling (AAL) (Tzourio-Mazoyer et al., 2002). Then, the average intensities inside each region are taken as features for the classification step. However, such fragmentation of the brain may not be suitable for Alzheimer's disease: the border of the affected areas do not necessarily represent those of the atlas. For this reason, (Fan et al., 2007) proposed an adaptive segmentation of the brain with a study group, to obtain a set of homogeneous regions. This method has been used in many studies such as (Christos et al., 2008; Fan et al., 2008; Misra et al., 2009). By statistically analyzing these voxel-wise measures, it is possible to determine which voxels are significantly different between the subject groups, and maps presenting the brain regions that are related to the disease can be created (Vemuri et al., 2008; Klöppel et al., 2008; Magnin et al., 2009; Stefan et al., 2007; Duchesne et al., 2010; Fan et al., 2008; Christos et al., 2008; Hinrichs et al., 2009). In addition, those voxel-wise measures can be taken as features, which are then fed to a classifier such as Support Vector Machines (SVMs), in the aim to discriminate between

normal controls and early-stage AD.

Here, the features are extracted at the voxel level, features may be voxel intensity from the probabilistic map of gray matter or CSF (Christos et al., 2008; Klöppel et al., 2008). For instance, in (Magnin et al., 2009),

each MRI scan were parcellated into ROIs. An histogram analysis of the intensity distribution in all voxels is then performed in order to identify the amount of WM, GM, and CSF in the ROI. The extracted parameter from this analysis represents the relative weight of GM compared to WM and CSF. Finally, based upon this parameter estimated in all the brain ROIs, the authors classify the subjects with an SVM.

Univariate and multivariate voxels-based analysis Traditional univariate voxel-based analysis quantifies changes in brain tissue density or volume between groups in a voxel-wise manner such that each voxel is individually compared. It neither consider group differences in the patterns of covariance across brain regions, nor explicitly tests the interrelationship among brain regions.

Recently there is a growing interest in studies using a multivariate approach to analyze brain imaging data in an attempt to overcome the limitations inherent to univariate voxel-based approaches. The Multivariate approach focuses on the analysis of the images by extracting features (voxels GM/WM/CSF density) to distinguish between AD and normal subjects. Multivariate pattern analysis is a machine-learning- based pattern recognition technique that can be used to classify data by discriminating between two or more classes (or groups). Multivariate approaches can provide unique information that is over-looked by univariate approaches. Whereas univariate analysis can reveal which particular brain regions differ on a relevant dimension (e.g., GM volume) between participant groups, multivariate analysis can show which set of brain voxels, in combination, can be used to discriminate between two participant groups. Among different morphometric approaches, we distinguish the following:

Voxel Based Morphometry (VBM) It is a well-known computational neuroimaging analysis (Ashburner and Friston, 2000). VBM compares regional patterns of brain between groups of subjects by performing statistical tests across all voxels in the MRI scan. VBM

has been widely applied to study the GM probability map (Busatto et al., 2003; Shiino et al., 2006; Mechelli et al., 2005; Vasconcelos et al., 2011; Frisoni et al., 2005). The probabilistic segmentations of the gray and white matter tissues are compared voxel by voxel. Figure 1.13 presents an example of GM density maps comparison.

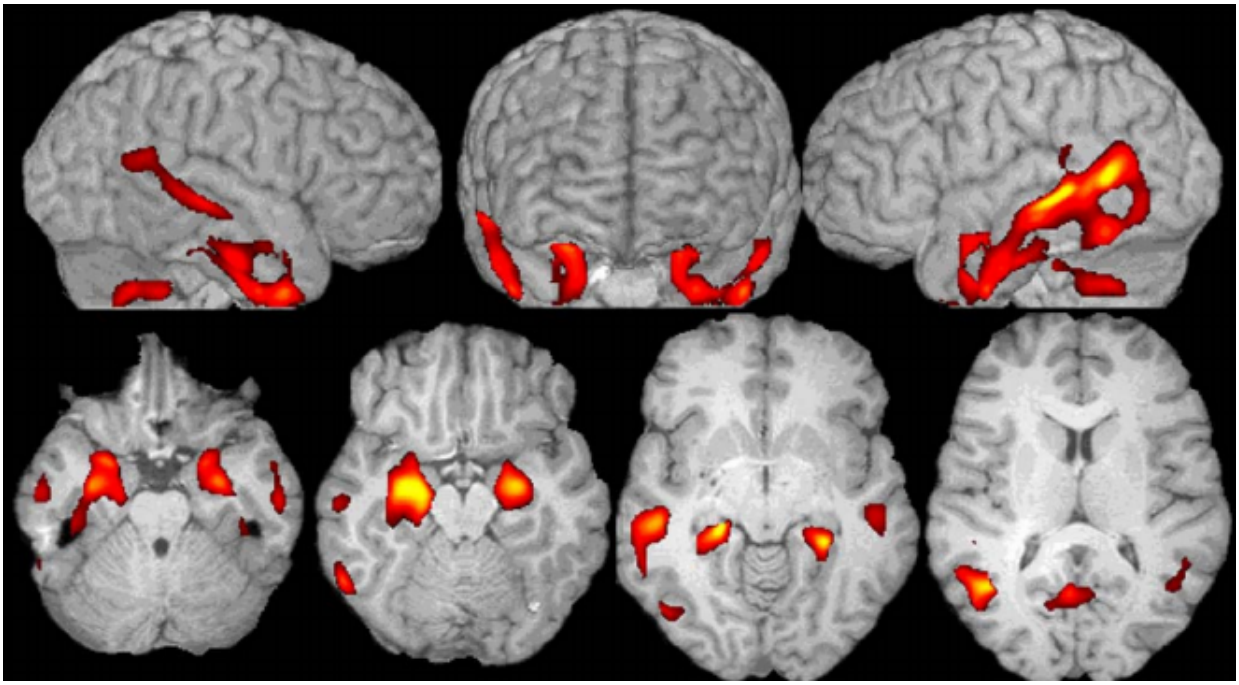

Figure 1.13: Example of VBM comparison results of AD patients and normal controls. Maps of significantly lower grey matter density (Lehericy, 2007)

Deformation-Based Morphometry (DBM) It considers the properties of the deformation field that results from the non-linear registration step (Gaser et al., 2001). The deformation field gives information about both position and volume differences.

Tensor-Based Morphometry (TBM) TBM (Studholme et al., 2006) is a variant of DBM and uses the voxel wise Jacobian determinant of this deformation field. This measure represents the volume change.

Object-Based Morphometry (OBM) It analyzes the deformation of specific pre-segmented anatomical structures of interest (Mangin et al., 2003).

Voxel based methods work directly on the voxel grid and are computationally very efficient. An advantage of these approaches,compared to the ROI-based volumetric methods, is the fact that they do not require a priori assumptions about the location, the size or number of ROIs to be analyzed, since they provide voxel wise measures determined in the entire brain. Nevertheless, they are less accurate due to the limited resolution of the voxel grid and less robust to noise. Then, and as mentioned above, these approaches always require an inter-subject registration to a template, in order to guarantee that the statistical analysis compares homologous structures across all subject brains. However, this kind of one-to-one correspondence between subjects need not be achieved for every case, mainly because of the inherent inter subject anatomical variability and the effects of a brain pathology. Indeed, not all subjects may have the same anatomical structure, or may exhibit different morphologies across the group. In addition, some pathologies may affect not only a single anatomical structure or interconnected regions, but specific structures localized far away from each other. This kind of patterns are difficult to find and analyze with the standard morphometrical techniques. To cope with this issue, features based methods, that can be able to model such patterns have been proposed. This will be further discussed in the next chapter.

1.4 Alzheimer's disease diagnosis using DTI

For nearly twenty years, considerable progress has been made in the acquisition and processing of MRI data. Alongside these advances, many studies have investigated the potential of these techniques in AD diagnosis.

1.4.1 Alzheimer's disease in DTI

Recent works have been focused on the use of diffusion MRI in the AD and MCI patients. Indeed, DTI measurements correlate with tissue damage that is not detectable in conventional sMRI. Increased MD and decreased FA in medial temporal lobe structures including the entorhinal cortex, hippocampus and parahippocampal white matter for both AD patients and MCI patients were reported (Mielke et al., 2009; B. Parente et al., 2008; Rose et al., 2008).

Microstructural abnormalities on DTI are promising biomarkers for AD. Indeed, progressive loss of the cellular barriers that restrict water molecules motion (neuronal loss) or degeneration of structural barriers can be sensitively detected by DTI as pathologically increased MD (Basser and Pierpaoli, 1996; Kale et al., 2006; Mielke et al., 2009). Hence, hippocampal shrinkage observed on diffusion tensor imaging may be a biomarker for AD diagnosis. A higher MD of the hippocampus compared with controls has been found in mild cognitive impairment or Alzheimer's disease subjects (Cherubini et al., 2010; Müller et al., 2007; Yakushev et al., 2010; den Heijer et al., 2012). (Müller et al., 2007) showed that high diffusivity within the hippocampus is more predictive than hippocampal volume atrophy in predicting dementia onset in mild cognitively impaired patients. Several MRI findings have shown that white matter is heavily affected in Alzheimer's disease, even at early stages (Medina et al., 2006; Naggara et al., 2006; Serra et al., 2010; Stahl et al., 2007; Liu et al., 2013). However, regional patterns of white matter (WM) damage are still difficult to study due to lack of discernible anatomical features of white matter in structural MRI. Here, DTI has become the method of choice for detecting white matter alterations in the human brain (Bihan, 2003). It has been reported that FA values of Alzheimer's disease (AD) subjects tend to be lower than those of NC subjects in several regions of white matter (Patil et al., 2013; Nir et al., 2013; Radanovic et al., 2013; Liu et al., 2013).

MD and FA maps are scalar values ranging from 0 diffusion to 1. Grayscale images, may be generated encoding values from the unitary interval $[0, 1]$ to the gray color space $[0, 255]$. From the level of intensities presented on the MD and/or FA maps we can deduce if the corresponding subject is healthy or presents an AD. The Figures below show the fractional anisotropy and the mean diffusivity maps of one healthy subject and on AD patient. Maps are selected from the ADNI dataset.

Note that the bright signal intensities in the grey-scale FA map (Figure 1.15) image due to high diffusion anisotropy highlight the ordered structures in which water moves in a preferred direction and the darker pixels regions of isotropic diffusion, for example ventricles full of CSF in the case of NC or the shrinked area in the case of AD. On the other hand, MD is higher in areas where the water is relatively unrestricted, like in the ventricles and surrounding CSF and it is lower in the WM where the diffusion of water is more restricted (Figure 1.14).

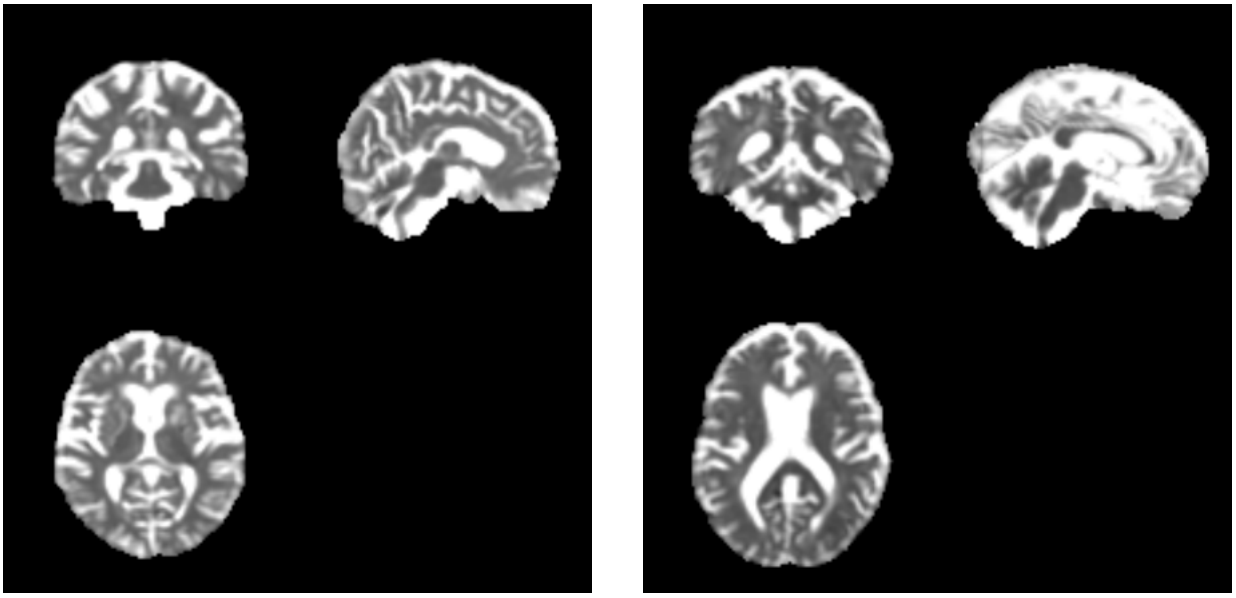

Figure 1.14: MD map of a Normal Control subject from the ADNI dataset : 021-S-4254 and MD map of AD patient from the ADNI dataset: 094-S-4089

Increased mean diffusivity in grey matter ROIs is due to the cells degeneration in those ROIs which may be a biomarkers for AD. MD increase is presented in the MD grey-scale image by bright pixels.

The number of studies employing DTI to investigate microstructural changes in AD and MCI has greatly increased over time. The next section presents the most used methods for structural changes detection and analysis.

1.4.2 DTI analysis methodologies

Several methods of DTI data analysis have been proposed. This section summarizes the main categories for patient-control comparison of diffusion MRI data. We can divide them in three main groups : Region-of-Interest (ROI)-based methods, voxel-based approaches and tract-based spatial statistics (TBSS). Those studies used DTI measures of MD and FA as markers of cerebral integrity.

Region-of-Interest (ROI)-based methods

DTI-studies mostly use fractional anisotropy (FA) and mean diffusivity (MD) measurements in a priori defined regions of interest (ROI) (Naggara et al., 2006; Bozzali et al., 2002; Stahl

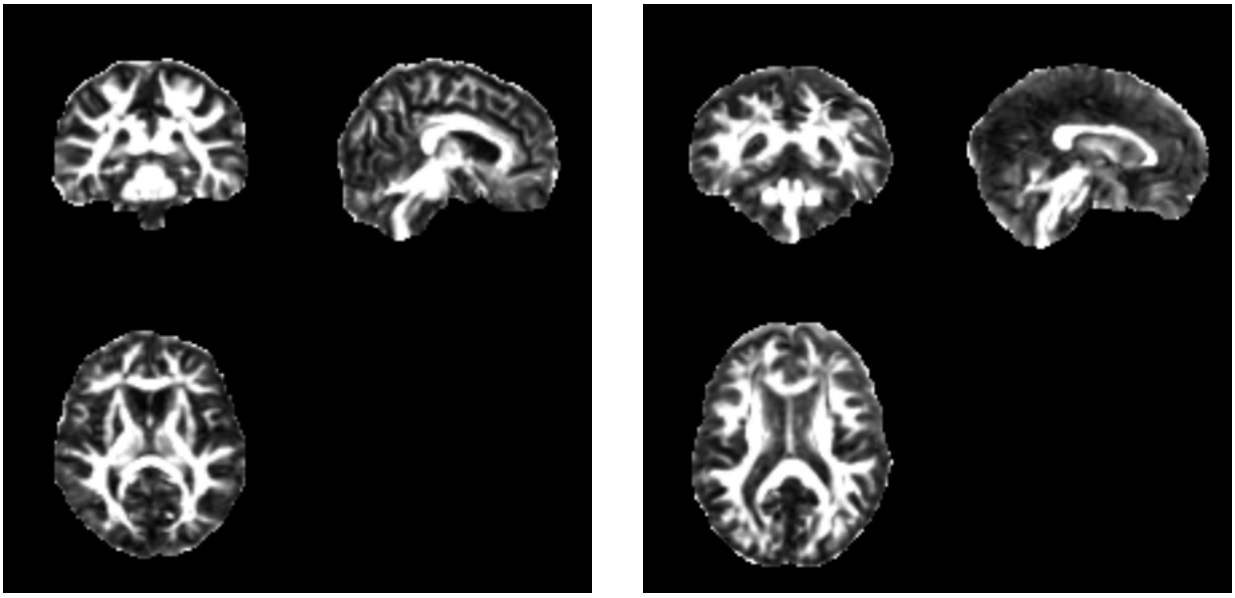

Figure 1.15: FA map of AD patient from the ADNI dataset: 094-S-4089 and FA map of a Normal Control subject from the ADNI dataset :021-S-4254

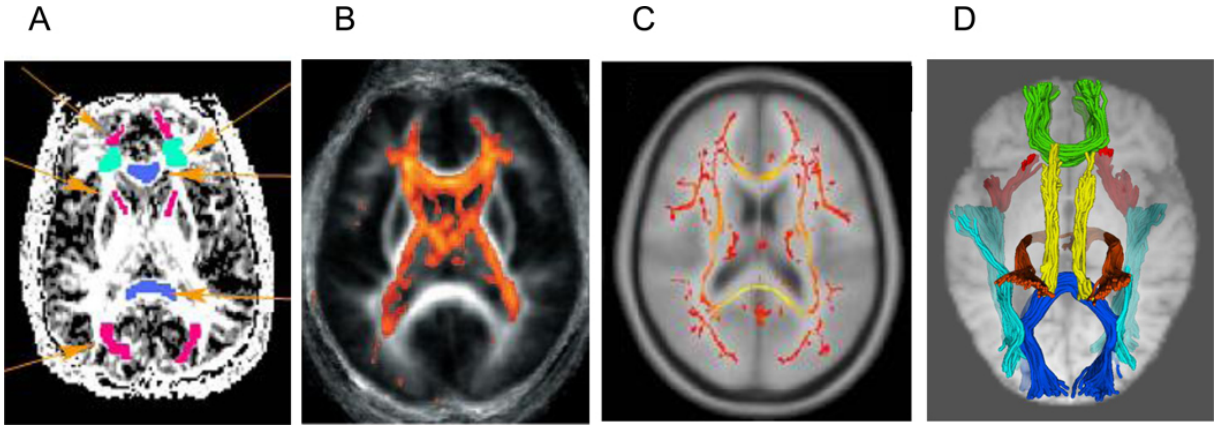

Figure 1.16: Methods for representing diffusion tensor imaging (DTI) data. A = regions of interest (in color) placed directly on DTI image; B = voxel-based morphometry (VBM); C = mean skeleton of white matter tracts from tract-based spatial statistics (TBSS); D = fiber tracking of white matter pathways. Image courtesy of Simon Davis, University of Cambridge (Madden et al., 2012).

et al., 2007; Zhang et al., 2007).

Hippocampus is one of the first brain region to be affected by AD pathology, and microstructural alterations within hippocampus have been quantified in vivo using DTI. Mean diffusivity, as a marker of microstructure, appears to be a more sensitive marker of hippocampal integrity than macrostructural measurements with MR volumetry (Clerx et al., 2011).

In contrast, FA is not as accurate for quantifying microstructural integrity of hippocampus in AD (Andreas and Igor, 2011). Recent works reported reduced FA in white matter regions as well as increased MD in the hippocampus and other medial temporoparietal regions using ROI approaches (Cherubini et al., 2010; Müller et al., 2007; Kantarci K, 2005).

Voxel-based methods

Voxel-based Approaches (VBA) are widely used in DTI studies to localize macro-structural changes related to AD (Takahashi S, 2002; Tabelow K, 2008; Stoub TR, 2005; Stricker NH, 2009; tebbins GT, 2007; Medina et al., 2006). A growing number of studies employ VBA using statistical parametric mapping (SPM) (Wellcome Department of Cognitive Neurology, [1] to compare voxels value extracted from FA or MD map. VBA is a fully automatic method.

Tract-Based Analysis Techniques (TBSS)

Voxel-based analysis and tract-based spatial statistics (TBSS) was recently introduced to perform voxel-wise statistical analyses of FA (Smith et al., 2006). TBSS has been found to overcome the drawbacks of VBA by minimizing the effects of misalignment and provides more consistent results across subjects and sessions. TBSS has been used in sevral studies to compare patients with AD and MCI with healthy controls (Haller et al., 2010; Zhuang et al., 2010; Damoiseaux et al., 2009; Liu et al., 2011; Serra et al., 2010). TBSS pipeline is provided in the FSL software package.

In addition, several DTI works for Alzheimer's disease extract FA and/or MD values together with stuctural MRI voxel values improves classification accuracies Dyrba et al. (2012) Mesrob et al. (2012) Cherubini et al. (2010) of AD subjects. (Haller et al., 2010; O'Dwyer et al., 2012) used support vector machines to classify MCI versus healthy controls using DTI data.

[1] http://www.fil.ion.ucl.ac.uk

1.5 Conclusion

In this chapter, we gave an overview of some important concepts related to the Structural MRI and Tensor Diffusion imaging modalities. Then, we briefly presented the main methods of AD diagnosis using those two modalities. Actually, most of the methods cited above were proposed for group analysis and cannot be used to classify individual patients. Thus, quantifying image features which may not be present in all subjects is a major challenge. In order to overcome all these limitations, computer vision tools and features-based approaches have been proposed. The next chapter introduces and elaborates the role of content-based image indexing and classification for the categorization of Alzheimer's disease patients.

Chapter 2

Features-based methods as a new trend in AD diagnosis research

Contents

2.1 Introduction

MRI can be described using either global or local features. Global features are calculated based on the whole image while local features extraction consists in describing the local image neighborhoods computed at specific region. Indeed, global features present significant limitations such as difficulties to reflect localized details of an image. Whereas, local descriptors are able to offer robustness against rotation and translation in localized regions of the images. Recently, a class of local features-based methods has demonstrated impressive level of performance for Alzheimer's disease related patterns description. In this chapter, we will introduce particularly the fundamental theory of content-based indexing and retrieval approach. Then, we will present the concept of CBIR-based CAD. Next, we will briefly review some recent research features-based methods for Alzheimer's disease diagnosis in the literature. Finally, a summary about state-of-the-arts classification-based CAD systems will be presented.

2.2 Generic methodology of MRI (CAD) system

The traditional diagnosis way is based on the clinician's experience and his wisdom of collecting useful information and interpreting medical images. Actually, the clinician looks carefully into the scan and identifies the corresponding patient's disease. To attain a correct diagnosis, clinicians need to learn and archive previous studied cases which may provide a valuable reference in a new case diagnosis. Actually, a good clinician does not need to have a particularly good eyes but a sensible ability to precise what he/she is looking for when examining a scan. However, clinician diagnosis is made based on subjective judgment. CAD has been proposed as a way to support clinicians decision.

The concept of CAD was founded by the University of Chicago, in the mid-1980s. The idea was to provide a computer output as a "second opinion" to aid radiologists in analyzing images.

Figure 2.1 shows a diagram of the CAD process. The system consists of several steps namely image preprocessing, ROI segmentation, feature extraction and final classification. Indeed, the extracted features are classified to build decision model. This model helps clin-

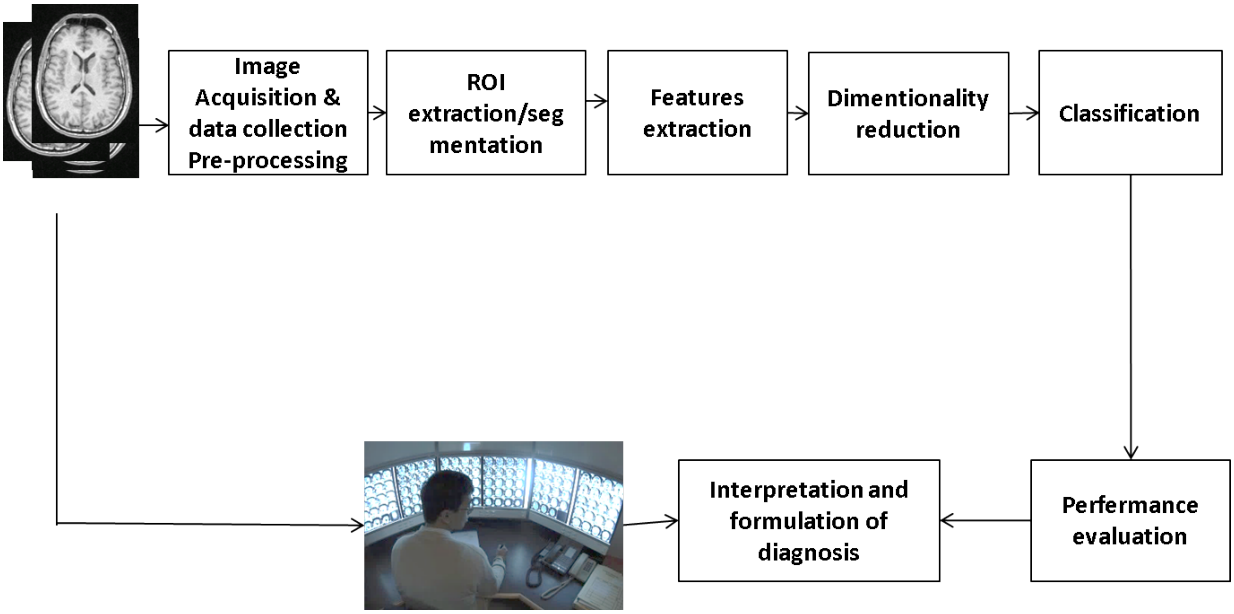

Figure 2.1: Typical Computer-assisted diagnostic-system flowchart according to (El-Dahshan et al., 2014)

icians making decision about the disease. Consequently, appropriate image processing tools and methods may improve the performance of the CAD system. The interpretation and the formulation of diagnosis consists in merging two main sources of clinical information: computer-extracted image features and radiologist-interpreted findings. Although CAD assists in decision support in the diagnosis process but the final decision is to be made by the doctor.

Hence, the application of general image analysis and classification techniques in this specialized domain is a well-established field of research. Recently, CBIR-based CAD or classification-based CAD systems have shown potential to provide clinicians with "visual aid" to make better decision with confident and quicker process as compared to the traditional manual diagnosis (Welter et al., 2012).

2.3 Content-Based Image Retrieval (CBIR)

Content-Based Image Retrieval (CBIR) also known as content-Based Visual Image Retrieval (CBVIR) has been active and fast advancing research area since the 1990s (Smeulders et al.,

2000). CBIR makes use of information directly derived from the content of images themselves rather than their textual information. Indeed, this technique refers to the use of visual descriptors to represent image content, and machine learning techniques to retrieve and compare those images. The visual content descriptor can be compared either globally (the whole image) or within an image region (locally). Traditional features include color feature, texture feature, and shape feature. Those features present the image or the ROI as a vector of n-numerical values in a n-dimensional space. Content-based image retrieval computes visual similarities between a given image and the images of a database. The system returns a number of images ranked by their similarities with the query image. To have optimal performance of visual content-based system, one needs to select appropriate descriptors for the specific type of images to be processed, and to find best distance metric to compare images. However, in many cases especially when the high-level concepts in the user's mind are difficult to express, the use of such low-level features can not give satisfactory retrieval results, this is the so-called "semantic gap" problem.

The challenge of CBIR here consists in optimizing and mapping the low-level features to high-level semantic concepts by using object ontology to define high-level concepts. That have been almost done by using machine learning tools to associate low-level features with query concepts, including user relevance feedback functionality, and combining the visual content of images with its textual information. Moreover, the choice of the important relevant features refereeing to the domain knowledge of the application contributes to effective image retrieval. Survey in CBIR can be found in (Long et al., 2003).

Actually, CBIR techniques have been intensively investigated in many applications such as image classification, fingerprint identification, biodiversity information systems, digital libraries, crime prevention, historical research and medicine for health care and computer-aided diagnosis. We can cite among others three prominent research projects on medical CBIR :

- cbPACS: the content-based Picture Archiving and Communication System (cbPACS): A Content-Based Retrieval Architecture for the PACS (picture archiving and communication system) which is an evolving health-care technology for the short and long term storage, presentation and distribution of medical images (Mortensen and Barrett,

1995).

- MedGIFT: the medical GNU Image retrieval system [1] is an adaptation of the GIFT, an open source CBIR framework developed at the Geneva University Hospitals.
- IRMA : the Image Retrieval in Medical Applications project [2] for the classification of images into anatomical areas, modalities and viewpoints (Lehmann et al., 2004).

2.4 CBIR-based Computer-Aided Diagnosis

Actually, Content-Based Medical Image Retrieval (CBMIR) is based on automatically extracted features that specify visual content such as morphology, shape, and texture. The popular approach to image-based CAD consists in providing image interpretation as a second opinion to radiologists. The CAD performance and reliability depends on a number of factors, including data preprocessing, features extraction and features classification. A review of medical image retrieval systems and future directions can be found in (Ghosh et al., 2011; Müller et al., 2004; Müller and Deserno, 2011; Kumar et al., 2013; Ridha et al., 2006). CBMIR have been applied to many diseases diagnosis such as breast cancer detection which is based on the visual analysis of mammograms (Nazari and Fatemizadeh, 2010; Quellec et al., 2011; Chen et al., 2011; Jiang et al., 2014; Kinoshita et al., 2007; Quellec et al., 2010), brain tumor detection (Huang et al., 2014; Arakeri, 2013; Huang et al., 2012; Kim et al., 2006; Zacharaki et al., 2009), Schizophrenia (Castellani et al., 2012, 2009) using MRI scans and more recently to Alzheimer's disease diagnosis (Unay, 2010; Toews et al., 2010; Agarwal and Mostafa, 2010; Akgul et al., 2009; Mizotin et al., 2012; Daliri, 2012; Rueda et al., 2012; Ridha et al., 2007; Felipe et al., 2003; Qin et al., 2013; Chen et al., 2014).

Up to now, few CBIR-based CAD systems have been integrated and evaluated in clinical practice. Nevertheless, they showed very promising results as that they can be accepted by the clinicians as a helpful tool allowing significant improvement in the diagnosis accuracy (Shyu et al., 1999; Aisen et al., 2003; Keysers et al., 2002). In terms of clinical diagnosis, MRI provides visual information regarding the brain ROI abnormalities. In that respect,

[1] http://medgift.hevs.ch/silverstripe/
[2] http://ganymed.imib.rwth-aachen.de/irma/

Content-Based Visual Information Retrieval (CBVIR) has become an attractive technique for computer-aided diagnosis (Dy et al., 2003; Balmashnova et al., 2007; Kim et al., 2006; Quellec et al., 2010; Tamaki et al., 2013; Müller et al., 2004; Toews et al., 2010). Therefore, the knowledge of the CBIR approach may be disseminated to discrimination between the normal and abnormal brain MRI based on extracted features.

2.5 Local Features-based approach for Alzheimer's disease diagnosis

Brain atrophy in the case of Alzheimer's disease is localized in some ROIs known to be affected at an early stage. Therefore, features-based approaches consider that the most reliable information in brain MRI is local and thus trend to describe image in terms of a local visual appearance.

2.5.1 Features-based methods: literature review

Several methods have been proposed to classify AD and NC subjects (Beg et al., 2013). Spherical harmonics (SPHARM) (Gutman et al., 2009; Gerardin et al., 2009) and Statistical Shape Models (SSMs) (Shen et al., 2011) are recently used to model the localized disease-related shape changes by performing the shape analysis upon the hippocampus. However, due to complex tissues present in the 3D MR brain, images classification through shape features is hard to achieve. In addition, the extracted ROI may be corrupted by occlusions or noise as a result of the image segmentation process. Recent methods show a tendency of using local features in disease discrimination, since they are able of identifying the subtle disease-specific patterns associated with the effects of the disease on human brain. In this section, we give an overview of this line of research.

Actually, CVBIR has been recently explored for research in medical diagnostics of Alzheimer's disease. In this area, the approaches used are fundamentally features-based. Here, features are the characteristic vectors computed on small areas-patches in images according to a chosen prior model. These patches can be selected around the so-called char-

acteristic points in image that exhibit signal singularities, or on the contrary, they can be chosen arbitrarily in an image space. The specific nature of MRI vs general purpose image databases requires in-depth studies of specific features which have to be designed to explain visible and invisible abnormalities in a diagnostics process. Attempts to follow the CBVIR approach with feature-based similarity were made for subject discrimination and showed performances that argue for pursuit of feature-based approaches. Table 2.1 presents a list of the major works conducted in the area of features-based methods in AD diagnosis and highlights the adopted features per work. The cited works used the structural MRI modality. However, no previous works on the DTI modality, which is a relatively new MR modality, have been reported. To the best of our knowledge, CBIR has not been yet investigated on DTI for AD diagnosis.

Works	Modalities	features
(Unay and Ekin, 2011)	sMRI	HOG
(Unay et al., 2010)	sMRI	LBP + KLT
(Li M1, 2014)	sMRI	LBP
(Toews et al., 2010)	sMRI	SIFT
(Wang et al., 2012)	sMRI	SIFT
(Agarwal and Mostafa, 2010)	sMRI	LBP+DCT
(Akgul et al., 2009)	sMRI	LBP+Intensity+Gradient
(Daliri, 2012)	sMRI	SIFT
(Rueda et al., 2012)	sMRI	SIFT
(Jiang et al., 2014)	sMRI	SIFT
(Lopes Simoes et al., 2012)	sMRI	Local texture maps
(Qin et al., 2013)	sMRI	SIFT
(Chen et al., 2014)	sMRI	SIFT

Table 2.1: Features-based CAD for Alzheimer's disease

In (Unay et al., 2010), the authors propose a ROI retrieval method for brain MRI, they use the Local Binary Pattern (LBP) and Kanade-Lucas-Tomasi (KLT) features to extract local structural information. The proposed method is invariant to intensity variations and geometric transformations. (Lopes Simoes et al., 2012) classifies between normal controls and MCI patients using local statistical texture maps (co-occurrence matrix based). In the latter, textural information is extracted from local neighborhood of each voxel. It does not take into

account the localization of the affected ROI. (Li M1, 2014; Nanni et al., 2010) differentiates AD or MCI from NC using gray-level invariant features (LBP) as well. The basic idea behind the LBP approach is to use the information about the texture from a local neighborhood. Other kind of descriptors can contain coefficients of a spectral transform of image signal, e.g. Fourier or Discrete Cosine Transform coefficients (DCT), statistics on image gradients (Rueda et al., 2012; Daliri, 2012), etc. In (Agarwal and Mostafa, 2010), the authors are focusing on integrating different types of information, including textual data, image visual features extracted from scans as well as direct user (doctor) input. Features used in (Agarwal and Mostafa, 2010) to describe brain images are LBP and DCT. (Akgul et al., 2009) uses visual image similarity to help early diagnosis of Alzheimer. (Akgul et al., 2009; Ridha et al., 2007) prove the performance of user feedback for brain image classification.

Some works on MRI classification for AD diagnosis such as (Daliri, 2012) and (Rueda et al., 2012) evaluate the suitability of the BoVW approach for automatic classification of MR images in the case of Alzheimer's disease. In (Daliri, 2012), the authors use SIFT descriptors extracted from the whole subject's brain to classify between brain with and without AD. In (Rueda et al., 2012), the authors show that the Bag Of Features (BOF) approach is able to describe the visual information for discriminating healthy brains from those suffering from the AD. However, both works do not address the MCI case which has become an important construct in the study of AD. The BoVW model represents a whole brain scan or a ROI as a histogram of occurrence of quantized visual features, which are called visual words. The latter received the name of visual signature of an image/ROI. (Unay and Ekin, 2011) presents an automated method for dementia diagnosis using search and retrieval of brain MRI with a tailored version of histogram of oriented gradients (HOGs) as features. (Qin et al., 2013) introduced the Gross feature recognition of Anatomical Images based on Atlas grid (GAIA), the proposed method describes image based on disease-related anatomical features, which should be helpful for diagnosis. (Chen et al., 2014) combined Feature Based Morphometry (FBM) and the SVM classifier, the latter used SIFT features to identify disease-related, healthy-related and noisy features then SVMs are applied to classify extracted features. An illustrating of SIFT features extraction on MRI brain is presented in Figure 2.2

In the next section, we presents the popular state-of-the-art local descriptors that have

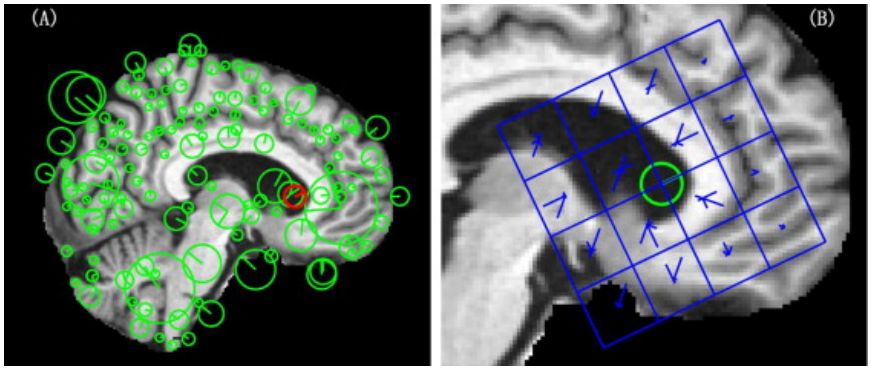

Figure 2.2: Example of a brain slice with identified SIFT features (Chen et al., 2014)

been used to extract visual information from MRI for a Alzheimer's disease diagnosis.

2.5.2 Local features

The development and analysis of low-level primitives in medical imaging have been extensively studied earlier. In the flowing we will present the state-of-the-art local descriptors: SIFT, SURF and the most successful descriptor in medical image indexing: the Local Binary Pattern (LBP). Appendix 7.1 A contains more mathematical of SIFT, SURF and LPB descriptors.

SIFT SIFT developed by (Lowe, 2004) is one of the most widely used descriptors in computer vision domain. It is stable in regard to change in rotation, scale and illumination. SIFT descriptros are well localized in both the spatial and the frequency domains, reducing the probability of disruption by occlusion, clutter, or noise.

SURF While SIFT is based on multi-scale space theory and the feature detector is based on Hessian matrix, (Bay et al., 2008) SURF (Speed Up Robust Features) descriptor is based on similar properties as SIFT. SIFT and SURF perform well in computer vision applications, and recently are investigated in medical image application (Sargent et al., 2009; Tamaki et al., 2013) such as image description (Lecron et al., 2012; Castellani et al., 2012), segmentation (Meijuan Yang and Yan, 2011), registration (Li-jia et al., 2009), and image retrieval (Lecron et al., 2012). In this thesis we will use both of those descriptors to extract

relevant information from MRI scans. Performances of those descriptors on Alzheimer's disease subject recognition will be compared to CHFs features which will be introduced and discussed in the next chapter.

LBP Texture is a commonly used feature in the analysis and interpretation of medical images. It is characterized by a set of local statistical properties of pixel intensities. Several descriptors have been used to extract texture features from MRI. Local Binary Pattern (LBP) is a computationally efficient non parametric local image texture descriptor. Indeed, the local primitives such as curved edges, points, corners, flat areas etc. can be also described using LBP. LBP operator is invariant to any monotonic lighting condition changes in gray-level, and it is very fast to calculate (Ojala et al., 2002). The idea is to analyze how similar or different are the texture in voxels neighborhoods. The application of LBP to medical images and specifically MRI images has been explored in (Nanni et al., 2010; Oliver et al., 2007; Chang et al., 2012; Unay et al., 2008; Oppedal et al., 2012). In addition to local descriptors, machines learning methods will be used to recognize diseased subject from healthy ones.

2.6 Classification-based CAD

Machine learning techniques have been widely used to support the diagnosis of neurological diseases such as AD. Classical CBIR approaches consist in comparing between sets of features or images signatures on an appropriate metric space. Hence, the response to a query are ranked according to the distance between signatures or appropriate distance function. Nevertheless, the methodological progress make the modern CBIR approach to become a classification task. Specifically in our case of CAD, we need to identify a category of query subject (AD, NC,MCI). Hence, In addition to CBIR-CAD system, Classifier-based CAD can be seen as good decision support in AD diagnosis. The estimation of the searched category can be seen as a binary classification problem between two classes. The task is to determine whether the two images are sufficiently similar for further consideration. This is treated as a two-class pattern classification problem. In this thesis, we consider the use of machine learning techniques such as Support Vector Machine (SVM) and the Bayesian classifier. In

the rest of this chapter we will review the use of SVM in AD diagnosis and we will introduce their mathematical background. In the end of section we will present the Bayesian Classifier technique.

2.6.1 SVM-based computer-aided diagnosis of the Alzheimer's disease

Pattern recognition techniques are widely used in CAD. In particular, Support Vector Machines (SVMs) classifiers have proven to be efficient to perform individual diagnosis. Here, the aim of SVM is to identify patterns that allow for the discrimination of individual subjects (for review, see (Haller et al., 2011). Thus, SVMs require a training group, i.e., well- characterized subjects (for instance healthy subjects and diseased patients), in order to categorize new subject, who belong to the so-called test group, into one of the classes the subjects of the training population belong to. It is noteworthy that SVMs analyses for individual classification are fundamentally different from the group level ROI or voxel-wise analyses presented in chapter 1. Indded, such voxel-wise analyses are univariate tests, which separately analyze each included ROI or voxel between two (or more) groups. Recently, SVMs have been used for computer-aided AD diagnosis using several MRI modalities (Bicacro et al., 2012; Ortiz et al., 2013; Fung and Stoeckel, 2007; Oppedal et al., 2012; Haller et al., 2011; Fung and Stoeckel, 2007; Montagne et al., 2013; Illán et al., 2011; Zhiqiang et al., 2004; Ramirez et al., 2013; Beg et al., 2013). SVMs have been successfully applied by several works for discriminating between AD patients, Normal control and MCI using structural MRI. Table 2.2 presents a literature review of some SVM-based methods for AD diagnosis. It is to note that most of literature works are focus in a binary classification (AD versus NC, NC versus MCI and AD versus MCI).

Work	Features	Groups comparison	Data
(Vemuri et al., 2008)	GM + WM + CSF voxels	NC vs AD	380
(Christos et al., 2008)	GM, WM and CSF volumes	MCI vs AD	30
(Fan et al., 2008)	voxels	NC vs AD NC vs MCI AD vs MCI	210
(Klöppel et al., 2008)	GM	NC vs AD	90
(Chupin et al., 2009a)	Hippocampus volumes	AD vs NC	59
(Gutman et al., 2009)	hippocampus shape	AD vs NC	112
(Gerardin et al., 2009)	hippocampal shape features (SPHARM)	NC vs AD NC vs MCI	71
(Cuingnet et al., 2011)	Various	AD vs NC, AD vs MCI	509
(Shen et al., 2012)	hippocampal shape features (Statistical shape models)	NC vs AD	237
(Magnin et al., 2009)	Histogram of voxels intensity distribution in GM, WM, and CSF regions	NC vs AD	38
(Zhang et al., 2011)	GM volume (93 ROIs)	NC vs AD	202
(Liu et al., 2009)	Neuropsychological tests,hippocampal volume, regional cortical thickness measures	NC vs AD NC vs MCI AD vs MCI	351
(Wee et al., 2013)	Correlation and ROI based morphological features	AD vs NC	598
(Yang et al., 2012)	CSF and hippocampus volume	NC vs AD NC vs MCI AD vs MCI	211
(Farhan et al., 2014)	GM, WM, CSF and hippocampus	AD vs NC	85

Table 2.2: Literature review of some SVM-based classification methods for Alzheimer's disease diagnosis with structural MRI

MCI case recognition is the most challenging task and it is actually the topic of interest in the current research related to AD diagnosis. Most of works extracted different features, including the hippocampus and the cortical thickness. The region of interest tends to be the GM, the WM, as well as the CSF. These features are the common used. Some other works use their own features (Gutman et al., 2009; Gerardin et al., 2009; Shen et al., 2012). High recognition rates are achievable (SVM) focused on brain ROI (Gerardin et al., 2009; Cuingnet et al., 2011; Gutman et al., 2009; Klöppel et al., 2008; Fan et al., 2008; Magnin et al., 2009; Zhang et al., 2011; Christos et al., 2008; Zhiqiang et al., 2004; Duchesne et al.,

2010; Vemuri et al., 2008; Liu et al., 2009; Apostolova, 2008; Chupin et al., 2009b). However, the lack of studies using multiple methods on the same data has made it difficult to directly compare the results of the different techniques. Recently (Cuingnet et al., 2011) compares ten high-dimensional classification methods applied to 509 baseline ADNI 1.5 T MR images. In the latter, two methods use only the hippocampal shape or volume, while the remainder are whole-brain approaches.

In addition, SVMs have been investigated for the DTI modality (Lee et al., 2013; Haller et al., 2010; O'Dwyer et al., 2012; Mesrob et al., 2012; Patil and Ramakrishnan, 2014). For instance, in (Haller et al., 2010), Fractional anisotropy and longitudinal, radial, and mean diffusivity were measured using Tract-Based Spatial Statistics. Statistics included group comparisons and individual classification of MCI cases using SVM.

Fundamentals

Support Vector Machine, known as SVM is a supervised learning technique developed in In 1992 by Boser, Guyon, and Vapnik (Boser et al., 1992). SVM have been successfully used in a number of image processing applications including content-based image retrieval (Tao et al., 2006) and medical imaging diagnosis (Chen et al., 2012)

Practically, SVM is committed to find the maximum margin between two classes. In author word, SVM can find the hyperplane that leaves the largest possible number of points of the same class on the same side, while maximizing the distance of either class from the hyperplane.

Given a training of instance label pairs $(x_i, y_i), i = 1, ..., l$ where $x_i \in R^n$ and $y \in \{1, -1\}$, x_i is the feature vector in n dimensions that describes the data point and y_i is the corresponding label of x_i we need to bridge a mapping between the instances and their labels. In this thesis, we only consider the binary classification. Therefore, if x_i is positive, its y_i is 1: otherwise, y_i is -1. The problem solution consists in finding a function $f(x)$, which is able to predict the y for each given x.

Linear SVM

From very beginning, the SVM was to classify two classes. In addition, it was assumed that there should be a linear function that could reach the goal.

$$w^T x + b = 0 \tag{2.1}$$

In Equation 2.1, $f(x)$ is the mapping that we have to find. The separated hyperplane can be parametrized by its normal vector w and a constant b. Two classes locate at opposite sites of the hyperplane. Therefore, we may use the hyperplane as the discriminant of the two classes. In each region, the data points which are closest to the hyperplane are called support vectors. They are considered to be the most important data from the training set, since they are the only data points used to determine the equation of the separating hyperplane.

H_+ and H_- are the hyperplanes which are parallel to the separating hyperplane and contain the support vectors. These hyperplanes are defined by:

$$\begin{aligned} H_+ &: w^T x_i + b = +1 \\ H_- &: w^T x_i + b = -1 \end{aligned} \tag{2.2}$$

Figure 2.3 illustrates the so-called decision boundary between regions classified as positive and negative of the classifier. The support vectors are presented by the circled points, the examples that are closest to the decision boundary. They determine the margin which separate the two classes. Note that any point from the training set falls between these two hyperplanes. Thus, every training data satisfy:

$$\begin{aligned} w^T x_i + b >= +1 \, then \, y_i = +1 \\ w^T x_i + b <= -1 \, then \, y_i = -1 \end{aligned} \tag{2.3}$$

These equations represent parallel bounding hyperplanes that separate data thay can compactly rewritten in the flowing way:

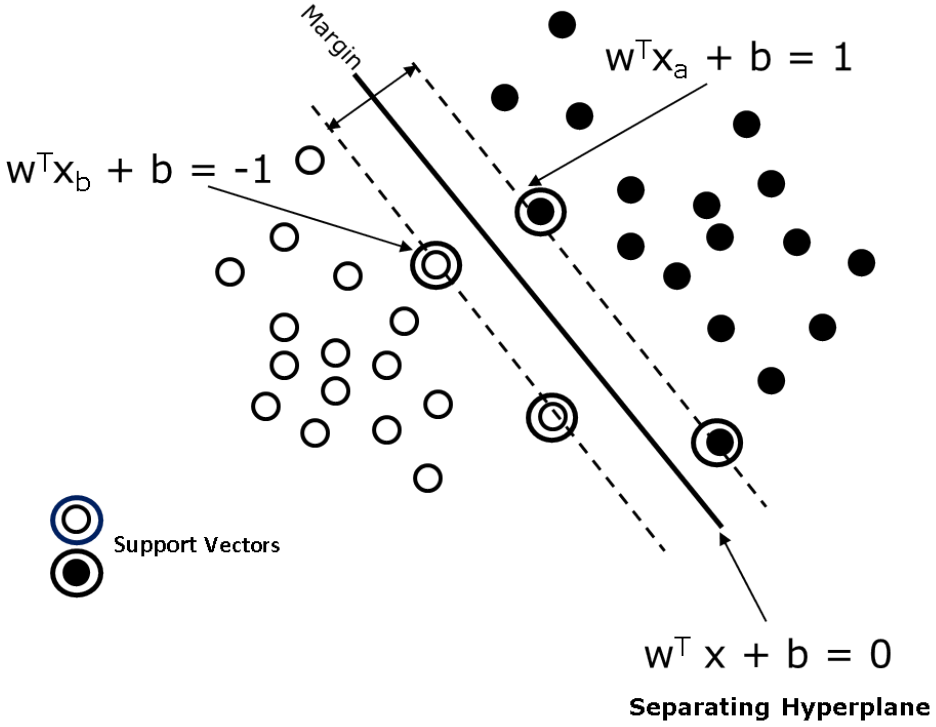

Figure 2.3: Illustrative example of a linearly separable binary example with SVM.

$$y_i(w^T x_i + b) >= 1 \forall i \tag{2.4}$$

To select the best hyperplane from this separating bounding hyperplanes, its margin should be maximized. The distance between the hyperplane and the nearest vector is given by:

The distances from H + and H - to the origin are, respectively,$\frac{b+1}{\|w\|}$ and $\frac{b-1}{\|w\|}$. The margin M is defined as the distance between H + and H- , that is:

$$M = \frac{b+1}{\|w\|} - \frac{b-1}{\|w\|} = \frac{2}{\|w\|} \tag{2.5}$$

The optimal hyperplane allows to separate data with the maximum margin possible and is determined by minimizing $\|w\|^2$, subject to constraints. This leads to a quadratic optimization problem

Therefore, to find the maximum margin is to minimize$\|w\|$. We can summarize it as a

particular in quadratic programming problem:

$$minimize_{w,b}\,\frac{1}{2}\|w\|^2 \tag{2.6}$$
$$Subject\,to\,y_i(w^T x_i + b) >= 1\,\forall i$$

The problem is a constrained optimization problem which cannot be solved directly. Lagrangian multipliers α_i (Fletcher, 1987a) is used to transform it into unconstrained form. The optimization problem is formulated as:

$$L = \frac{1}{2}\|w\|^2 - \sum_{i=1}^{N}(\alpha_i\left[y_i(w^T x_i + b) - 1\right] \tag{2.7}$$
$$subject\,to\,\alpha_i >= 0$$

L_p must be minimized with respect to w, b and maximized with respect to α_i . The solution is given by the saddle point [10]. This is a convex quadratic optimization problem, since the objective function is itself convex and the points satisfying the constraints also form a convex set. For this reason, it is possible to make use of the Karush-Kuhn- Tucker (KKT) conditions to solve the problem [ref] and, therefore, the gradient of L should vanish:

$$\frac{\partial L}{\partial w} = 0 \Rightarrow w = \sum_{i=1}^{N}\alpha_i y_i x_i \tag{2.8}$$
$$\frac{\partial L}{\partial b} = 0 \Rightarrow \sum_{i=1}^{N}\alpha_i y_i = 0 \tag{2.9}$$

The primal form of the Lagrangian L 2.8 may be equivalently written in dual form by substituting the above expression for w. The dual form expresses the optimization criterion in terms of inner products of the feature vectors:

$$max_\alpha L\ (\alpha) = max_\alpha \left\{ \sum_{i=1}^{N} \alpha_i - \frac{1}{2} \sum_{i,j} \alpha_i \alpha_j y_i y_j x_i x_j \right\} \tag{2.10}$$
$$subject\, to\, \alpha_i >= 0\, and \sum_{i=1}^{N} \alpha_i y_i = 0$$

The decision surface is thus expressed in terms of the support vectors, since only their corresponding α_i are non-zero (According to the quadratic programming theory). b is found by the average of a N_{sv} support vectors:

$$b = \frac{1}{N_{sv}} \sum_{i=1}^{N_{sv}} (w^T x_i - y_i) \tag{2.11}$$

This is an important property for the creation of nonlinear SVM classifiers.

Soft-margin SVM

In the case of noisy data where no linear hyperplane can separate the data, the soft-margin SVM formulation is applied and slack variables ϵ_i are introduced. Those variables measure the degree of misclassifcation of the feature vectors. The optimization becomes trade-off between maximizing the margin and minimizing the degree of misclassifcation. This trade-off is controlled by the penalty parameter C, such that the constrained optimization may be expressed as:

$$min_{w,\epsilon,b} \left\{ \frac{1}{2} \|w\|^2 + C \sum_{i=1}^{N} \epsilon_i \right\} \tag{2.12}$$
$$subject\, to\, y_i(w^T x_i + b) >= 1 - \epsilon_i\, and \epsilon_i >= 0 \forall i$$

By using Lagrange multipliers, the problem may be re-expressed as the unconstrained optimization

$$L = \frac{1}{2}\|w\|^2 + C\sum_i \epsilon_i - \sum_{i=1}^{N}(\alpha_i\left[y_i(w^T x_i + b) - 1 + \epsilon_i\right] - \sum_i \mu_i\epsilon_i \tag{2.13}$$

$$subject\,to\,\alpha_i >= 0$$

Again, according to the KKT conditions (Karush- Kuhn-Tucker) (Fletcher, 1987b) , the derivatives of L are set to zero:

$$\frac{\partial L}{\partial w} = 0 \Rightarrow w = \sum_{i=1}^{N}\alpha_i y_i x_i \tag{2.14}$$

$$\frac{\partial L}{\partial b} = 0 \Rightarrow \sum_{i=1}^{N}\alpha_i y_i = 0 \tag{2.15}$$

$$\frac{\partial L}{\partial \epsilon_i} = 0 \Rightarrow C - \alpha_i - \mu_i = 0 \tag{2.16}$$

The dual for of Equation 2.14 is written as:

$$max_\alpha\, L\ (\alpha) = max_\alpha \left\{\sum_{i=1}^{N}\alpha_i - \frac{1}{2}\sum_{i,j}\alpha_i\alpha_j y_i y_j x_i x_i\right\} \tag{2.17}$$

$$subject\,to\, 0 =< \alpha_i <= C\, and \sum_{i=1}^{N}\alpha_i y_i = 0$$

Kernel SVM

The main idea of Non-Linear SVM is to apply a suitable non-linear transformation to map the problem to a new space, called the feature space, where a linear model can be used. The linear model in the feature space corresponds to a non-linear model in the input space (I). This is known as the "Kernel Trick". In cases where the data are not linearly separable in the input feature space, a nonlinear function $\phi(x)$ maps data points into higher-dimensional (H). The d Kernel trick consists in replacing the inner product of the original points with the inner product of point with kernels and then the non-linear problem is transformed inti

linear classification problem, which could be solved by SVM. AS it is Illustrated in Figure 2.4, the original data is non-linearly separable. After the mapping of a trick function ϕ, they can be linearly separate.

$$\phi : I \rightarrow H \tag{2.18}$$

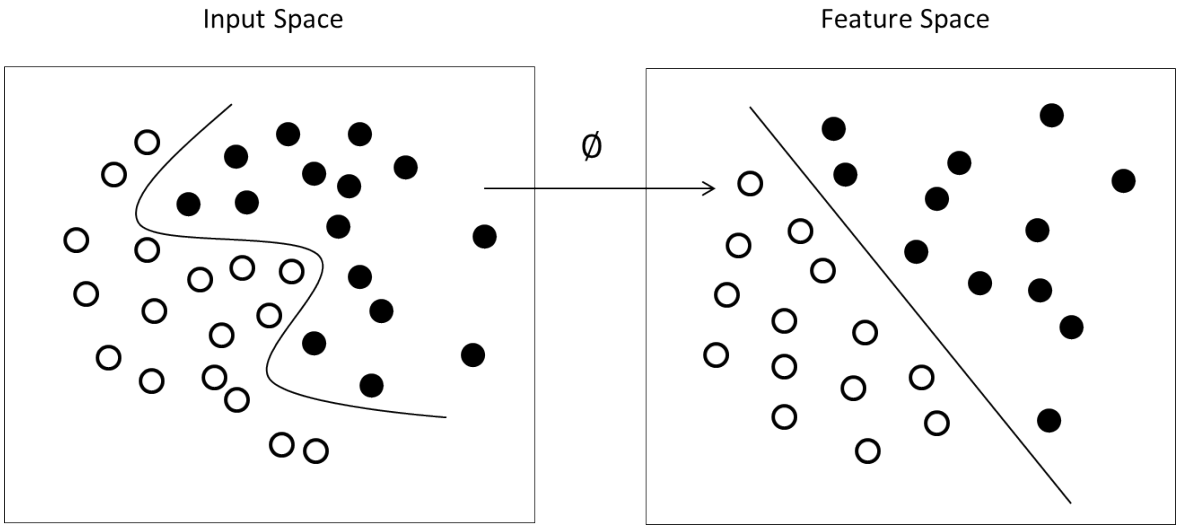

Figure 2.4: Illustrative example of a non linearly separable data.

This function use a kernel K witch take data points from the input space I and return their inner product in the feature space

The function $K(x_i, x_j) = \phi(x_i)\phi(x_j)$ is known as the kernel function.

The two parameters w and b of the hyperplane are determined by solving a constrained minimization problem using Lagrange multipliers α_i. The final decision function is as the flowing:

$$f(x) = sgn(\sum_{i=1}^{N} y_i \alpha_i K(x_i, x_j) + b \tag{2.19}$$

Several kernel may be used to map data, for instance:

- Radial Basis Function: $K(x_i, x_j) = exp(-\gamma * |x_i - x_j|^2)$
- Sigmoid: $K(x_i, x_j) = tanh(\gamma * x_i^T * x_j + r)$

2.6.2 Bayesian Classifier

Bayesian methods are being used increasingly in clinical research (Berry, 2004). A naive Bayes is a probabilistic classifier based on the application of Bayes theorem.

Given a set of feature vectors, $x_1, x_2, ...x_n$, the objective is to construct the posterior probability for the class C_j among a set of possible outcomes set of classes $C_1, C_2, ..., C_m$.

Using the Bayes theorem, the posterior probability of class C_j being X can be written as follows:

$$p(C_j|X_1, ..., X_n) = \frac{p(C_j)p(X_1, ..., X_n|C_j)}{p(X_1, ..., X_n)} \tag{2.20}$$

where $p(C_j)$ is the prior probability of class C_j, $p(X_1, ..., X_n|C_j)$ is the likelihood of X given C_j and $p(X_1, ..., X_n)$ is the evidence.

In fact, only in the numerator of that fraction is of interest, since the denominator does not depend on C and the values of the features X are known, so that the denominator is constant. The numerator is equivalent to the flowing probability model:

$$\begin{aligned} p(C_j, X_1, \ldots, X_n) &= p(C_j)P(X_1, \ldots, X_n|C_j) \\ &= p(C_j)p(X_1|C_j)p(X_2, \ldots, X_n|C_j, X_1) \\ &= \cdots = p(C_j)p(X_1|C_j)p(X_2|C_j, X_1)\ldots p(X_n|C_j, X_1, X_2, \ldots, X_{n-1}) \end{aligned} \tag{2.21}$$

The nave conditional independence assumptions guarantees that each feature vector X_i is conditionally independent of every other feature vector X_k for $\neq i$. This means that:

$$p(X_i|C_j, X_k) = p(X_i|C) \tag{2.22}$$

and thus the joint model can be expressed as:

$$p(C_j, X_1, \ldots, X_n) = p(C_j)p(X_1|C_j)p(X_2|C_j)\ldots p(X_n|C_j) \tag{2.23}$$
$$p(C_j) = \prod_{i=1}^{n} p(X_i|C_j)$$

The naive Bayes classifier combines the model above with a decision rule. One common rule is to choose the hypothesis that is most probable. This is known as the maximum a posterior (MAP) decision rule. The corresponding classifier is the equation defined as follows.

$$\widehat{C}(X_1, \ldots, X_n) = max_c p(C_j) \prod_{i=1}^{n} p(X_i|C_j) \tag{2.24}$$

The use of this independence assumption is at the basis of the naive Bayesian classifier.

Tow major advantages of the use of Bayes classifier. First, it is robust to missing values because these values are simply ignored in computing probabilities and thus have no impact on the final decision. Second, it is with reduced computational time for training because it requires relatively small set of training data to estimate classification's parameters. Naive Bayesian classifiers have proven to be powerful probabilistic models for solving classification problems in a variety of domains. Most notably in computer aided diagnosis domain (Nissan et al., 2010; Hani et al., 2010)

2.7 Conclusion

In this chapter, we firstly gave a brief introduction to both concepts of CBIR and Computer-Aided Diagnosis system. Then, we presented an overview of recent researches related to the local features-based methods for Alzheimer's disease diagnosis. Finally, we introduced some mathematical backgrounds of descriptors and classifiers used in this thesis. In addition, an overview of recent researches related to the image-based classification of AD subjects has been presented. The later chapters incorporate more focused and detailed review of the most recent related research in both medical and image processing fields. The following

four chapters will give the main contributions of this thesis. Next chapter will present the preprocessing and the features extraction methods used to build a signature-related atrophy.

Chapter 3

Visual disease-related signature generation: methods and materials

Contents

3.1 Introduction

As we showed in Chapter 1, ROIs-based methods which are focus on extracting features from specific regions of the brain are of growing interest. Indeed, ROI's segmentations performed by an expert or by a specific software are challenging. In fact, they are time-consuming and can present poor results in a boundary detection of brain regions. On the other hand, atlas-based parcellation can be used as a standard and automated method for automatically labeling ROIs on MR brain images. However, the latter reveals less inter-subject variability and then is not able to represent atrophy information. Hence, in this chapter, we will present and explain our methodology in generating Alzheimer's disease-related signature using an atlas ROI extraction method. The intuition is that the variations in the brain/ROI anatomy can be represented as a set of local features illustrating the presence or absence of atrophy in the specific tissue overlapping with atlas parcels. In this chapter, we will start by explaining the adopted MRI preprocessing pipeline. Then, we will present the visual disease-related signature generation method. Next, we will introduce the CHFs descriptors and present their interest in extracting MRI local information. Finally, we will introduce the data used to test our methods.

3.2 Spatial normalization of MRI data

Brain scans alignment is mandatory for ROIs extraction. Two types of alignment: linear or non-linear can be applied accordingly to the common practices (Salmond et al., 2002). The linear transform, either "rigid body" or affine, allows only a coarse registration of global geometrical differences, e.g. rotation and magnification. Fine anatomical structures will not be aligned precisely by the linear transform because of natural inter-subject anatomical variance. Non linear deformable registration allows a more precise alignment of fine brain structures. However, it is difficult to guarantee that images are not "over-aligned", which would mean the loss of the individual patterns in brain structures. A more detailed analysis of this problem is presented in (Ridha et al., 2007). The authors note several shortcomings of the Voxel-Based Mophometry (VBM) approach, which is based on nonlinear registration. First, the deformable registration is not desirable for feature-based approaches, as it deforms

the features itself, while we want to preserve specific local patterns. Second, our approach analyzes the brain ROIs slice-by-slice (Chapter 5 and Chapter 6). Linear registration gives us roughly corresponding slices for the selection of ROIs. The similar slice-based technique was used in (Akgul et al., 2009). In addition, affine registration preserves specific local patterns. Thus, in our work we adopt to an affine registration of all scans to the MNI 152 brain template (Frisoni et al., 2005) through using the freely available VBM8 toolbox [1] using the Statistical Parametric Mapping (SPM)[2] software as illustrated in Figure 3.1.

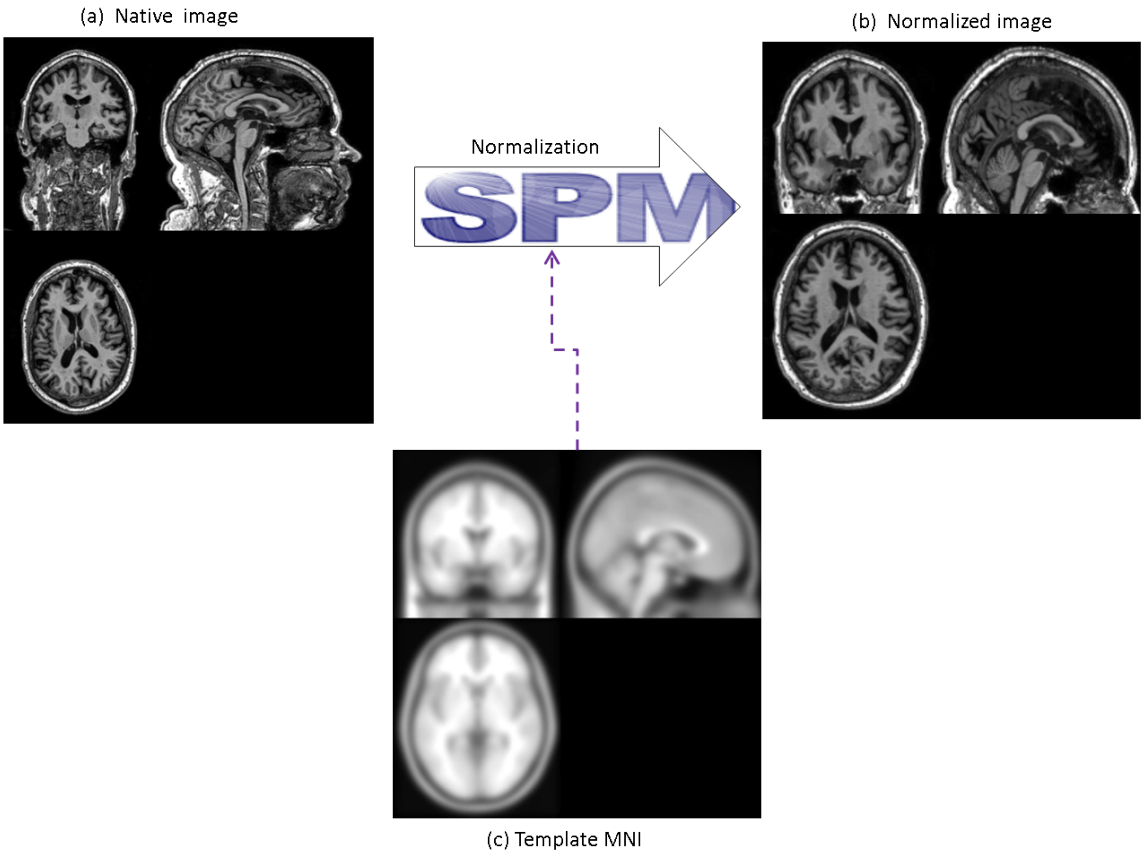

Figure 3.1: MRI spatial normalization to the MNI space using the SPM software (Image are structural MRI of an AD patient from the ADNI dataset)

[1] http://dbm.neuro.uni-jena.de/vbm/
[2] http://www.fil.ion.ucl.ac.uk/spm/software/

3.2.1 The Montreal Neurological Institute (MNI) template

This is the most common template used for spatial normalization. It is developed by the Montreal Neurological Institute (ICBM, NIH) [3]. The MNI is designed to define a brain that is more representative of the population. Indeed, it is average of large numbers of T1-weighted images of 152 healthy individuals who have been registered into a common space.

In SPM, the standard space is defined by the template image "T1.nii" supplied with the SPM toolbox. The default configurations include source image smoothing with 8 mm, affine regularization with ICBM space template, a nonlinear frequency cutoff of 25, 16 nonlinear iterations. Figure 3.2 shows a screen shot of the spatial normalization results done by the SPM software. We normalized here an NC subject from the ADNI dataset to the MNI template (left), the spatially normalized image is on the right.

3.2.2 Affine normalization

Generally, the affine transformation includes translation, rotation, scaling and shearing and it preserves collinearity and proportions on lines (Ashburner et al., 1997). SPM uses a 12-parameter affine transform to fit the source image f to a template image g.

For each point $\mathbf{x}= (x_1, x_2, x_3)^T$ from f, the transformation to point $\mathbf{y}=(y_1, y_2, y_3)^T$ in g is defined as follows:

$$\begin{pmatrix} y_1 \\ y_2 \\ y_3 \\ 1 \end{pmatrix} = \begin{pmatrix} m_1 & m_4 & m_7 & m_{10} \\ m_2 & m_5 & m_8 & m_{11} \\ m_3 & m_6 & m_9 & m_{12} \\ 0 & 0 & 0 & 1 \end{pmatrix} \begin{pmatrix} x_1 \\ x_2 \\ x_3 \\ 1 \end{pmatrix} \tag{3.1}$$

This transformation can be broken down into a product of translation, rotation, scale and shear in x-, y- and z-axis:

[3] http://www.mni.mcgill.ca

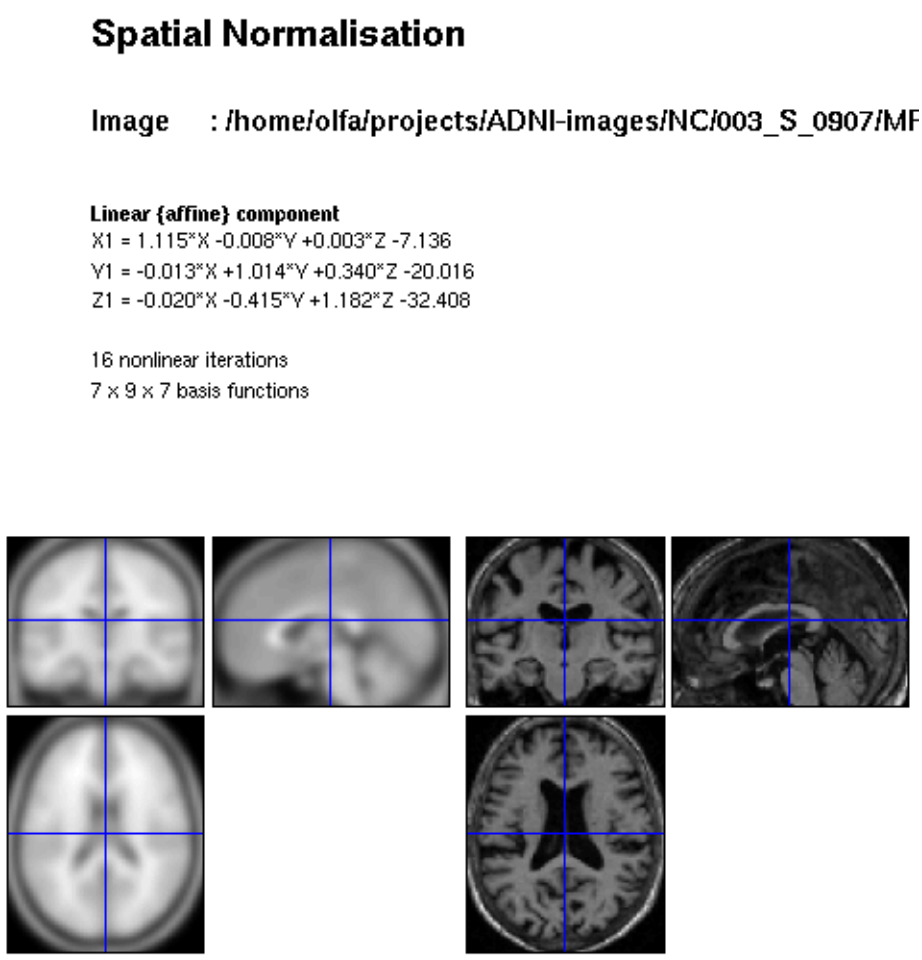

Figure 3.2: SPM8 screenshot after spatial normalization of NC subject from the ADNI dataset. The MNI template is in the left, the spatially normalized image is on the right.

$$M = M_{Translation} * M_{Rotation} * M_{Zoom} * M_{Share} \tag{3.2}$$

The parameters q_1,q_2, q_3 correspond to 3 translation parameters, q_4, q_5 and q_6 correspond to 3 rotations parameters. q_7, q_8 and q_9 to 3 zooms and finally q_{10}, q_{11} and q_{12} are the 3 shares corresponding parameters.

where,

$$M_{Transtation} = \begin{pmatrix} 1 & 0 & 0 & q_1 \\ 0 & 1 & 0 & q_2 \\ 0 & 0 & 1 & q_3 \\ 0 & 0 & 0 & 1 \end{pmatrix}$$

$$M_{Rotation} = \begin{pmatrix} 1 & 0 & 0 & 0 \\ 0 & \cos(q_4) & \sin(q_4) & 0 \\ 0 & -\sin(q_4) & \cos(q_4) & 0 \\ 0 & 0 & 0 & 1 \end{pmatrix} * \begin{pmatrix} \cos(q_5) & 0 & \sin(q_5) & 0 \\ 0 & 1 & 0 & 0 \\ -\sin(q_5) & 0 & \cos(q_5) & 0 \\ 0 & 0 & 0 & 1 \end{pmatrix} * \begin{pmatrix} \cos(q_6) & \sin(q_6) & 0 & 0 \\ -\sin(q_6) & \cos(q_6) & 0 & 0 \\ 0 & 0 & 1 & 0 \\ 0 & 0 & 0 & 1 \end{pmatrix}$$

$$M_{Zoom} = \begin{pmatrix} q_7 & 0 & 0 & 0 \\ 0 & q_8 & 0 & 0 \\ 0 & 0 & g_9 & 0 \\ 0 & 0 & 0 & 1 \end{pmatrix}$$

$$M_{Share} = \begin{pmatrix} 1 & q_{10} & q_{11} & 0 \\ 0 & 0 & q_{12} & 0 \\ 0 & 0 & 1 & 0 \\ 0 & 0 & 0 & 1 \end{pmatrix}$$

The normalization function done with 12 degrees of freedom, minimizing the sum of squares of intensity differences (SSD) (Equation 3.3) between each subject image and the brain template (Ashburner and Friston, 1999).

$$SSD(f,g) = \frac{1}{N} \sum_{(x,y) \in N} (f(x,y) - g(x,y))^2 \tag{3.3}$$

Thus, normalization can also be used within modalities exclusively. If we want to normalize an individual T1-weighted anatomical scan, we have to fit it onto a T1 template.

3.3 Disease-related signature generation

Alignment of individual brain scan to a common template deforms the individual morphology. Hence, in our approach we do not segment the aligned scan. We propose to generate a visual signature of ROI using a statistical description, which is supposed to be robust to such deformation. Hence, we need only roughly localize ROI in the scans. Therefore, we resort to an Atlas-based method for ROI selection.

Broadly speaking, MRI signal varies across tissue characteristics and/or types. Quantification of the amount of brain cell loss in terms of signal variation across individual brains may provide information about the disease. In this section, we present the process of visual signature or the so-called "disease-related signature" generation. A signature per subject is generated to reflect brain atrophy at the individual level. We will not use a segmentation step to extract region of interest to be described, we propose an atlas-based features generation approach. We use the atlas parcels to characterize brain abnormalities in terms of intra-ROI local pattern. The pattern overlapping with the extracted ROI mask shows different signals presented inside the ROI itself, those signals present the ROI atrophy and then this signal variations inside the ROI anatomy will be represented as a set of local features. Extracted features are leveraged to distinguish normal from abnormal ROI area. It should be noted that we are working in the 2D plane and image processing is done slice by slice.

Using global descriptors, local details of an image are hard to be reflected. Hence, in the current work, we investigate the local features, which will be discussed further below. We use local descriptors because they are able to offer robustness against translation and rotation and in localized points of the image. Also ensure that the extracted features is well related to the AD, we have to extract feature from ROIs known to be involved in the AD. This is our interest in the next sections.

3.3.1 ROI extraction using AAL

Since each brain image is affinely mapped with a normalized atlas in 3D space and resliced in the same way as the atlas, we are able to identify a region of interest (ROI) by mapping the image with the atlas slice by slice. The regions investigated in this work are suggested

by our medical partners. These are regions known could have potential relevance to disease classification of individual MR scans. To select the ROIs, we used a brain atlas called Automated Anatomical Labeling (AAL) (Tzourio-Mazoyer et al., 2002). The AAL atlas is a single-subject atlas based on the MNI Colin27 T1 atlas. Figure 3.3 shows the standard AAL template (different projections) which comprises 116 brain anatomical regions. The selection process consists in superimposing geometrically aligned individual brain volume and the AAL.

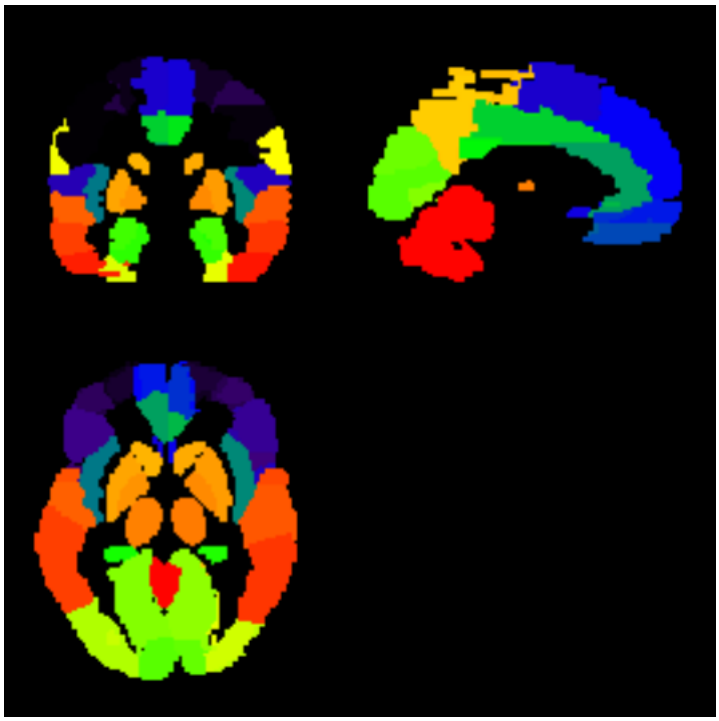

Figure 3.3: The Automated Anatomical Labeling (AAL) (axial, coronal and sagittal projections)

3.3.2 Features extraction and signatures generation

After brain alignment and ROIs selection, we compute image features. As it was already noted, we need to extract only those features that contain visual information related to the presence or absence of the Alzheimer's disease. Hence, in the current research SIFT and SURF descriptors are used to extract local information from brain tissues. In addition, we use the Circular Harmonic Functions (CHFs). An important issue here lies in the representation

of extracted features for comparison purpose. One of the most popular models in CBVIR is the Bag-of-Visual-Words. It is an adaptation of the bag-of-words scheme proposed in the text retrieval problem area and it was further adapted for image analysis (Csurka et al., 2004; Sivic and Zisserman, 2009). This model represents a whole image or a ROI as a histogram of occurrence of quantized visual features, which are called "visual words". The histogram received the name of "visual signature" of an image/ROI. Some works in MRI classification for diagnostics of AD evaluate the suitability of the BoVW approach. In (Daliri, 2012), the authors use SIFT features extracted from the whole subject's brain to classify brains with and without AD. Successful results with BoVW approach are also reported in (Rueda et al., 2012). The two last mentioned works used an SVM to classify signatures obtained by BoVW representation on the open-access dataset OASIS [4]. However, (Daliri, 2012), (Rueda et al., 2012) and (Toews et al., 2010) have not addressed the MCI case which is considered in our work.

The good tissue contrast of T1-weighted MRI enables to obtain accurate structural MRI analysis, which may be used as a biomarker for diagnosing AD. In the current work, additionally to conventional SIFT and SURF descriptors we propose the use of Circular Harmonic Functions (CHFs) descriptors. CHFs are used for selection of contrasted patterns in brains, and their coefficients form the descriptors of these patterns. In the flowing section, we will introduce the CHFs descriptors.

Circular Harmonic Functions keypoints detector and descriptors

The choice of the initial description space (features) is of a primary importance as it has to be adapted to the nature of the images. Indeed, despite the good performances of SIFT features reported in (Rueda et al., 2012), there is still place for an intensive investigation of the descriptors choice. SIFT or their approximated version SURF (More computational details are given in Appendix 7.1), widely used in classification of general purpose image data sets, are not optimal for MRI with the lack of pronounced high frequency texture and clear structural models.

Circular Harmonic Functions (CHFs) give interesting approximations of blurred and noisy

[4] http://www.oasis-brains.org/

signal as we have it in MRI. CHFs were first introduced in the pattern recognition domain (Sorokin et al., 2011). They have several advantages over other descriptors particularly for MRI. CHFs present a decomposition of image signal on the orthonormal functional brains. They allow for capturing local direction of image signal as this is the case in SIFT and SURF. But what is even more important, they allows for capturing intermediate frequencies in the signal similarly to Fourier decomposition. This is not the case of SIFT and SURF. We hypothesize that this propriety is more convenient for MR images with smooth contrasts.

According to (Sorokin et al., 2011; Sorgi et al., 2006), these descriptors in some cases are superior to SIFT which is a current benchmark. Furthermore, computing the CHFs descriptors on densely sampled patches in brain brings the statistical variety necessary for overcoming the problem of inter-subject instability of signal singularities. Furthermore, these features as computed on patches inside the ROI or selected on the whole brain, convey local structural information of image signal. Figure 3.5 presents an example of (SIFT and CHFs) keypoints placement in selected MRI slices.

CHFs, these are complex, polar separable filters, characterized by harmonic angular shape allowing the descriptors to be rotationally invariant. CHFs were yet proposed for rotation invariant pattern recognition in (Arsenault and Sheng, 1986). They possess the interesting characteristic of being efficacious to extract visual relevant features and rich frequency extraction .

LG-CHF is complete orthogonal set of functions on the real plane. Thus, the image $I(x, y)$ can be expanded in the analysis point x_0 , y_0 for fixed scale σ in Cartesian system. The coefficients of the partial expansion of local neighborhood can be used as a feature descriptor. The advantages of these features are such that they capture both the direction and smooth variations of image signal. Their drawback is in a rather slow convergence, hence a sufficient number of coefficients has to be retained for image description. The number of coefficients retained define the dimensionality of the descriptor. The reasonable dimensionality of 150 coefficients (Mizotin et al., 2012) was used in the present work. Hence, the dimension of the descriptor is comparable with that one of conventional SIFT.

Keypoint detection

Let us consider a family of complex orthonormal and polar separable functions:

$$\Psi(r,\theta;\sigma) = \Psi_n^{|\alpha|}(\frac{r^2}{\sigma})e^{i\alpha\theta} \tag{3.4}$$

$$\Psi_n^{|\alpha|}(x) = \frac{1}{\sqrt{n!\Gamma(n+\alpha+1)}}x^{\frac{\alpha}{2}}e^{\frac{-x}{2}}L_n^{\alpha}(x) \tag{3.5}$$

where $n = 0, 1, ...; \alpha \pm 1, \pm 2...$ and $L_n^{\alpha}(x)$ are Laguerre polynomials. r, θ are polar coordinates, σ is a scale parameter and Γ is a gamma function.

$$L_n^{\alpha}(x) = (-1)^n x^{-\alpha}e^x\frac{d}{dx^n}(x^{n+\alpha}e^{-x}) \tag{3.6}$$

The Laguerre functions $\Psi_n^{\alpha}(x)$ can be calculated using the following recurrence relations:

$$\Psi_{n+1}^{\alpha}(x) = \frac{(x-\alpha-2n-1)}{\sqrt{(n+1)(n+\alpha+1)}}\Psi_n^{\alpha}(x) - \sqrt{\frac{n(n+\alpha)}{(n+1)(n+\alpha+1)}}\Psi_{n-1}^{\alpha}(x), \tag{3.7}$$

$$n = 0, 1..., \Psi_0^{\alpha}(x) = \frac{1}{\sqrt{\Gamma(\alpha+1)}}x^{\alpha/2}e^{-x/2}, \Psi_{-1}^{\alpha}(x) \equiv 0$$

These functions Ψ_n^{α}, called Laguerre-Gauss Circular Harmonic (GL CH) functions, are referenced by integers n (referred by "radial order") and α (referred by "angular order") (Figure 3.4).

The LG-CH functions are self-steerable, i.e. they can be rotated by the angle θ using multiplication by the factor $e^{i\alpha\theta}$. They also keep their shape invariant under Fourier transformation and they are suitable for multi-scale and multicomponent image analysis.

For a brain scan slice $S(x, y)$ defined on the real plane from one projection plane R^2, due to the orthogonality of the Ψ_n^{α} family, the slice $S(x, y)$ can be expanded in the analysis points $(x_0\ ,\ y_0)$ for fixed σ in Cartesian system as follows:

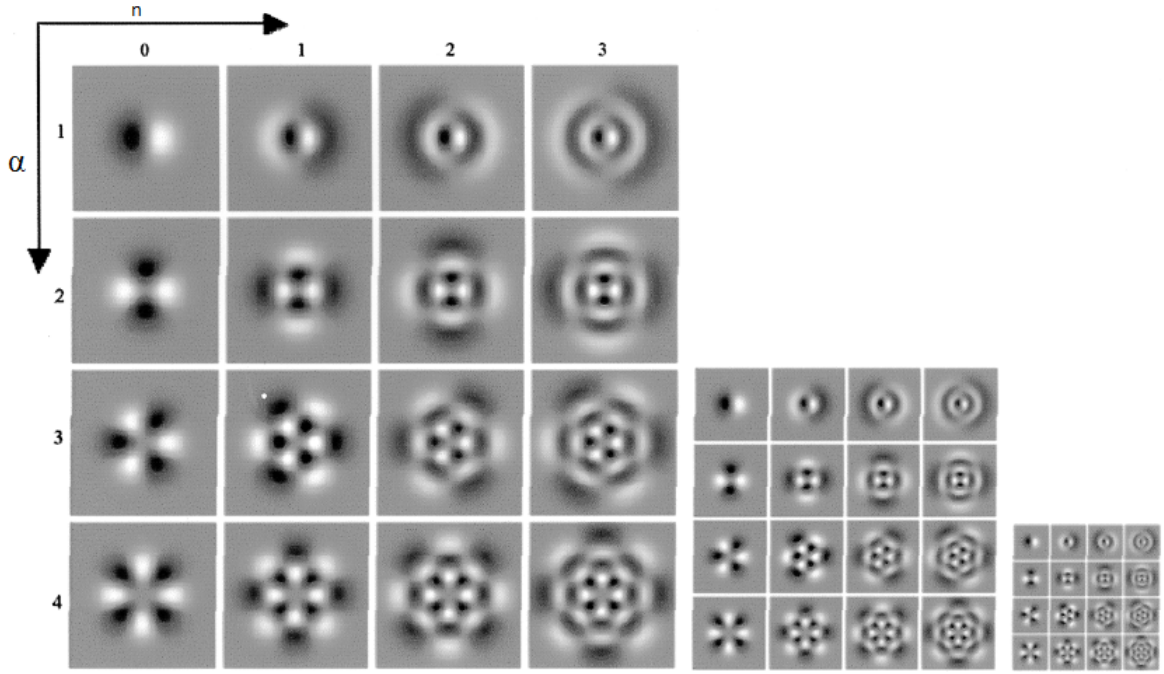

Figure 3.4: Illustrating of Laguerre Gauss Pyramid at different scales

$$S(x_0, y_0) = \sum_{\alpha=-\infty}^{\infty} \sum_{n=0}^{\infty} g_{\alpha,n}(x_0, y_0; \sigma) \Psi_n^{\alpha}(r, \theta, \sigma), \tag{3.8}$$

where

$$g_{\alpha,n}(x_0, y_0; \sigma) = \int_{-\infty}^{\infty} \int_{-\infty}^{\infty} S(x_0, y_0) \overline{\Psi_n^{\alpha}(r, \theta, \sigma)} dx dy,$$

And

$$r = \sqrt{(x - x_0)^2 + (y - y_0)^2},$$

$$\theta = arctg(\frac{y - y_0}{x - x_0})$$

For more details on the use of these functions in image analysis we refer the reader to (Sorokin et al., 2011).

Gauss-Laguerre Keypoint descriptors

For the keypoint description, which are in our case the centers of a regular grid of patches, each point $\overline{K} = (\overline{x}, \overline{y}, \overline{\sigma})$ is associated to a local descriptor $\overline{\chi} = \{\overline{\chi}(n, \alpha, j)\}$. This is a complex valued vector consisting of local image projection to a set of LG-CH functions Ψ_n^α at $2j_{max}$ scales neighbor to the keypoint $\overline{K}$ reference scale $\overline{\sigma}$. The $\overline{\chi}$ elements are defined as:

$$\begin{aligned} &\overline{\chi}(n, \alpha, j) = A_{norm}.g_{\alpha,n}(x, y; \sigma_j)e^{-i\alpha\phi_j}, \\ &n = 0, ..., n_{max}, \alpha = 1, ..., \alpha_{max}, \\ &j = -j_{max}, ..., j_{max}. \end{aligned} \tag{3.9}$$

Where σ_j is the j^{th} scale following $\overline{\sigma}$ if $j > 0$, or preceding the $\overline{\sigma}$ if $j < 0$ in discretized scale space. A_{norm} is the normalization coefficient that makes descriptor invariant to illumination changes. The phase shift $e^{-i\alpha\phi_j}$ is used to make descriptors invariant to the keypoint pattern orientation, where $\phi_j = arg(g_{1,0}(\overline{x}, \overline{y}; \sigma_j))$.

Construction of the Bag-of-Visual-Words signature

Recently BoVW has been successfully applied in various tasks of medical image classification and retrieval and specially for computer aided diagnosis. This method represents an image as a distribution of local salient (or dense) patches. Usually, there is two ways to localize relevant features would be extracted. The Keypoint-based analysis and dense-sampling. In this thesis, we used a dense sampling scheme with a regular-grid-based extraction. This is done by partitioning images using a regular grid, and taking each grid item as a patch of fixed size. Such sampling scheme may provide a rough model of clinician vision and results in a good coverage of the entire scan and a constant amount of features per image area. Regions with less contrast contribute equally to the overall image representation. As illustrated in Figure 3.6 , the visual words construction process can be decomposed into three main steps :

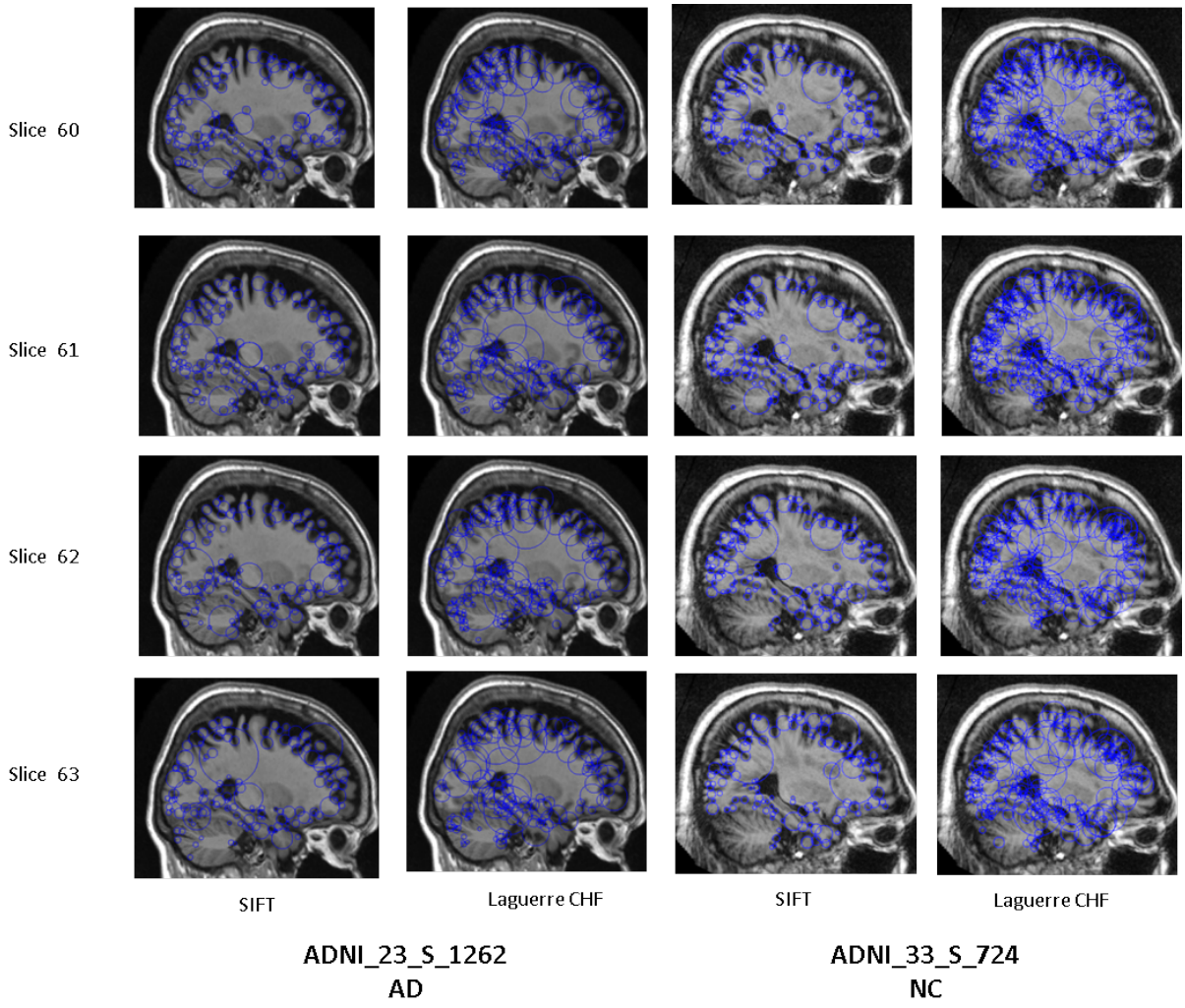

Figure 3.5: Example of features placement in MRI slices (from slice number 60 to slice number 63), extracted features here are SIFT and CHFs

First stage: Visual words detection

The first stage through the Bag-of-Visual-Word approach consists in extracting small patches from the images. To extract visual features from the images, several descriptors are used such as SIFT, SURF and CHFs.

Second stage: Learning the visual vocabulary

Derived from local image descriptors, the visual vocabulary is computed through clustering of all descriptors calculated from the training images. This is done using the k-means clustering

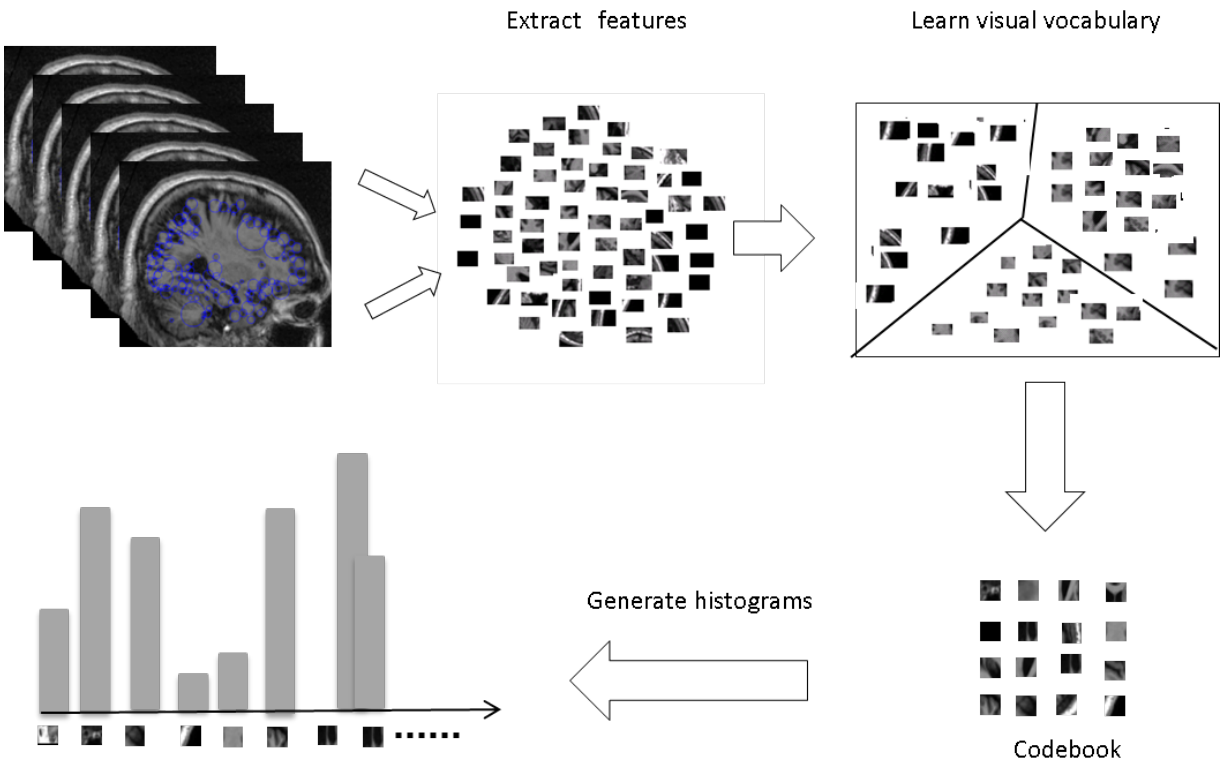

Figure 3.6: Process of the BoVW representation illustrating the three steps 1) Local features extraction, 2) Visual vocabulary construction 3) Histogram generation

method (Jain et al., 1999) which is one of the simplest but well known clustering algorithms. It simply aims to cluster n vectors or features into k clusters and return the k cluster centers (Algorithm 1).

Algorithm 1 Features clustering: K-means

Input: The number of clusters k and the set of n features $F := f_1, f_2, ..., f_n$

Output: A set of k clusters C_j.

Step 1: Choose $a_1, a_2.., a_k$ centroids randomly as the initial centers of the clusters

Step 2: Repeat

2.1: Assign each feature to their closest cluster center using Euclidean distance.

For every i, $c_i := argmin_j \|f_i - a_j\|^2$

2.2: Compute new cluster center: For every j, $a_i = \frac{\sum_{i=1}^{n} 1\{c_i=j\} f_i}{\sum_{i=1}^{n} 1\{c_i=j\}}$

Until

No change in cluster center or No feature changes its clusters.

Third stage: Visual words quantization to construct the histogram

Finally, once the cluster centers are identified, each feature vector in an image is assigned to the closest cluster centroid using the Euclidean metric. Each image is then represented by a k-bin histogram of these cluster centers by simply counting the occurrence of the words appear in an image. The obtained histogram is called image signature.

3.4 MRI Alzheimer's disease Data

Data used in the experiments of the current research come from two sources. First, we used subsets of the Alzheimer's Disease Neuroimaging Initiative (ADNI) dataset. Second, we used a real cohort of a large French study. Those two data are explained in detail in the next section. It is to note otherwise that only baseline images have been used in the current work. Also, only one scan per subject has been used.

3.4.1 ADNI data

Data used in the preparation of this work were obtained from the ADNI database [5]. The goal of the ADNI is to determine and validate MRI, PET images, and cerebrospinal fluid (CSF) as predictors and outcomes for use in clinical trials of AD treatments (Weiner et al., 2010). *"The ADNI was launched in 2003 by the National Institute on Aging (NIA), the National Institute of Biomedical Imaging and Bioengineering (NIBIB), the Food and Drug Administration (FDA), private pharmaceutical companies and non-profit organizations, as a 60 million, 5-year public-private partnership. The primary goal of ADNI has been to test whether serial magnetic resonance imaging (MRI), positron emission tomography (PET), other biological markers, and clinical and neuropsychological assessment can be combined to measure the progression of mild cognitive impairment (MCI) and early Alzheimer's disease (AD). Determination of sensitive and specific markers of very early AD progression is intended to aid researchers and clinicians to develop new treatments and monitor their effectiveness, as well as lessen the time and cost of clinical trials. The Principal Investigator of this initiative is*

[5] adni.loni.usc.edu

Michael W. Weiner, MD, VA Medical Center and University of California San Francisco. ADNI is the result of efforts of many co-investigators from a broad range of academic institutions and private corporations, and subjects have been recruited from over 50 sites across the U.S. and Canada. The initial goal of ADNI was to recruit 800 subjects but ADNI has been followed by ADNI-GO and ADNI-2. To date these three protocols have recruited over 1500 adults, ages 55 to 90, to participate in the research, consisting of cognitively normal older individuals, people with early or late MCI, and people with early AD. The follow up duration of each group is specified in the protocols for ADNI-1, ADNI-2 and ADNI-GO. Subjects originally recruited for ADNI-1 and ADNI-GO had the option to be followed in ADNI-2".

Images used in this thesis are T1-weighted scans obtained from different scanner types using the volumetric MPRAGE sequence. All image are preprocessed as described in the ADNI website [6]including distortion correction and B1 non uniformity correction.

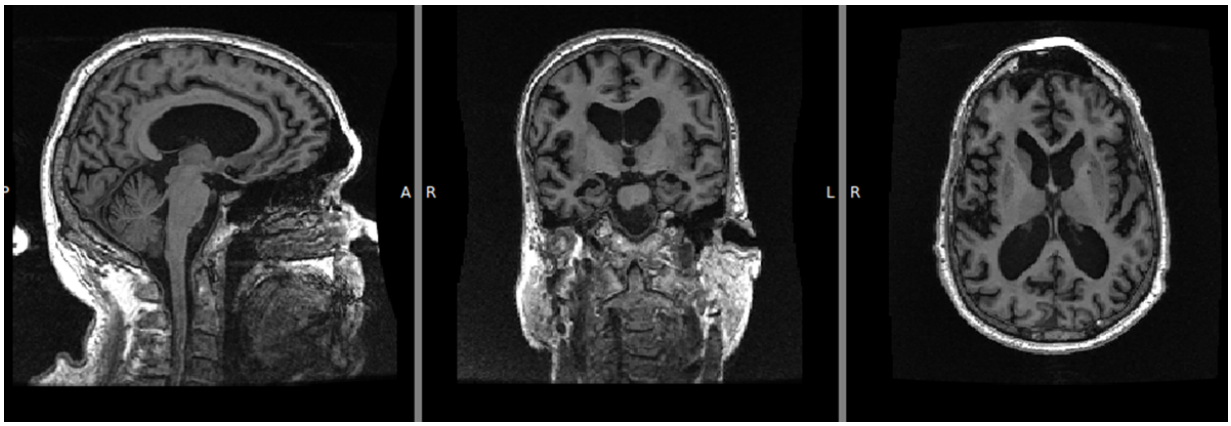

Figure 3.7: Example of an MRI scan of an AD subject of the ADNI data set: subjectID: 003S4136

3.4.2 Bordeaux-3City cohort

Second data used in this work is a subset from the 10-year follow-up of a population-based cohort (Bordeaux-3City) from of the Three-City (3C) study [7].

The Three-City (3C) study was established in 1999 to investigate the influence of vascular factors on the risk of dementia and cognitive impairment. The Three-City Study, a French

[6] http://www.adni.loni.usc.edu/
[7] http://www.three-city-study.com/the-three-city-study.php

prospective study designed to evaluate the risk of dementia in persons aged 65 years and older. Participants were recruited from three French cities: Bordeaux (South-West), Dijon (North-East) and Montpellier (South-East). The 9,294 eligible participants who participated in the baseline examination have since been invited to three waves of follow-up, 2001-2002, 2003-3004, and 2006-2007. At the time of the baseline examination, 60% of the participants were female and they were, on average, 74 years old. The participants are a subset from the Bordeaux site (2104 subjects) of the Three-City (3C) study , a longitudinal multicenter population-based cohort designed to evaluate risk factors of dementia. Subjects were non institutionalized individuals age 65 years and older and were randomly recruited from electoral lists. The study protocol was approved by the ethics committee of Kremlin-Bicetre University Hospital (Paris, France), and all participants provided written informed consent.

MRI data were collected at 1.5 T using a Gyroscan Intera system (Philips Medical Systems, Best, The Netherlands) equipped of 20 mT/m gradients and a quadrature head coil. Each subject underwent a high-resolution 3D T1-weighted anatomic scan with acquisition parameters as followed: TR/TE = 8.5/3.9 ms. A total of 124 slices (thickness 1 mm), were acquired with a 256 x 256 matrix and a field of view (FOV) of 240 mm (voxel size = 0.9 mm x 0.9 mm x 1 mm). The diffusion weighted imaging was performed by using single shot spin-echo echo-planar imaging with the following parameters: TR/TE = 6940/89 ms. Diffusion gradients were applied in 6 spatial directions. The b values used were 0 s/mm2 and 800 s/mm2. Diffusion data results from 8 signal averages. Images were acquired with a 96 x 96 matrix, which were reconstructed to 128 x 128 over a FOV of 230 mm. The resulting voxel size was 1.8 mm x 1.8 mm x 2.5 mm (number of slices = 35, with no gap). The imaging sections were positioned to make the section parallel to the anterior commissureposterior commissure plan (ACPC). Head motions were minimized by the use of tightly padded clamps attached to the head coil. The total scan duration was 11 min 06.(Catheline et al., 2010; Pelletier et al., 2013).

3.4.3 Subjects used in the current research

Here, subjects are selected randomly and their clinical and demographic informations are reported.

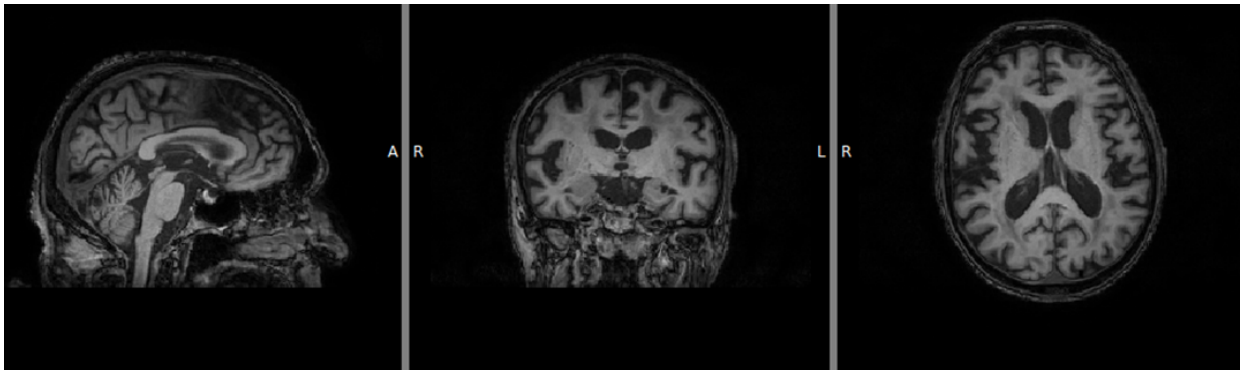

Figure 3.8: Example of slices of the MRI data from subject f4395. Left column: Coronal plane. Middle column: Sagittal plane. Right column: Transverse plane.

- Demographic informations contain gender (M/F) and age.
- Clinical Examination: The Mini-Mental State Examination (MMSE), is a brief 30-point questionnaire test that assess different cognitive abilities, with a maximum score of 30 points. An MMSE score of 27 and above is suggestive of not having a Dementia related disease.

Structural Data

In this thesis, three groups of structural MRI data were collected:

Group 1 (ADNI) contains a total of 188 baseline structural MRIs from the ADNI dataset. Table 3.1 presents a summary of the demographic characteristics of the selected subjects (including the number, age, gender and MMSE of the subjects).

Diagnosis	Number	Age	Gender (M/F)	MMSE
AD	41	72.5 ± 8.79	16/25	24.5± 2.1
NC	60	75.2 ± 4.74	23/37	29.1± 0.6
MCI	87	75.06 ± 7.75	55/32	27 ± 1.3

Table 3.1: Demographic description of the **ADNI** studied population **(Group 1)**. Values are denoted as mean ± standard deviation

Group 2 (ADNI) contains 218 baseline structural MRIs from the ADNI dataset with 35 Alzheimer's Disease (AD) patients, 72 cognitively normal (NC) and 111 Mild Cognitive

Impairment (MCI) subjects. Images are standard 1.5 T screening baseline T1-weighted obtained using volumetric 3D MPRAGE protocol. Demographic information about this group is given in Table 3.2.

Diagnosis	Number	Age	Gender (M/F)	MMSE
AD	35	74 ± 7	20/15	22± 2
NC	72	76 ± 5	37/35	30± 0.8
MCI	111	74 ± 6.8	77/34	26 ± 1

Table 3.2: Demographic description of the **ADNI** subset **(Group 2)**. Values are denoted as mean ± standard deviation

Group 3 ("Bordeaux-3City") The third group of subjects is selected from a study of AD on a real cohort, called "Bordeaux-3City" [8] (Catheline et al., 2010). This group contains 37 structural MRIs (16 AD and 21 NC). Table 3.3 presents the demographic characteristics of the selected subjects (including the number, age, gender and MMSE of the subjects)

Diagnosis	Number	Age	Gender (M/F)	MMSE
AD	16	77.6 ± 9.7	9/7	20.3 ± 3
NC	21	82.7 ± 4.5	9/12	27 ± 1

Table 3.3: Demographic description of **"Bordeaux-3City"** dataset (**Group 3**). Values are denoted as mean ± standard deviation

Diffusion Tensor Imaging Data

Three groups of subjects are used: we first selected a subset of Diffusion Tensor Imaging and their corresponding structural MRI from the Alzheimer's Disease Neuroimaging Initiative (ADNI) database. Table 3.4, Table 3.5 and Table 3.6 present a summary of the demographic characteristics of the studied groups (including the number, age, gender and MMSE of the subjects).

Group 4 (ADNI) This group contains 25 AD and 32 NC subjects.

[8] http://www.incia.u-bordeaux1.fr/

Diagnosis	Number	Age	Gender (M/F)	MMSE
AD	25	77.3 ± 4.1	10/15	22.6± 0.3
NC	32	74± 3.3	12/20	28.7± 1

Table 3.4: Demographic description of the **ADNI** studied population **(Group 4)**. Values are denoted as mean ± standard deviation

Group 5 (ADNI) This group contains 25 NC, 24 AD and 21 MCI subjects.

Diagnosis	Number	Age	Gender (M/F)	MMSE
AD	24	68 ± 5.3	10/14	24.1± 2.4
NC	25	72.3± 3	12/13	29.7± 1.3
MCI	21	73 ± 2.9	8/13	27±0.8

Table 3.5: Demographic description of the **ADNI** studied population with MCI cases (**Group 5**). Values are denoted as mean ± standard deviation

Group 6 ("Bordeaux-3City") A subset of a real cohort: the 10-year follow-up of a population-based cohort "Bordeaux-3City" (Pelletier et al., 2013). We select 21 NC subjects. However, for the AD group, we have only 7 DTI scans with their corresponding structural MRI.

The resolution of DTI scans is 224 x 224, with 60 slices, and with a voxel of size 1 x 1 x 1.5 mm^3. Informations about this group is presented in Table 3.6

Diagnosis	Number	Age	Gender (M/F)	MMSE
AD	7	85.5 ± 3	2/5	25.57 ± 2.4
NC	21	82.7 ± 4.5	9/12	27 ± 1

Table 3.6: Demographic description of **"Bordeaux-3City" (Group 6**). Values are denoted as mean ± standard deviation

3.5 Conclusion

In this chapter, we introduced the preprocessing pipeline of MRI data. We presented the feature extraction approach which is guided by a ROIs atlas-based parcellation method. Next, we presented the Bag of Visual Words approach and the Circulars Harmonic Functions detectors and descriptors theory. Finally, we presented the imaging data used in this

thesis. In the next chapter, we will present a late fusion scheme of visual features-based classifiers. Investigated features are extracted from the the most involved region in AD called "Hippocampus".

Chapter 4

Alzheimer's disease diagnosis using late fusion of hippocampal visual features-based classifiers

Contents

4.1 Introduction

The multimodal nature of multimedia data yielded an active research in fusion of heterogeneous data for classification purposes (Ayache et al., 2007). Nevertheless, an efficient application of image classification methods in Computer-Aided Diagnosis of AD is not straightforward. Indeed, the specific nature of MRI collections vs general purpose image databases requires an in-depth study of the specific features that explain visible and invisible abnormalities for the diagnosis process.

Hence, in this chapter we develop an automatic content-based framework for recognition of Alzheimer's disease subjects using MRI scans. There are three different categories of subjects to recognize: Normal Control (NC), Alzheimer's Disease (AD) patients and the most challenging group Mild Cognitive Impairment (MCI). We extract visual features from the hippocampal region to emphasize the difference or similarity of subjects with respect to AD. Two kinds of features are extracted: visual local descriptors using SIFT, SURF and CHFs and the amount of CSF pixels in the hippocampal area. These features are of different nature. Hence, it is appropriate to deploy the multimedia fusion approaches despite we are working with the same imaging modality. Hence, we propose a late fusion scheme, where the probabilistic outputs of classifies on both local features and the amount of CSF are fused to perform the final classification of the MRI scans. Our approach has been evaluated on the baseline MR images of 218 subjects from the Alzheimer's Disease Neuroimaging Initiative (**ADNI**) database and then on the MRI subset **"Bordeaux-3City"** (see Section 3.4). The rest of this chapter is structured as follows: section 2 explains the visual interpretation of hippocampus atrophy. In section 3, we explain the visual content description with its particularities for this kind of data. In section 4, we present the late fusion scheme for subjects classification. In section 5, we give experiments and results and the final section concludes the chapter.

4.2 Visual interpretation of hippocampus shrinkage referring to the domain knowledge

In AD, the most common pronounced change in the brain structure is the reduction of the hippocampus volume (Villain et al., 2008). Several works in the literature use extracted features from the hippocampus region of interest (ROI) for the purpose of diagnosis (Gerardin et al., 2009; Chupin et al., 2009a; Cuingnet et al., 2011; Gutman et al., 2009). Most of the recently proposed approaches do not take into account the local visual morphological changes in brain regions, which is our goal. Furthermore, the most of proposed methods for AD diagnosis are built on the basis of a fine image segmentation. However, hippocampus is not sufficient for the separation of subject with MCI and AD. Other features derived from known biomarkers can be of help. Recent studies on AD diagnosis found that the quantity of Cerebrospinal Fluid (CSF) in hippocampal region is a biomarker of AD (Shaw et al., 2009). Indeed, smaller hippocampal volume is associated with greater CSF amount. Also, the authors in (Yang et al., 2012) proved that the combination of CSF amount and MRI biomarkers provides better prediction than either MRI or CSF alone. From Figure 4.1, one can see the difference between a normal and an affected hippocampus ROI. It is clear to see from the presented T1-weighted MRI slices that hippocampus structure undergoes a significant cells loss in the AD stage and CSF volume increases to fill the extra space (black area).

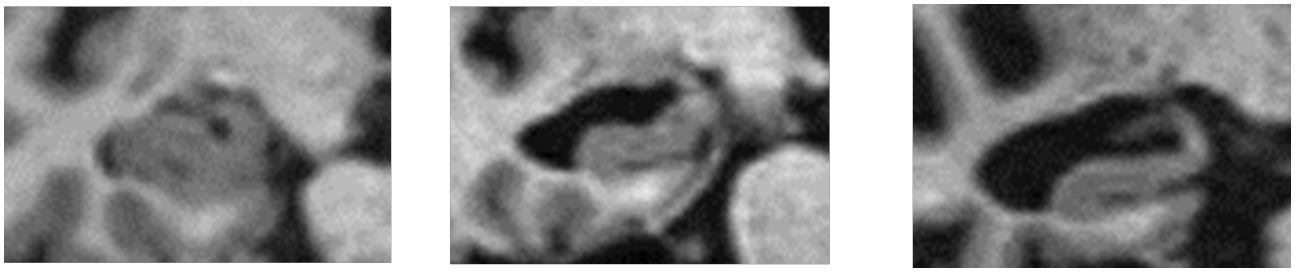

Figure 4.1: From left to right: Bounding box around hippocampus ROI of respectevely NC, MCI and AD subjects from the ADNI dataset

4.3 Visual content description

Two kinds of features are extracted here to quantify the hippocampus atrophy: structural local features of the hippocampus ROI and the amount of CSF in this ROI.

4.3.1 Extraction of local features from hippocampal area

The overall bloc diagram for visual pattern description of the hippocampus ROI is presented in Figure 4.2. We first select the ROI. Then, visual features are extracted and finally signature is build using the BoVW approach. We will detail each step in the next sections.

Actually, visual features extraction is a common step in the overall processing chain yielding image interpretation and classification. Applied to MRI, it has to be populated by particular techniques already in use for brain MRI analysis.

Hippocampus ROI extraction

As the visual information has to be extracted from a specific anatomical region, an atlas-based selection of this region has to be performed. Hence, in this work, an affine registration is applied to the MRIs to the MNI space because we look for preserving a specific pattern of the ROI and avoiding features deformation. For more detail, reader can refer to Section 3.1. Since each brain scan is affinely registered with the MNI template in 3D space and resliced in the same way as the atlas, we superimpose the registered brain slice by slice with AAL and only voxels which are labeled in AAL as hippocampal are selected. An example of labeled hippocampus ROI for one slice on three planes is presented in Figure 4.3.

Local descriptors extraction

In this work, Circular Harmonic Functions (CHFs) were used for selection of contrasted patterns in brains. In addition the SIFT and SURF descriptors are used for comparison purposes with CHFs. We have already given the reason why we privilege CHFs descriptors over conventional SIFT in Chapter 3. Here, we extract also SIFT ans SURF feature from the hippocampus ROI.

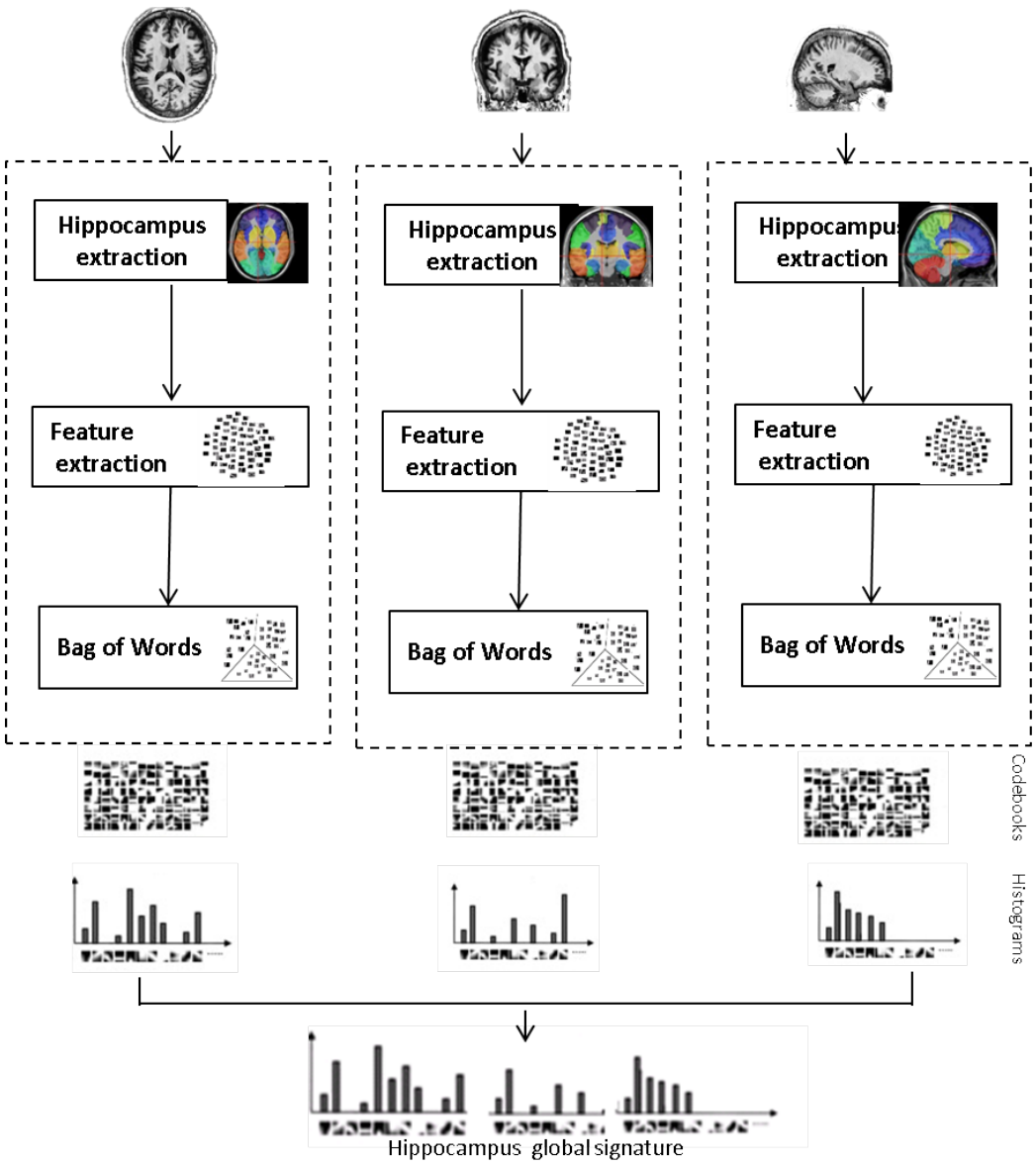

Figure 4.2: Visual feature extraction from the hippocampus ROI and signature generation

We use a "dense sampling" strategy to capture all the relevant information. Thus, the scans are densely sampled in a selected hippocampal ROI by a grid of circular patches and the signal decomposition on a CHFs basis is computed for each patch. These patches could cover the hippocampal area at a microscopic level. Figure 4.4 shows the CHFs features placement on the hippocampus ROI (axial, coronal and sagittal projections). The extracted feature points "support areas" (i.e. where the descriptors are computed) are denoted with yellow circles. We perform 2D CHFs transform computation slice-by-slice. Hence, the whole

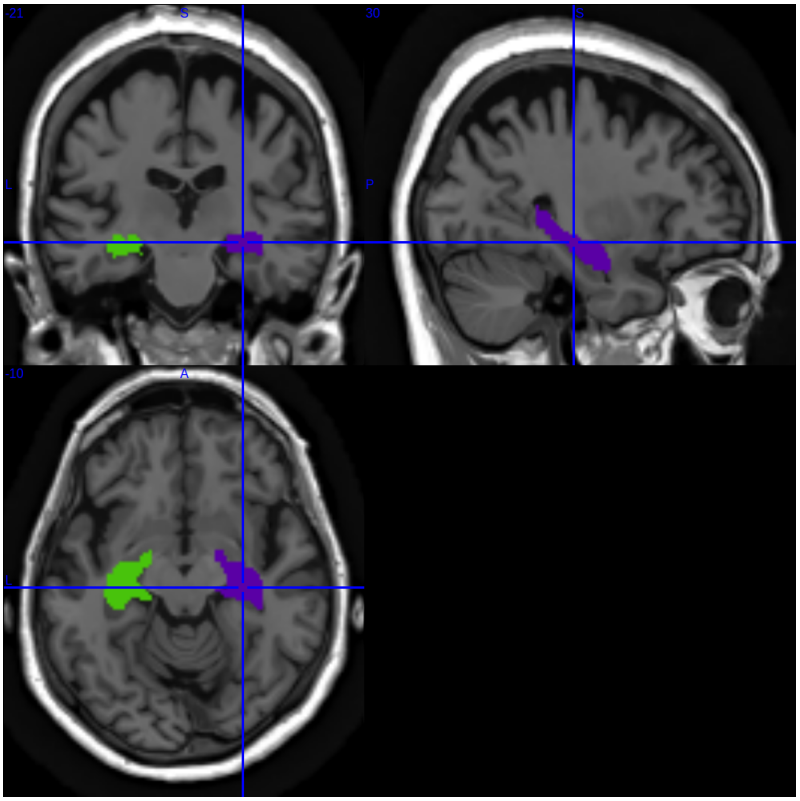

Figure 4.3: Hippocampus ROI selection in three planes of an MRI slice

description of the hippocampal volume is a collection of 2D CHFs descriptors for each slice and each projection of the selected volume. It is to note that the CHFs coefficients extracted from several areas overlapping with the AAL mask are different and hence depend on the signal presented in the ROI (atrophy or not).

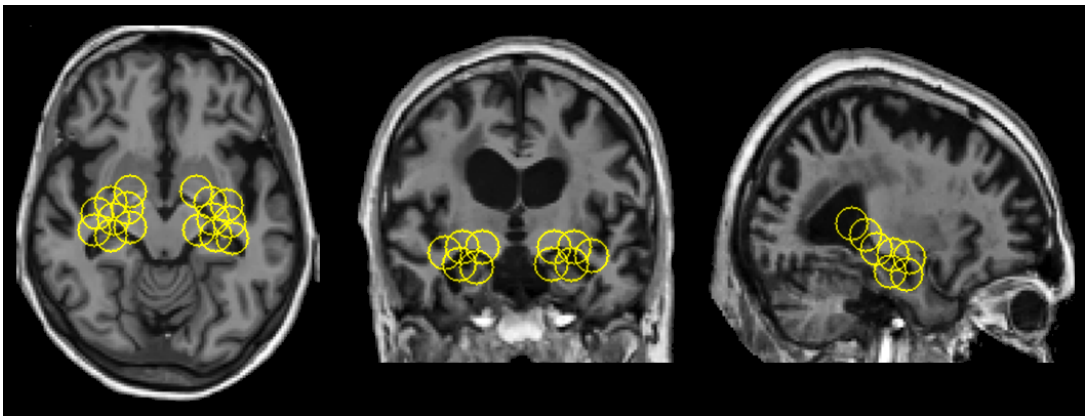

Figure 4.4: CHFs features placement on the hippocampus ROI (axial, coronal and sagittal planes) of an MRI slice of an **ADNI** subject

Signature generation: ROI-specific bag of words generation

The Bag-of-Visual-Words (BoVW) approach is used to model the hippocampus ROI pattern. The role of BoVW model is to cluster extracted features from hippocampus in order to build a visual vocabulary. The region's shape differs from one projection to another. Thus, we choose to perform clustering three times from different planes (sagittal, axial and coronal) and to generate one visual vocabulary per projection. This allows to capture the maximum of atrophy information. Firstly, all features $f^s_{n,i}$, here n and i stand respectively for slice and feature indexes, are extracted from the ROI on all slices for the sagittal projection then features are clustered by k-means algorithm. The same is done for axial and coronal projections. All features $f^s_{n,i}$, $f^a_{n,i}$, $f^c_{n,i}$ and centers of clusters c_{sk} ,c_{ak}, c_{ck} obtained by k-means (where K is the codebook size) here have the same dimensionality of the descriptor being used. In case of SIFT it is 128 and for CHF it is 150. According to the BoVW approach, we then call cluster centers "visual words". Once the visual words have been determined, the image signature per projection is generated. Each feature is assigned to closest visual word using the distance $d(f^s_{n,i}, c_s)$, in our case the Euclidean distance is used. Then each projection is represented by a normalized histogram of occurrence of visual words. The image signature h is built by concatenating the histograms from all projections $h = [h_s h_a h_c]$.

The difference between our proposed scheme and the traditional BoVW model explained in (Chapter 3) is that only features extracted from the hippocampus ROI are used rather than all image's pixels in an scan to create the vocabularies. This process makes the created vocabularies more region-specific and make the signature more disease-specific.

4.3.2 CSF volume computation

The increased quantity of CSF in the hippocampal region is an important visual biomarker for AD diagnosis. Indeed in the case of AD, the hippocampus shrinks and the liberated volume is filled with CSF. To analyze the shrinkage, we count the CSF pixels in the region of the hippocampus. In the MRI T1 scans the CSF is appearing as dark areas (Chapter 1), thus we can select it just by thresholding.

$$B^*(x, y, z) < T_{dark}$$

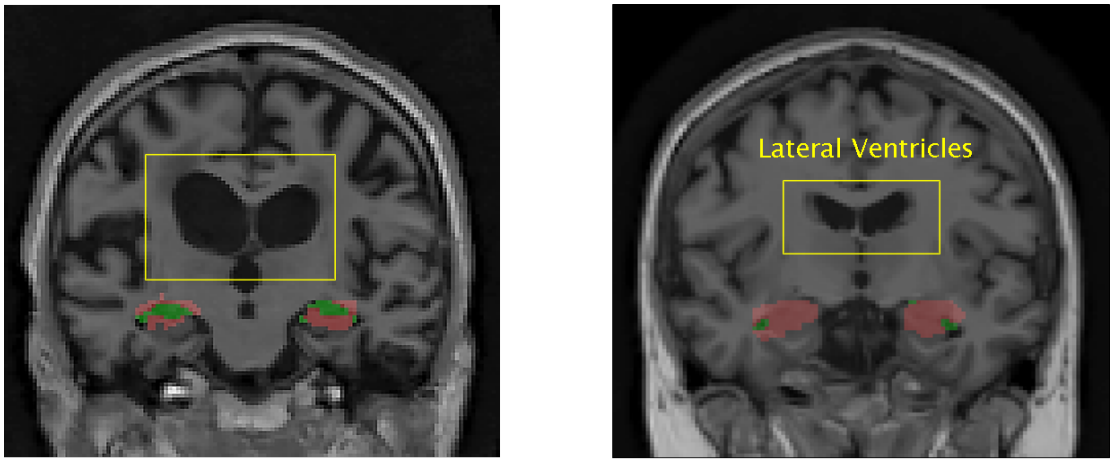

Figure 4.5: CSF on the hippocampus region : a) AD brain, b) Healthy: MRI slices in coronal projection

The choice of T_{dark} is not straightforward due to the large difference in brightness and contrast of MRI scans. Hence, all scans need to be transformed in such a way that, similar intensities will have similar tissue-specific meaning. In our work, we perform the grey-scale normalization method proposed in (Nyúl et al., 2000) which consists in equalization of histograms of all scans. In order to select the optimal threshold, the following procedure is performed: all voxels from the hippocampus regions from all scans are collected together and the threshold between dark (hyposignal) and bright (hypersignal) voxels is estimated using Otsu's method (Otsu, 1979). In fact, one threshold for all images is computed. However, normal patients have a little CSF amount in the hippocampus area. Thus, to ensure correct delineation when computing the threshold by Otsu's method (mathematical details are presented in Appendix .3), we add additional regions where CSF is always present: The Lateral Ventricles (LV) by referring to the domain knowledge. In addition, adding some pixels from the Lateral Ventricles may improve the discrimination results because AD patients show more CSF in the LV than do MCI and NC subjects. Using this procedure, the volume of the CSF in a normalized hippocampal area is measured in a quantity of voxels. It will be later denoted by V. Figure 4.5 illustrates the results of detection of CSF (in green) in hippocampal region. The CSF (green color) is situated around the hippocampus (red color)

boundaries. The added region is marked with a yellow rectangle (LV). It can be seen that the quantity of CSF in the case of AD (a) is higher.

4.4 Late fusion scheme for subjects classification

The proposed classification approach aims to combine the two sources of information: visual signature and the amount (volume) of CSF in a global decision framework to discriminate between AD versus NC, NC versus AD and AD versus MCI subjects. Taking into account the advances in multimedia fusion research in the literature, we propose to do it by a late fusion scheme. The overall diagram of the approach is presented in Figure 4.6. Classifiers are applied separately on the two kind of features and the probabilistic outputs of each classifier are concatenated and provided as inputs of another SVM. The CHF-based visual signatures are first classified between the categories two by two with a state-of-the art SVM approach with an Radial Basis Function (RBF) kernel. The classification of subjects on the basis of the CSF volume is performed by a Bayesian classifier. Indeed, we have here a scalar feature and the class probabilities can reasonably be a priori trained (AD are much more rare in patients cohorts, than NC and MCI for instance). Both classification schemes give a decision output. We transform it into an homogeneous probabilistic output and form the second order feature vectors of dimension 2. The latters are then submitted to the trained SVM binary classifier for each classification problem given above.

We stress that in this work we address a binary classification problem as the goal is to assess the discriminative power of using both hippocampal shape expressed by CHFs features and CSF volume biomarkers in an automatic classification of cohorts. In the following, we will present the details of each step of the approach.

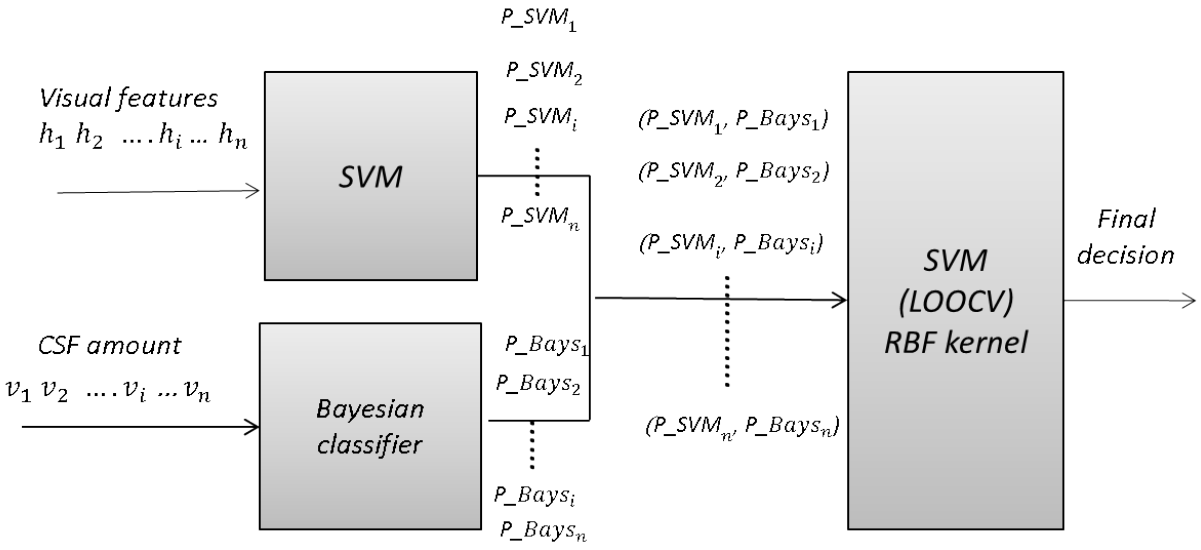

Figure 4.6: Late Fusion scheme

4.4.1 Support Vector Machines classifier for visual signatures classification

In the current research, we solve a set of binary classification problems AD vs NC, NC vs MCI and AD vs MCI. The unknown subject is classified by maximizing the score of these three classifiers. We use the well known SVMs classifier in the visual description space of signatures built with CHFs descriptors. At training step it separates a given set of training data of instance label pairs $(x_i, y_i), i = 1, ..., l$ where $x_i \in R^n$ and $y \in \{1, -1\}$ by maximizing the distances to the hyperplane that separates the two classes in a kernel-transformed space. Then the classification of unknown data is performed in this space accordingly to their position with regard to the hyperplane. For more details on SVMs we refer the reader to Section 2.6.1. In this work, we use the RBF kernel defined by: $exp(-\gamma * |u - v|^2)$. In many settings, for a given input sample and for a given classifier we are more interested in the degree of confidence that the output should be +1. In such cases it is useful to produce a probability $P(y = 1|x)$. Given k classes, for any x, the goal is to estimate

$$p_i = P(y = i|x), i = 1....k$$

We first estimate pairwise class probabilities by Platt approximation (Platt, 1999)

$$r_i = \frac{1}{1+e^{Af_i+B}}$$

where f is the decision value at x. A and B are estimated by minimizing the negative log likelihood of training data (using their labels and decision values). For each binary classifier we will have the probabilistic output $P_{SVM_i}(x)$.

4.4.2 Bayesian classifier for CSF based features classification

The Bayesian classifier (Section 2.6.2) uses the parametric model of Probability Density Function (PDF) for each class which we suppose Gaussian. It gives the most likely class for a given observation. Let V denote the CSF volume for a given subject, Y is the subject class label ($Y = AD$, NC or MCI), and $C = 2$ (binary classification) is the number of classes. The problem consists in classifying the sample v to the class c_* maximizing $P(Y = c|V = v)$ over $c = 1, , C$. Applying Bayes rule gives:

$$P(Y = c|V = v) = \frac{P(V=v|Y=c)P(Y=c)}{P(V=v)}$$

and reduces the original problem to:

$$c_* = argmax_{c=1,...C} P(V = v|Y = c)P(Y = c)$$

we denote the related probability of a sample by $P_{Bayes_i}(x)$

4.4.3 Fusion Strategy: Probabilistic information fusion

The probabilistic outputs of SVM-based signature classification and CSF volume-based Bayesian classification are now available for each binary classification problems. We form the 2 dimensional feature vectors as flows:

$$Z_i(x) = (P_{SVM_i}(x), P_{Bayes_i}(x))^T$$

Finally, the obtained vectors are submitted as inputs to the second SVM classifier in cascade using Leave-One-Out Cross-Validation. The classification method is presented in Figure 4.6. The latter use a linear SVM kernel.

4.5 Experiments and results

4.5.1 Metrics of evaluation

Metrics used to evaluate final late fusion classification performance are :

- $Accuracy\ (Acc) = \frac{(TP+TN)}{(TP+TN+FN+FP)}$
- $Sensitivity\ (Sen) = \frac{TP}{(TP+FN)}$
- $Specificity\ (Spe) = \frac{TN}{(TN+FP)}$
- $BAC = 0.5 * (Sensitivity + Specificity)$

Here True Positives (TP) (True Positives) are AD patients correctly identified as AD, True Negatives (TN) are controls correctly classified as controls, False Negatives (FN) are AD patients incorrectly identified as controls and False Positives (FP) are controls incorrectly identified as AD. Similar definition is hold for other binary classification problems NC vs MCI and AD vs MCI.

4.5.2 Data groups

In this chapter, we selected from the **ADNI** dataset the same subjects number as (Yang et al., 2012), with the a comparable demographic information for each of the diagnosis groups (NC, AD and MCI). The data sample consists of 218 baseline structural MRIs with 35 AD patients, 72 NC and 111 MCI subjects **(Group 2)**. The second source of data is the **"Bordeaux-3City"** data **(Group 3)**. comprising 37 structural MRIs (16 AD and 21 NC). Demographic characteristics of the selected subjects are given in Section 3.4.3 (Respectively presented in Table 3.3 and Table 3.2)

4.5.3 Results and discussion

CSF volume computation

In this section we give the figures showing the credibility of CSF quantity biomarker extracted with our method (see Section 4.3.2). Table 4.1 presents the quantities of CSF voxels within

the hippocampal ROI. Here, one can note that the amount of CSF increases from NC to AD images.

Class	Volume (mean ± sd)
NC	212 ± 101
MCI	316 ± 104
AD	402 ± 126

Table 4.1: CSF amounts

Classification results

Table 4.2 presents the classification performance. It summarizes classification results of AD versus NC, NC versus MCI and AD versus MCI for the **ADNI** subset **(Group 2)**. We also present classification results of AD versus NC obtained on the **"Bordeaux-3City"** in Table 4.3. Since the latter does not contain MCI cases, relative classification problems are not addressed in our experiments.

Firstly, we compare the performance on CHFs visual features with regard to conventional SIFT and SURF descriptors. It can be seen that the proposed CHFs features systematically outperform SIFT and SURF in all three quality metrics: Accuracy, Specificity and Sensitivity. We note that the SURF features with the lowest dimension (64) between three classes of descriptors are not applicable in our problem. In fact, they are less precise than SIFT and give a very low sensitivity (25.73%) in a difficult case of MCI vs AD. The CHFs descriptors are of a comparable dimension (150) with SIFT (128), but outperform them. The results presented for visual features alone, correspond to the optimal sizes of visual vocabularies. Codebook sizes were estimated experimentally optimizing the accuracy criterion. For SIFT features, the size of visual dictionary per projection was 100 yielding to the dimension of 3x100 of the BoVW. For SURF features, it was of 150 yielding the signature size of 3x150. Finally, for the CHFs features, the dictionary consisted of 150 visual words yielding a dimension about 3x150 of the visual CHFs signature. The low cardinality of the optimal codebook can be explained by a reasonably limited number of descriptors. Indeed, the dense sampling is performed only on the hippocampal ROI in a limited number of slices (70 for sagittal, 97 for axial and 42 for coronal projections respectively).

AD versus NC				
Features	Specificity	Sensitivity	Accuracy	BAC
Hippo VF (CHF)	94.45%	65.72%	85.05%	80.05%
Hippo VF (SIFT)	93%	51.43%	79.44%	72.21%
Hippo VF (SURF)	91.67%	60%	81.3%	75.83%
CSF volume	72.29%	70.5%	78.5%	71.93%
Hippo VF (CHF) + CSF	100%	75.5%	87%	87.75%
NC versus MCI				
Features	Specificity	Sensitivity	Accuracy	BAC
Hippo VF (CHF)	85.59%	57%	74.32%	71.29%
Hippo VF (SIFT)	84.69%	52.78%	72.14%	68.73%
Hippo VF (SURF)	83.78%	56.95%	73.23%	70.36%
CSF volume	48%	66%	58.47%	57%
Hippo VF (CHF)+ CSF	83.34%	70.73%	78.22%	77.03%
AD versus MCI				
Features	Specificity	Sensitivity	Accuracy	BAC
HippoVF (CHF)	63.97%	42.86%	58.9%	53.41%
Hippo VF (SIFT)	55.85%	40%	52.05%	47.92%
Hippo VF (SURF)	57.6%	25.73%	50%	41.66%
CSF volume	67.39%	60%	62.33%	63.69%
Hippo VF (CHF) + CSF	70%	75%	72.23%	72.5%

Table 4.2: Classification results: **ADNI** dataset **(Group 2)**

AD versus NC				
Features	Specificity	Sensitivity	Accuracy	BAC
Hippo VF (CHF)	80%	70%	79%	75%
Hippo VF (SIFT)	76.19%	56.26%	67.56%	66.22%
Hippo VF (SURF)	40%	85.71%	66.67%	62.85%
CSF volume	72%	60%	80%	66%
Hippo VF (CHF) + CSF	81%	76%	85%	78.5%

Table 4.3: Classification results: **"Bordeaux-3City" (Group 3)**

Using visual features of the hippocampus on the ADNI subset, we achieved an accuracy of 85.05% and 74.32% respectively for AD versus NC and NC versus MCI classification. However, structural change on hippocampus is not sufficiently accurate to be an absolute diagnostic criterion to separate AD from MCI cases. In the case of MCI versus AD classifica-

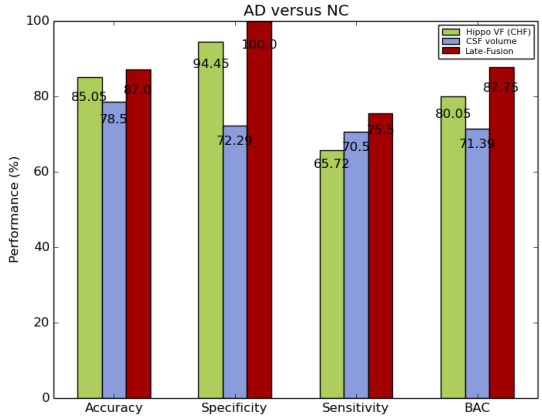

Figure 4.7: AD vs NC Performance comparison **(ADNI (Group 2))**

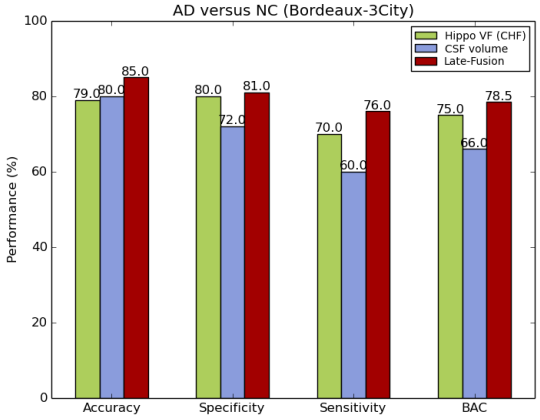

Figure 4.8: AD vs NC Performance comparison **("Bordeaux-3City")**

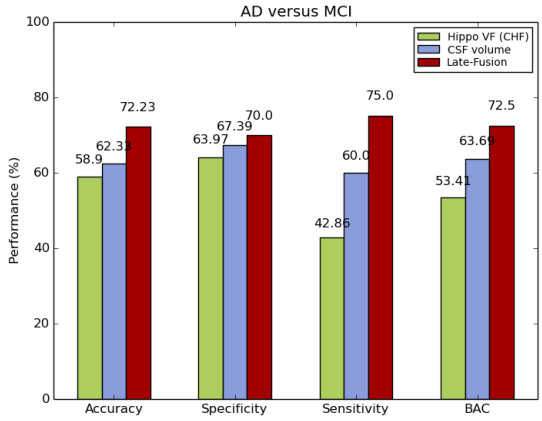

Figure 4.9: AD vs MCI Performance comparison **(ADNI Group 2)**

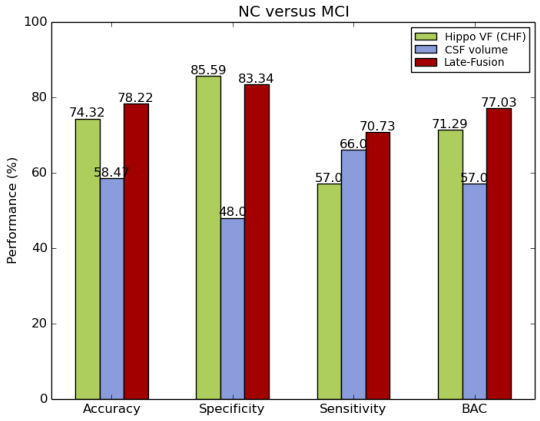

Figure 4.10: NC vs MCI Performance comparison **(ADNI (Group 2))**

tion, performance drops to 58.9%. We aimed to deal with this challenging category (MCI). To enhance the results, CSF amount measurement was added. The CSF amount classification using Bayesian classifier gives an accuracy of 62.33% and 58.47% for the recognition of the MCI cases respectively from the AD and NC subjects. Moreover, we note that adding supplementary voxels from the Lateral Ventricles helps to boost the performance of CSF delineation and thus improve the classification results. Indeed, the accuracy of AD vs NC classification by CSF amount increases from 74.1%to 78.5%. Hence, we retained this finding for classification and all results in Table 4.2 were obtained with this approach. Since those

two kinds of features were extracted from the same brain (hippocampus), our assumption that they could provide complementary information for classification was correct.

For AD versus MCI classification, using the late fusion, we achieved 72.23% of accuracy compared to 58.9% using only CHF features. For the NC versus MCI classification, accuracy increases from 74.32% to 78.22%. As we can see from Figures 4.9 and 4.10, the sensitivity values of both AD vs MCI and NC vs MCI classification accuracies undergo a significant increase (from 42.86% to 75% for the MCI vs AD cases for example) when we use the late fusion. These results show that CSF volume improves the classification accuracy by an average of 9% when combined with the visual signatures especially for the MCI cases classification which is the most challenging task due to the strong heterogeneity of this class.

We compare our work with results obtained in (Yang et al., 2012). First, the authors used the volume and the shape of hippocampus to perform subjects categorization and second, they added CSF bimomarkers and volume and shape of the lateral ventricles to improve results in the case of AD and MCI recognition. From Table 4.4, we can see that our content-based approach outperforms most of the achieved results on (Yang et al., 2012). In fact, the BAC metric is always better in our case. In the case of the use of only the hippocampus ROI, we achieved better classification accuracies than those reported in (Yang et al., 2012) when the volume the hippocampus is used.

For example better classification accuracy was achieved in AD versus MCI and NC versus MCI classification tasks using hippocampus volume is 61.9% and 42.3% respectively, which is lower than results obtained in our present work (74.32% and 58.9% respectively). In addition our proposed late fusion performs better than combining hippocampus volume with Lateral ventricles and CSF volumes (Yang et al., 2012) on all three binary classification tasks. In the case of AD or MCI categorization we reached better results (accuracy of 72.23%, a specificity of 70% and a sensitivity of 75%) compared to (Yang et al., 2012) in which the authors obtained only 69.9% of accuracy, 68.6% of specificity anda 70.7% of sensitivity.

We can conclude that combining visual features of AD biomarkers performs better than using volume or shape. Also, in (Yang et al., 2012), the authors use the Freesurfer software [1] to select region which is a very time consuming (about hours of processing) task contrarily

[1] http://freesurfer.net/

to the atlas mapping used in our work. Therefore, the ability to efficiently classify MCI and AD patients based on visual features of structural MRI might shed light on the ability to predict the conversion from MCI to AD, which is of clinical interest.

Features	Results	AD vs NC	MCI vs NC	MCI vs AD
Volume of Hippcampus (Yang et al., 2012)	Acc	65.5%	61.9%	42.3%
	Sens	57.8%	57.7%	45.3%
	Spe	73.3%	66.1%	39.2%
	BAC	65.55%	61.9%	42.25%
CHFs Hippcampus our method	Acc	85.05%	74.32%	58.9%
	Sens	65.72%	57%	42.86%
	Spe	94.45%	85.59%	63.97%
	BAC	**80.08%**	**71.29%**	**53.41%**
Hippocampus volume+LV+CSF (Yang et al., 2012)	Acc	85.4%	72%	60.9%
	Sens	88.8%	70.1%	80.4%
	Spe	82%	73.9%	41.4%
	BAC	85.4%	72%	60.9%
CHFs hippocampus + CSF our method	Acc	87%	78.22%	72.23%
	Sens	75.5%	70.73%	75%
	Spe	100%	83.34%	70%
	BAC	**87.75%**	**77.03%**	**72.5%**

Table 4.4: Classification results comparison between our method and the volumetric approach proposed in (Yang et al., 2012)

Alzheimer's disease is not just a disease of old age. Alzheimer's affects people young people. Distinguishing criterion in this case are in same cases hard to detect because the correlation between brain structures abnormalities of both young AD patients and normal old subjects. In the next section we aim to classify between very old subjects and AD patients using the proposed Late fusion approach.

AD versus Normal very aged subjects

In a second part of experiments, we selected 15 MRI scans of AD (60 ± 3 years old) and 12 aging subject from the Normal control category (80 ± 6 years old) of the **ADNI** dataset. Our approach distinguishes well between young Alzheimer's disease and the aging normal control subjects with an accuracy of 85% and sensitivity of 76%. Hence, adding CSF amount not only improved MCI cases classification but also helped to separate very old healthy subjects from those suffering from AD.

4.6 Conclusion

In this chapter, we developed an automatic classification framework for AD recognition in structural Magnetic Resonance Images (MRI). The main contribution consists in considering visual features from the most involved region in AD (hippocampal area) and in using a late fusion of classification outputs of hippocampus features and CSF amount. The experiments showed that this late fusion gave better accuracy especially when discriminating between AD and MCI than using either visual features extraction or CSF volume computation separately. The experimental results show that our classification of patients with AD versus NC (Normal Control) subjects achieves the accuracies of 87% and 85% for **ADNI** subset and **"Bordeaux-3City"** respectively. For the most challenging group of subjects (MCI), we reached accuracies of 78.22% and 72.23% for NC versus MCI and AD versus MCI respectively on **ADNI** Group. The late fusion scheme improves classification results by 9% in average for the three groups. Results demonstrate very promising classification performance and simplicity compared to the state-of-the-art volumetric AD diagnosis approaches. The overall volumetric or shape analysis of the hippocampus does not describe the local change of its structure, which is helpful for diagnosis contrary to our local features-based method which describe the hippocampal atrophy in more details.

While in this chapter we applied a late fusion scheme of features-based classifiers outputs from one ROI (hippocampus). In the next chapter we will propose an early fusion scheme to combine features derived from two brain ROIs: hippocampus and Posterior Cingulate Cortex.

Chapter 5

Alzheimer's disease diagnosis on structural MR Images using late Fusion of hippocampus and Posterior Cingulate Cortex features

Contents

5.1 Introduction

Numerous structural analysis involved hippocampus ROI as the most efficient hallmark of AD. However, hippocampal atrophy alone is not sufficient to discriminate MCI cases and other structures may be a more sensitive biomarker in AD diagnosis (Dickerson et al., 2001). Therefore, fusion of measurements from many different regions or biomarkers can potentially build signature of high discriminative power and improve diagnostic decisions. In addition to hippocampal atrophy, PCC hypometabolism has been considered as a hallmark of early stage of AD (Minoshima et al., 1997). Indeed, many studies have shown PCC hypometabolism in incipient AD (Huang et al., 2002; C Nestor et al., 2003; Huang et al., 2002) associated with PCC atrophy (Callen et al., 2001; Jones et al., 2006; Choo et al., 2010; Kemp et al., 2003; Shiino et al., 2006). (Pengas et al., 2010) confirm that PCC atrophy is present from the earliest clinical stage of AD and that this region is as vulnerable to neurodegeneration as the hippocampus. Here, the question arises: *Whether atrophy of both the hippocampus and the PCC could be a more efficient criterion in Alzheimer's disease diagnosis than hippocampus atrophy alone.*

To increase classification performance, some works typically used techniques to reduce the dimensionality of neuroimaging data and to select the most discriminative features before

applying SVM. Principal Component Analysis (PCA)(Jolliffe, 2002) is often used for this type of application (Christos et al., 2008). We opted for PCA as well, as the visual signatures can be sparse and of a high dimensionality. In terms of prior information, classification can be improved by focusing on local visual features extraction from ROIs known to be involved in AD. Thus, in this chapter we hypothesize that hippocampal and PCC structures are more efficient than hippocampus alone to detect insidious case of AD.

In order to test this hypothesis, we first design a Content-based image retrieval approach and then we propose a classification framework. The rest of this chapter is organized as follows: Section 2 presents the early fusion of the Hippocampus and the PCC features. In section 3, we explain the content-based MRI retrieval methods. Then, in section 4 we present the AD subjects classifications framework. Discussion is given in section 5 and finally, section 6 concludes the chapter.

5.2 Early fusion of Hippocampus and PCC features

In this research, we follow the same methodology presented in Chapter 4. Local features extraction is applied separably for hippocampus and PCC ROIs to build representative signatures. In fact, a BoVW approach is applied to the extracted features and then a signature is generated for each ROI. Figure 5.1 presents the methodology of combined signature building. It is to note that the same strategy is applied to the two other projections (coronal and sagittal) and the final ROI signature is the concatenation of the tree signatures. The global image signature of a subject is obtained by concatenating both Hippocampus and PCC. In order to reduce the (high) dimensionality of signatures, a Principle Component Analysis (PCA) is applied. This late fusion will be integrated in two traditional approaches for computer-aided diagnosis: First, in a CBIR approach then, in a classification framework. Indeed, the first approach aims to retrieve relevant brain scans from an MRI data that are similar to the query image. In the second, SVM classifiers are used to classify the subject's brain into NC, MCI or AD category.

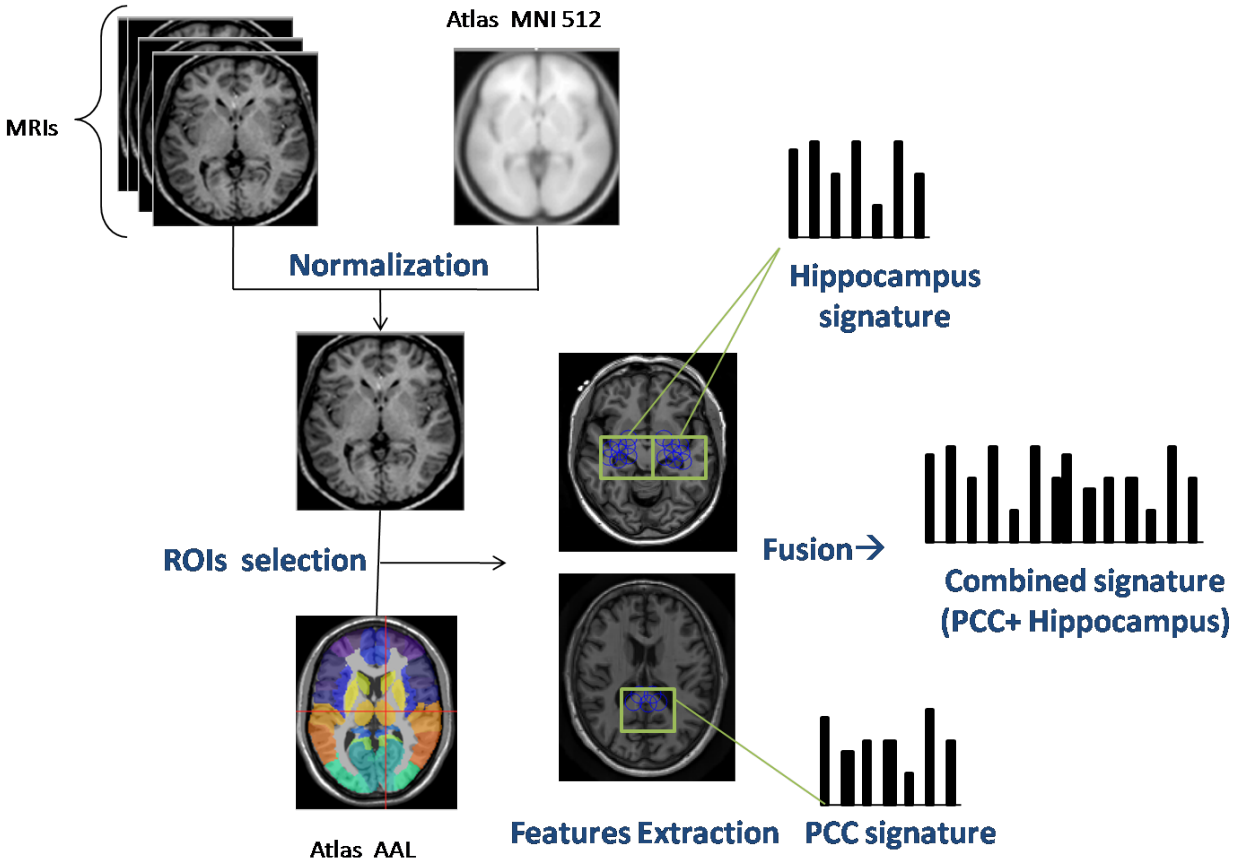

Figure 5.1: Framework description: Visual description of the combined signature generation in axial projection. The method starts with brain image normalization. Then, Regions-of-Interest (hippocampus and PCC) are extracted from normalized images to be described by local visual descriptors and quantified in the BoVW framework.

5.2.1 Hippocampus and Posterior Cingulate Cortex ROIs Selection

The first stage of visual feature extraction aligns MRI scans to a standard brain template. We use here the same methods explained in Chapter 3 and used in Chapter 4. All the scans are spatially normalized to the MNI template using an affine transformation. Since each brain image is affinely registered with a digital atlas in 3D space and resliced in the same way as the atlas, we are able to extract the region of interest (ROI) by mapping the brain volume with the atlas slice by slice. The regions investigated in this study are suggested by our medical partners. To extract the two ROIs (hippocampus and PCC), we used the

Automated Anatomical Labeling (AAL) Atlas.

5.2.2 Local feature extraction

After PCC and hippocampus ROIs selection, we extract features from the region overlapping with the obtained masks. In this chapter, we apply a "dense sampling" strategy. Based in our previous results, we resort to the use of CHFs as descriptors. Here, signal variations inside the ROI anatomy can be represented as a set of local CHFs coefficients.

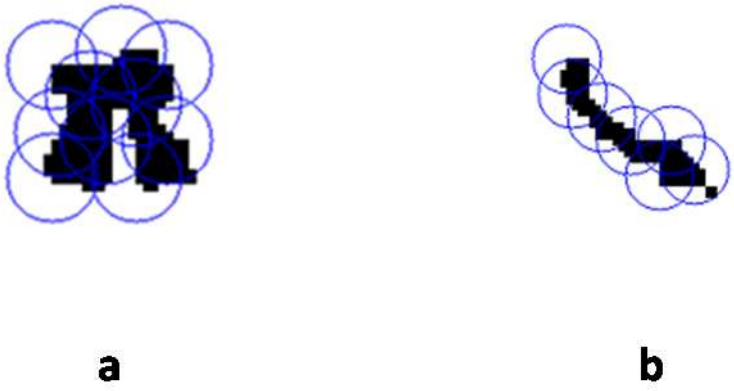

Figure 5.2: Illustrating of CHF feature extraction in PCC (a) (coronal slice) and in hippocampus (b) (axial slice) masks. Masks are extracted using the AAL atlas. Circles represent the locations of features (support area). The descriptor support areas are selected by simply scanning the mask line by line and by placing the feature centers in masked pixels of each slice. The extracted feature points "support areas" (i.e. where the descriptors are computed) are denoted with circles and the ROI is marked with black.

Dense feature placement is illustrated in Figure 5.2, the support regions of the fixed size are first generated with their centers on the regular grid including the mask and then only regions overlapping with the mask are selected. CHFs coefficients extracted from several areas overlapping with the mask may be different and depend on the signal variation inside each ROI. Therefore, this signal variations may characterize between affected (diseased) and normal tissues.

We note that these features are computed on each 2D slice separately. Figure 5.3 presents the descriptors extraction from both hippocampus (a) and PCC (b) from one slice in three MRI-planes.

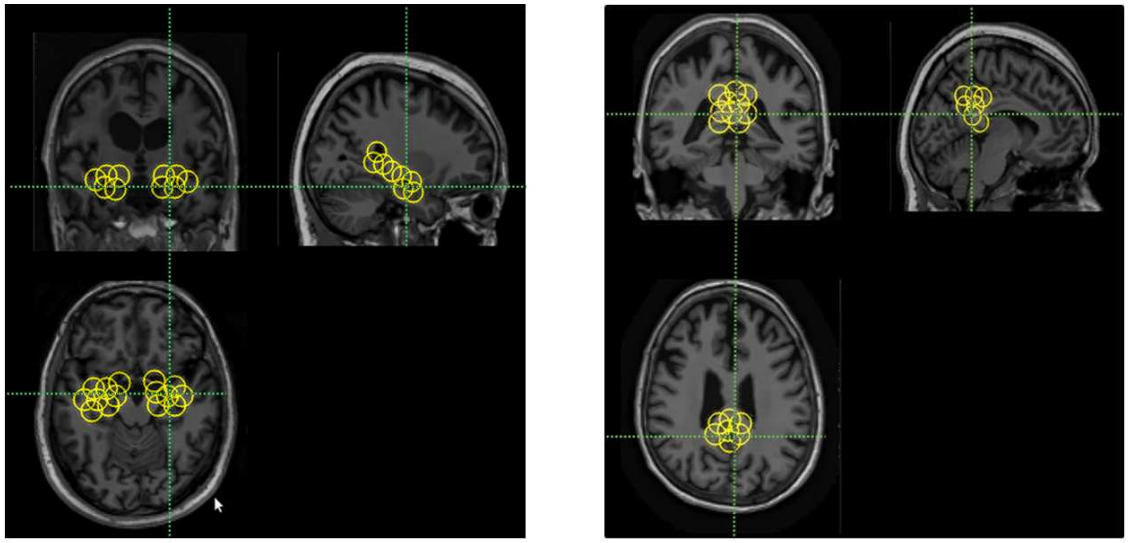

Figure 5.3: CHF Keypoints detection on MRI brain : Example of dense placement of local features on brain scans of a subject from the **ADNI** dataset. Extracted local feature is the descriptor of a circular support area, defined by each point of the grid and the radius of the support area in the ROI. (a) descriptors extraction of the hippocampus ROI (sagital, coronal and axial projections), (b) descriptors extraction on the PCC ROI (sagital coronal and axial projections). Here, CHFs capture the image variations and extract local visual features of each ROI.

5.2.3 Combined signature generation

In our work, we treat each ROI as a set of local features. Hence, the BoVW approach model is applied separately to the two ROIs (hippocampus and PCC). The first stage of BoVW approach is to cluster extracted features from the whole database in order to build the so-called visual vocabulary (codebook). As the shapes of PCC and Hippocampus differ, each ROI requires its proper codebook. Moreover, the region's shape differs from one projection to another. Thus, we choose to perform the clustering process three times from different projections (sagittal, axial and coronal) and to generate one visual vocabulary per projection and per ROI. The size of the resulting brain signature is $3 * 2 * codebook_{size}$.

First, all features $f^s_{n,i}$, where n and i stand respectively for slice and feature indexes, are extracted from the ROI on all slices from the sagittal projection (s) then the features are quantized by the k-means algorithm. The centers c^s_k, $k \in [1, K]$, are then calculated, where K is the codebook size given as a parameter to the k-means algorithm. The same is done for

axial and coronal projections. All features $f^s_{n,i}$,$f^a_{n,i}$,$f^c_{n,i}$ and centers c^s_k, c^a_k, c^c_k here have the same dimensionality of CHFs descriptor (150). Once the cluster centers have been computed, the image signature per projection is generated. Each feature is assigned to the closest center using the distance $d(f^s_{n,i}, c^s_k)$. Here we use the Euclidean distance. Then each projection is represented by an histogram of visual words occurrence. The image signature per ROI h is acquired by the concatenation of the histograms from all projections: $h = [h^s, h^a, h^c]$. The final scan signature is obtained by concatenating hippocampus and PCC signatures.

5.2.4 Dimensionality reduction

To obtain a meaningful representation of features, we have to remove noisy, irrelevant and redundant features. Features dimensionality reduction could improve the performance of the learning algorithm and reduce memory cost and computation time. Hence, to reduce the resulting image signature dimension, we use the PCA (Jolliffe, 2002) which is a useful mathematical technique for reducing vector dimensionality and finding an optimal combination of variables in a smaller set. In addition, MRI data are heavily impacted by noise. In order to avoid modeling noise, less significant components produced by PCA are excluded from the feature set based on the assumption that these components tend to account more for noise than for meaningful information. In the next section, we will present the retrieval approach using an hybrid fusion scheme of visual features.

5.3 Content-based retrieval of AD subjects using Hybrid fusion

5.3.1 Early fusion for subjects retrieval

Generally, we present a framework to help early diagnosis of AD from MRI using visual descriptors, this research was initialized in (Mizotin et al., 2012). It has been shown in (Mizotin et al., 2012) that image signature contains too much individual brain structural information which is not relevant to characterize the disease. Also in the latter, retrieval performances drops significantly when interring the MCI case. Hence, in the current research,

we tackle the MCI class from CBVIR perspective and make the following contributions:

First we propose to reduce the dimensionality of the scan signature and to retain only relevant information, we use here the PCA technique. Then, we propose to add an early fusion scheme to improve the recognition performance especially in MCI class. Actually, the early fusion of features is achieved by concatenating the hippocampus and the PCC signatures (Described in Section 5.2).

Here, we propose two modes of early fusion:

- Simple concatenation.
- PCA applied on concatenated signatures.

This early fusion is the part of a global hybrid fusion approach using the preliminary classification proposed in (Mizotin et al., 2012).

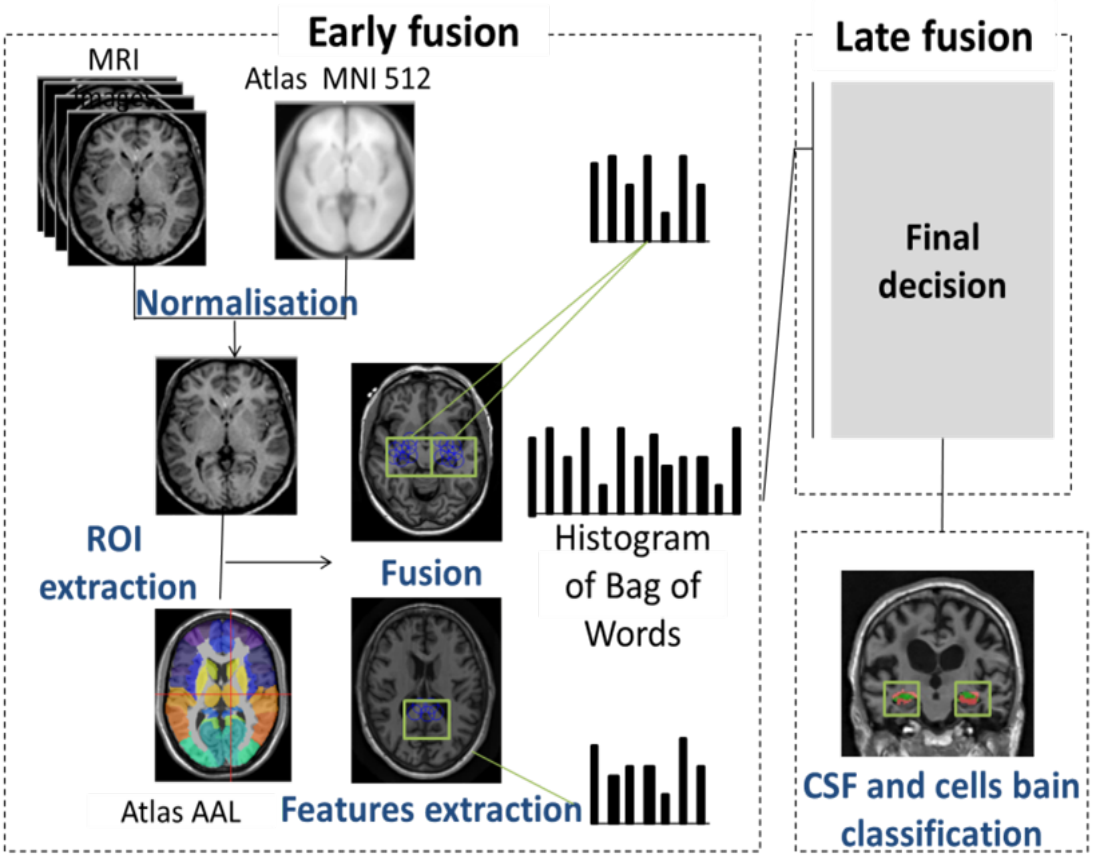

Figure 5.4: Hybrid Fusion framework description

5.3.2 Late fusion for subjects retrieval

In (Mizotin et al., 2012), the preliminary classification was combined with similarity measurement and several schemes of CBVIR were tested (Equation 5.2) but no significant difference of results with different sampling strategies: dense or sparse for the proposed scheme of brain image retrieval has been found. This fact corresponds with the results of the paper (Nowak et al., 2006). Minor advantages and limits however exist. An overview of the proposed hybrid fusion approach is presented in figure 5.4.

For a given query scan $Q(x, y, z)$, the features are computed using the same process resulting in its signature h^*. Image similarity is established by comparing the signatures, smaller distance means more similarity. For histogram comparison, the metric that has been chosen is $L1$:

$$d_q = D(h^*, h^q) = \sum_{i=1}^{6K} |h^* - h^q| \tag{5.1}$$

Were h^q is a signature of a brain q in a database and K is the codebook size.

The concatenation of histograms and application of PCA constitute the early fusion process. Using the Bayesian classification approach from completely different perspective, namely the presence of CSF on Hippocampus ROI, we define for the query image $Q(x, y, z)$, the probabilities to belong to three classes (AD, NC, MCI respectively). The combined dissimilarity is then obtained by multiplication fusion operator:

$$d_n^{class} = (-\ln(p_{classof(n)}) * d_n) \tag{5.2}$$

Finally,

$$similarity\,to\,n^{th}\,image = 1/d_n^{class} \tag{5.3}$$

This is the late fusion part of our hybrid fusion approach. We apply this fusion as it proved to be efficient on classification into three classes in (Mizotin et al., 2012).

5.3.3 Experiments and results

To perform the test, the ground truth data on the image similarity is needed; this information however is not available. Moreover, the similarity from a medical point of view would be different for different experts. Thus, in our testing procedure we only test for correct class correspondence (AD, NC, and MCI). Indeed, the images from the same class should be more similar than images from other classes and the retrieval precision can be calculated as the percentage of correct image classes in the first N retrieved images. To increase the number of experiments and precision of statistics full cross-validation is performed, (we are repeating the test for each image in our test dataset taking as the database the rest of the images). We compute average precision at N which is a variant of Average precision where only the top N ranked images are considered:

- *Precision at* N^{th} *= Number of images correctly classified/N*

Data used in this section consist in subset from of the **ADNI** database **(Group 1)**. In addition, **"Bordeaux-3City"** data **(Group 3)** is used to evaluate the proposed method. Informations about subjects are given in Section 3.4.

AD-patients versus Normal Controls using only hippocampus ROI

In the first part of experiments, we evaluated the BoVW approach on the hippocampus area to distinguish between AD and NC. For **ADNI** subset **(Group1)**, we varied the codebook size from 50 to 400. The best recognition rate was obtained for a codebook size of 210. Retrieval results are plotted in Figure 5.5.

The performance, presented by precision at 1^{th}, of the BoVW reaches 77.2% in the case of only 2 classes (NC and AD) compared to (Mizotin et al., 2012) (74% and 68% were obtained respectively with "CHF one to one" and "CHF-BOF "schemes). For the SIFT descriptor, we obtain 69% which is better than retrieval rate reached by "SIFT one to one" scheme (64%) (Mizotin et al., 2012).

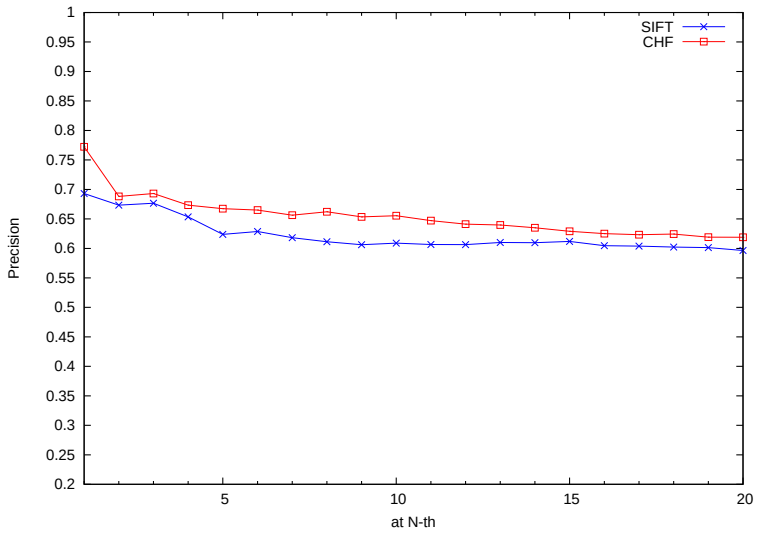

Figure 5.5: Precision of retrieval at N^{th} on the **ADNI** subset **(Group 1)**: AD versus NC. Both SIFT and the CHF descriptors are tested. Features used are extracted from only the Hippocampus ROI (K=210).

MCI retrieval using Hippocampus and PCC ROIs features fusion

The MCI category is the most difficult to recognize, as the structural changes in the characteristic brain regions are very unequal.

Precision (%)	Descriptor	Hippocampus	Early Fusion	Hybrid fusion
At 1^{th}	SIFT	37.6%	46.1%	50.8%
	CHF	45.7%	52%	51.32%
At 3^{th}	SIFT	39%	44.3 %	48.68%
	CHF	41.7%	48.1%	48.4%
At 10^{th}	SIFT	37.4%	41.7%	45.71%
	CHF	40 %	42%	46.26%
At 20^{th}	SIFT	37.4 %	41%	43.67%
	CHF	38.6%	42%	44.21%

Table 5.1: Average precision at N^{th} using only Hippocampus features, early fusion of both Hippocampus and PCC signatures and hybrid fusion. **ADNI** subset **(Group 1)**(AD, NC and MCI).

In the case of three classes retrieval, performance using only hippocampus drops to 37.6% for SIFT descriptor (see Table 5.1), the most likely reasons are that MCI class is a transition between AD and NC thus the bounds are uncertain. As we mentioned in the previous sections, the PCC alteration can be a predictive biomarker of rapid conversion to AD and hence should characterize the MCI cases. Therefore, we extract features from both hippocampus and PCC

areas. In the first BoVW experiment, we apply an early fusion approach and concatenate hippocampus and PCC signatures in global BoVW from three projections and both regions are thus concatenated in the description space. The most relevant precision was obtained with a codebook $K = 350$ yielding a signature size of 2100: $(K * projectionsnumber * 2)$. In the second experiment, we used the PCA technique to reduce the signature size to 69 for CHF and to 24 for SIFT. These dimensions were obtained experimentally by varying the number of principal components on **ADNI** group. In this case, the performance was higher by 4% for PCA on concatenated signatures compared to early signatures fusion without PCA (Figure 5.6).

As shown in Figure 5.7, the precision of the descriptor based retrieval when using PCC and Hippocampus signatures fusion is greater than precision when using only hippocampus area.

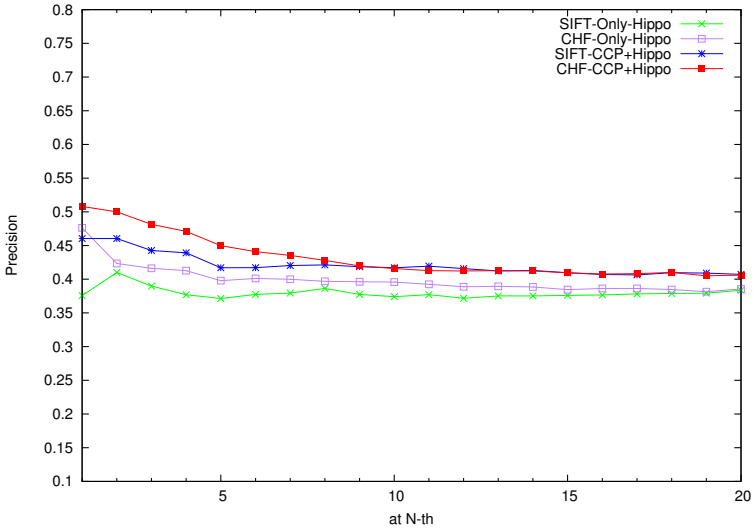

Figure 5.6: Precision of retrieval at N^{th} on the **ADNI** subset **(Group 1)**: Precision at Nth with and without PCA concatenation.

Fusion strategy increases results by an average of 6% while the fusion by dark pixel volume primary classification proposed in (Mizotin et al., 2012) gave only 5% of amelioration to only hippocampus classification. From Table 5.1 it can be seen that: The performance of image retrieval is substantially:

- improved by 10% using the hybrid fusion compared to classification using only hippocampus.

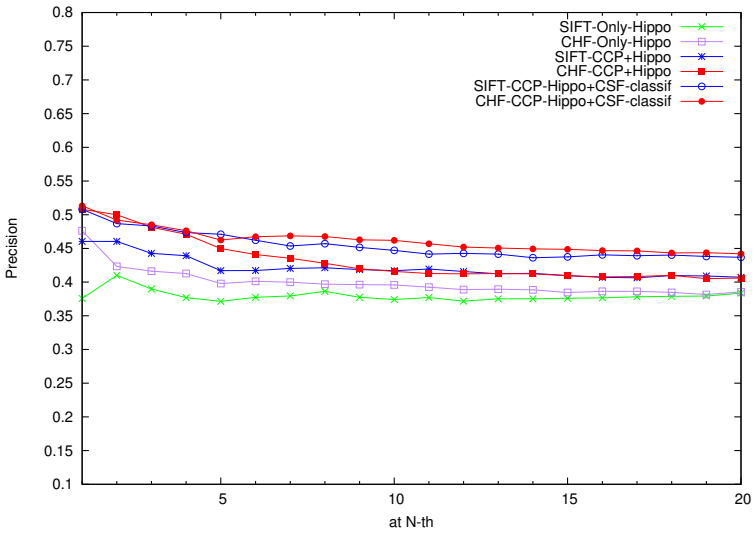

Figure 5.7: Precision of retrieval at N^{th} on the **ADNI** subset **(Group 1)**: Hybrid fusion

- obtained results exceed the reported results in (Mizotin et al., 2012) at 10^{th} as well at 20^{th} which are the more challenging.

- When using our early fusion approach to describe images (CHFs case), retrieval precision at 1^th is about 52% while when using only preliminary classification, precision drops to 45% (Mizotin et al., 2012).

Compared to the results presented in (Mizotin et al., 2012), the precision at 10^{th} and 20^{th} obtained on the same data are higher in the case of our full fusion schemes. In Table 5.1, we have 46.2% (column 5 line 3) versus 42% and 44.2% (column 5 line 4) versus 38%. Although we used only a pure visual image description, we obtain better results than (Agarwal and Mostafa, 2010) in which authors combine visual features with textual data.

In a second part of experiments, we evaluate the proposed approach on the **"Bordeaux-3City"** data **(Group 3)** (Section 3.6). The obtained results are presented in Figure 5.8.

Precision reaches 68% for CHF descriptors and 57% for SIFT descriptors.

From obtained results, CHFs features outperform SIFT by ($\Delta = 3 \pm 2$ %) on the **ADNI** subset **(Group 1)** and by ($\Delta = 4.8 \pm 3.9$ %) on the **"Bordeaux-3City"** subset **(Group 3)**.

From this section, we can conclude that using visual similarity between MRI images allowed us to provide the clinicians with semantic similarity, and thus could potentially

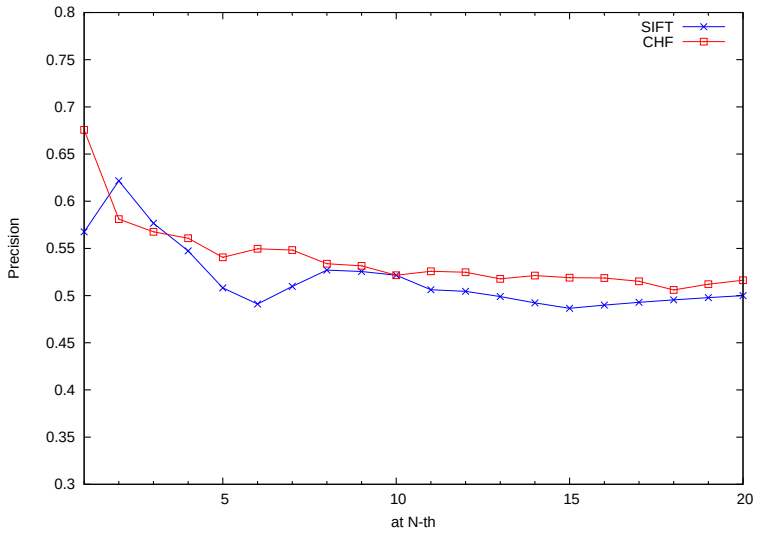

Figure 5.8: Precision of retrieval at N^{th} on **"Bordeaux-3City" (Group 3)**: AD versus NC subjects. Both SIFT and CHF descriptors are tested. Features used are visual descriptors extracted in Hippocampus and PCC ROIs.

support their diagnostic decision. PCC and hippocampus features fusion improve accuracy on MCI case retrieval. Across a range of tests, useful level of recognition rates were achieved with a small signature sizes for both CHFs and SIFT descriptors. In the next section, we will increase the number of subjects and use a supervised learning approach to classify between subjects.

5.4 Content-based classification of AD subjects using late fusion and CHFs

In this section we propose a computer-aided approach based on classification of AD subjects. We use features extraction from both ROIs: Hippocampus and PCC to build a signature-related atrophy. Referring to the previous chapters, CHFs prove to be more efficient than SIFT or SURF descriptors. Thus, in this section we retain the image decomposition on the basis of Circular Harmonic Functions on those areas to extract representative features. Figure 5.9 depicts a block-diagram of the classification framework. The approach we propose in this section also starts with brain image normalization, which is a standard step in brain image comparison. Then, ROIs are extracted from normalized images to be described by

local visual descriptors and quantified in the BoVW framework. To reduce dimensionality, we consider percentages of total energy which is obtained from cumulative energy vector. As the percentage of energy is reduced, the number of coefficients required also drastically reduces, and according the candidate feature vector size is reduced for classification.

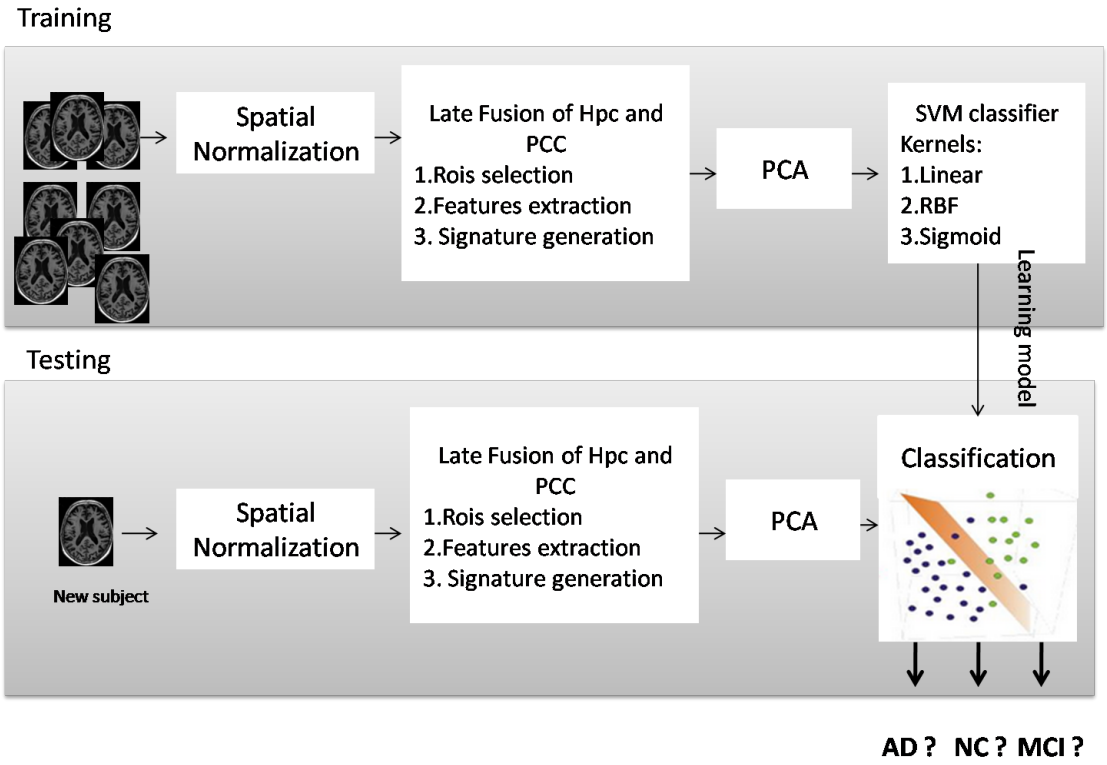

Figure 5.9: Classification framework.

In this work, libSVM package [1] was used for the binary classification (two classes (In our case: (AD versus NC, NC versus MCI and AD versus MCI)). Different kernels were applied: linear, sigmoid and Radial Basic Functions (RBF) kernels. Note that typically an SVM requires a fixed length vector that characterizes globally the subject to be classified. This is the case in our method: due to the BoVW representation, a subject brain is encoded by a set of quantized local features.

[1] http://www.csie.ntu.edu.tw/~cjlin/libsvm/

5.4.1 Choice of SVM optimal parameters

SVM searches to find the optimal hyperplane that best separates the positive and negative training samples. The optimization problem to resolve, in the case of the so-called "soft margin" classification, is the following:

$$\begin{aligned} &minimize_{w,\xi} \quad \frac{1}{2}\|w\|^2 + \frac{C}{n}\sum_{i=1}^{n}\xi_i \\ &subject\,to \quad y_i(w^T x_i + b) \geq 1 - \xi_i, \xi_i \geq 0 \end{aligned} \tag{5.4}$$

The ξ_i are the so-called slack variables relaxing class-separators constraints and C is a cost parameter that controls the trade-off between allowing training errors and forcing rigid margins. The kernel function may transform the data into a higher dimensional space to make the separation possible. In this section, several kernels are tested:

- Linear kernel : $\gamma u^T * v$, $\gamma = 1$
- Radial Basis Function: $exp(-\gamma * |u - v|^2)$
- Sigmoid : $tanh(\gamma * u^T * v + r)$

Parameter setting for Support Vector Machines is critical to obtain good performance. Hence, we need to select optimal kernel function parameters and the soft margin parameter C. We use a grid search on the log ratio of the parameters associated with cross validation. Then, value pairs (C, γ) are assessed using cross validation and then the pair with highest accuracy is chosen. The value of C and γ are exponentially varied ($C = 2e^{-6}, 2e^{3}, ..., 2e^{14}$; $\gamma = 2e^{-15}, ..., 2e^{10}$). Thus, the grid search has built dozens of SVM models with various parameter settings, and optimal parameters relatively to the training data were selected. Figure 5.10 illustrates an example parameters optimization using grid search in the case of NC versus MCI classification. The kernel used is a Gaussian kernel: The numbers at the top are what we are most interested in. The first number (32) is C, and the second number (0.5) is γ. Note that the current cross-validation accuracy is 67.033%.

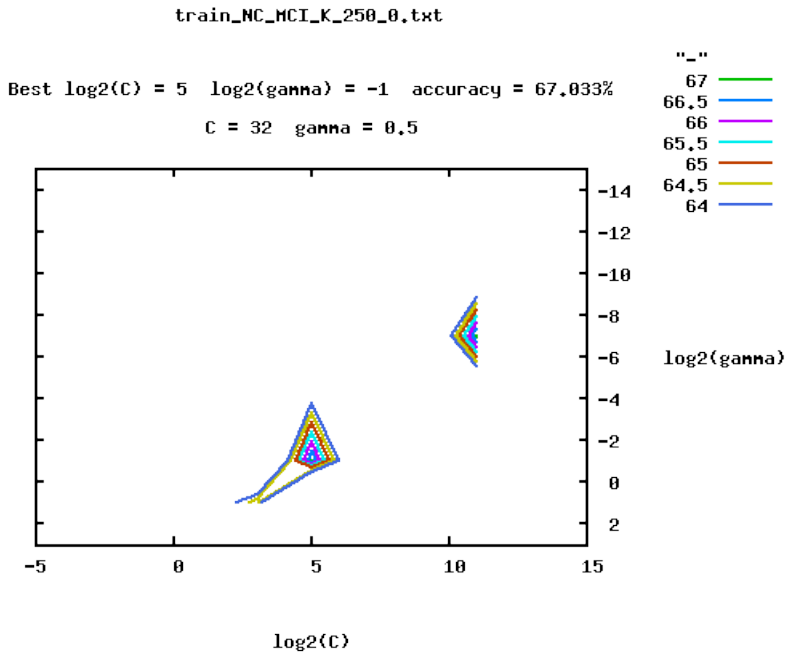

Figure 5.10: Contour plot of grid search result showing optimum values for SVM parameters.

5.4.2 Metrics of evaluation

To evaluate classifier performance, we computed overall classification accuracy, sensitivity, and specificity . These metrics describe the degree to which hippocampus and PCC features are informative when predicting NC vs AD, NC vs MCI and AD vs MCI. See Section 4.5.1.

5.4.3 Experiments and results

Data used in this sections are **Group 1**, **Group 2** and **Group 3**(More details in Section 3.4). Pattern classification with SVM was applied separately in each of two groups (NC vs AD, NC vs MCI and MCI vs AD).

We start by testing the classification approach on the **Group 1**. For that, we use a (Leave One Out Cross Validation (LOOCV)) method. This approach has become increasingly popular in Neuroimaging. Cross-validation is primarily a way of measuring the predictive performance of a model. Therefore, the original sample set was randomly divided into k folds. Then, one fold was used as test and the remaining $k-1$ folds were used as training

data. Classification results are given in Table 5.2

	Only Hippocampus			Hippocampus and PCC		
	Linear	RBF	Sigmoid	Linear	RBF	Sigmoid
AD versus NC						
Accuracy	73.27%	76.2%	73.24%	79.21%	80.2%	75.25%
Specificity	73.92%	78.13%	76.2%	74%	84%	77.78%
Sensitivity	71.88%	72.98%	68.43%	83.34%	75.61%	71.06%
BAC	72.9%	75.6%	72.31%	80.4%	80%	74.42%
NC versus MCI						
Accuracy	64.2%	64.67%	66.22%	74.33%	78.38%	77.71%
Specificity	70.12%	70.46%	70.22%	76.05%	79.79 %	79.59%
Sensitivity	55.74%	56.67%	59.26%	71.16%	75.93%	74.55%
BAC	62.93%	63.57%	64.74%	73.60%	77.86%	77.05 %
AD versus MCI						
Accuracy	70.78%	70.78%	70.08%	73.23%	74.02%	78.75%
Specificity	90.81%	91.96%	89.66%	93.11%	82.76%	90.81 %
Sensitivity	27.5 %	25%	27.5%	30%	55%	52.5%
BAC	59.16 %	58.48%	58.5 %	61.11%	68.87%	71.65%

Table 5.2: Classification results for **Group 1**: Performance comparison for classification of AD versus NC, MCI versus NC and AD versus MCI on only Hippocampus features and the fusion of both Hippocampus and PCC features. Classification is done using SVM with several kernels: Linear, Radial Basic Function (RBF) and Sigmoid. Metrics of evaluation are accuracy, specificity, sensitivity and BAC.

AD-patients versus Normal Controls

Comparing AD versus NC on **Group 1** we found an accuracy of 76.2%, a 72.98% of sensitivity and a specificity of 78.13% using hippocampal CHF features alone. Combining both PCC and hippocampus signatures resulted in an accuracy of 80.2%, a sensitivity of 75.61% and a specificity of 84%. The best results are obtained using an RBF kernel.

Normals Controls versus Mild Cognitive Impairment

We also classified NC versus MCI subjects of the **Group 1** using the hippocampus and PCC visual features. We achieved an accuracy of 78.38%, a sensitivity of 75.93 and a specificity of 79.79%.

AD-patients versus Mild Cognitive Impairment

Comparing AD with MCI on **ADNI** subset **(Group 1)**, we found an accuracy of 78.75%, a sensitivity of 52.5% and a specificity of 90.81%. The best results are obtained using an sigmoid kernel.

In the second part of experiments we take data of **Group 2** for a comparison propose with a volumetric approach proposed in (Yang et al., 2012). We used 10 fold cross validations to evaluate classification performance. We repeated the 10 fold cross-validation 50 times for a more general performance estimation of the classifier. Each time the 10 randomly selected folds were generated and the final result is the average accuracy, sensitivity and specificity of the 50 experiments. Table 5.3 summarizes the averaged results. We reported the 95% Confidence Interval (CI) of accuracy, sensitivity and specificity. We tested classification methods on Hpc features alone and then on Hpc and PCC features combined together.

Experiments were conducted first on the scans of **Group 2** and then on the structural MRI data from the **"Bordeaux-3City"** subset **(Group 3)** (Table 5.4). It should be noted that metric values presented in Table 5.4 and Table 5.3 as well as confidence interval's boundaries are rounded to the nearest decimal number using the Gaussian rounding method.

In this section the accuracy, sensitivity and specificity of the classifier are considered as the average accuracy of N tests. Estimating the error and the confidence intervals (CI) in an observation is a crucial issue in statistics if one wants to make predictions about what is likely to happen when repeating the experiment any number of times. The CI provides information about what is expected to result from a test, with a certain confidence level $1 - \alpha$, α value between 0 and 1 . In other words, this interval is the range of values in between the variable is expected to be located, with a probability $1 - \alpha$.

AD-patients versus Normal Controls

When comparing performance of classification methods, we select the best results according to the BAC metric. Comparing AD with Normal controls on the **Group 2** of the **ADNI** data, the best results achieved with Hippocampus ROI alone are 80.4% accuracy, 74.2% specificity and 82.8% sensitivity. The best results achieved with early fusion of hippocampus and PCC features are better. Namely, we obtain an increase of 3.3% in accuracy, 4.6% in

	Only Hippocampus			Hippocampus and PCC		
	Linear	RBF	Sigmoid	Linear	RBF	Sigmoid
AD versus NC						
Acc%[95%CI]	75.3[74.8 75.9]	80.4[80 80.9]	79.5[79 79.7]	80.17[80 80.4]	83.7[83.2 84.3]	82.9[82.8 83]
Spe%[95%CI]	64.1[63.1 64.9]	74.2[73.5 74.8]	72.4[72.1 72.5]	71.9[71.6 72.2]	78.8[78 79.5]	75.1[74.8 75.3]
Sen%[95%CI]	79.9[79.4 80.2]	82.8[82.5 83.1]	82.1[82 82.6]	83.7[83.5 83.8]	85.7[85.6 86]	86.5[86.4 86.7]
BAC%	72	78.5	77.25	77.8	82.25	80.8
NC versus MCI						
Acc%[95%CI]	60.1[59.6 60.2]	62.2[61.6 62.8]	62[61.1 62.9]	65.8[65.6.66]	66.7[66.3 67.2]	65.2[64.9 65.4]
Spe%[95% CI]	68.3[67.7 68.9]	69.1[68.6 69.6]	68.7[68 69.4]	66.8[66.6 66.9]	68.3[68 68.6]	71.3[71 71.4]
Sen%[95%CI]	51.8[51.1 52.5]	51.9[51.2 52.6]	51.8[50.6 52.9]	62.1[61.6 62.6]	62[61.1 62.9]	55.8[55.4 56]
BAC %	60.1	60.5	60.2	64.4	65.2	63.5
AD versus MCI						
Acc%[95%CI]	70[69.8 70.3]	74.2[74 74.3]	70.1[68.8 70.2]	74.5[74.1 74.9]	76.5[76.2 76.9]	75.9[75 76.3]
Spe%[95% CI]	32.6[32.1 33]	39.3[38.6 40]	32.7[32.2 33]	45.3[44.2 46.4]	52.8[52.2 54]	49.6[49.1 50]
Sen%[95% CI]	77.8[77.7 78]	77.5[77 77.7]	77.9[77 80]	80.6[80.4 80.7]	78.9[78.6 79.2]	79.9[79.6 80.1]
BAC %	55.2	58.4	55.3	62.95	65.85	64.75

Table 5.3: Classification results for **Group 2**: Performance comparison for classification of AD versus NC, MCI versus NC and AD versus MCI on only Hippocampus features and the fusion of both Hippocampus and PCC features. Classification is done using SVM with several kernels: Linear, Radial Basic Function (RBF) and Sigmoid . Metrics of evaluation are accuracy, specificity and sensitivity and BAC.

	Only Hippocampus			Hippocampus and PCC		
	Linear	RBF	Sigmoid	Linear	RBF	Sigmoid
Acc%[95% CI]	64.7[63.9 65.4]	65.7[65 66.3]	65.1[63.8 66.2]	73 [72.2 73.7]	78[77.3 78.6]	73.6[72.1 75.1]
Spe%[95% CI]	70.5[69.8 71.2]	69[68.3 69.7]	67.4[66.5 68.2]	78.5[77.8 79.2]	80.4[79.9 80.9]	77.9[76.4 79.3]
Sen%[95% CI]	58.3[57.5 59.1]	60.9[60.1 61.6]	61.3[59.5 63.1]	67[66.1 67.9]	74.7[73.8 75.6]	68.9[67 70.7]
BAC (%)	64.4	64.9	64.3	72.7	77.6	73.4

Table 5.4: Classification results: **Group 3**: Performance comparison for classification of AD versus NC on only Hippocampus features and the fusion of both Hippocampus and PCC features. Classification is done using SVM with several kernels: Linear, Radial Basic Function (RBF) and Sigmoid. metrics of evaluation are accuracy , specificity, sensitivity and BAC.

specificity and 2.9% in sensitivity. In both cases, results have been achieved with an RBF kernel. For the **"Bordeaux-3City"** group (see Table 5.4), the performance improvements when using the fusion of ROIs features are even stronger. Indeed, the reported increase in all metrics is more than 11%.

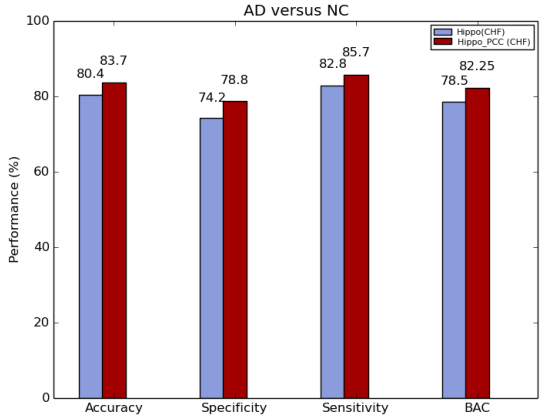

Figure 5.11: AD vs NC Performance comparison (ADNI subest)

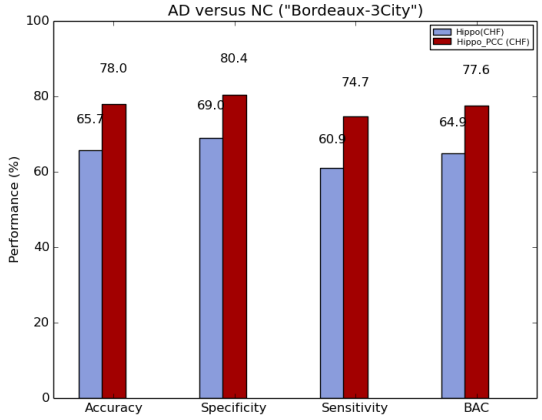

Figure 5.12: AD vs NC Performance comparison (Bordeaux-3City subset)

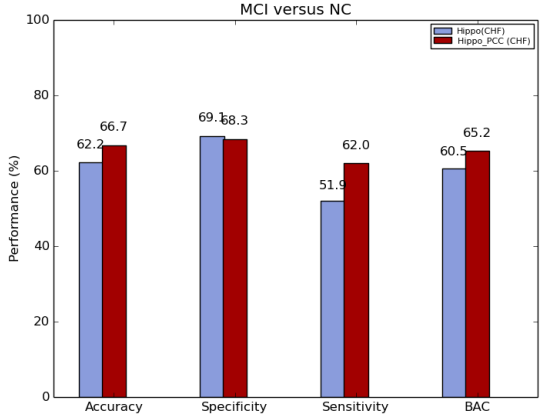

Figure 5.13: MCI vs NC Performance comparison (ADNI subest)

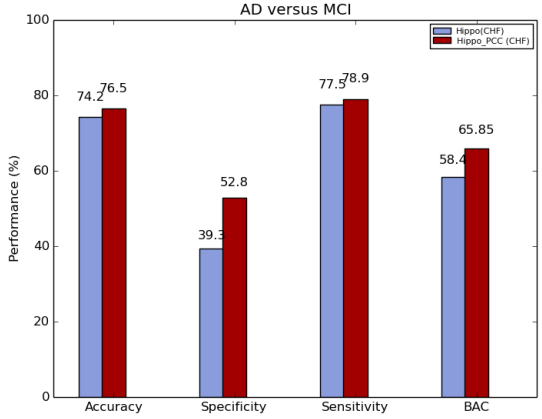

Figure 5.14: MCI vs AD Performance comparison (ADNI subest)

Normal Controls versus MCI patients

We also classified NC versus MCI subjects of the **Group 2** of the **ADNI** dataset using Hippocampus and PCC visual features. When using the proposed fusion method, the accuracy increases by 4.5%. Sensitivity is 10.1% higher and specificity is slightly lower (0.8%).

AD patients versus MCI patients

Comparing AD with MCI on the ADNI dataset, the use of combined visual features extracted from two ROIs increases accuracy by 2.3% specificity by 13.5% and sensitivity by 1.4%. We

note that when the MCI category is considered, the fusion of visual features derived from both Hpc and PCC regions gives strong increase in reported results. Heterogeneity of MCI class Accounts for such results. In fact, the MCI is a transition state between the Normal and Alzheimer state and structural changes on hippocampus are not yet clearly pronounced.

We can clearly conclude that the fusion of both ROIs features outperforms the use of hippocampus features alone. It is noteworthy that we made higher improvements in the more challenged and important tasks: classifying AD versus MCI and NC versus MCI for early diagnosis and treatment.

5.4.4 Statistical evaluation

To further validate the effectiveness of fusion scheme, we also assessed the statistical significance of differences between values of accuracy, sensitivity and specificity obtained when using Hpc alone versus the fusion of hippocampus with PCC. Paired student t-tests were conducted using the classification measures values corresponding to each of cross validation runs, with the null hypothesis being no improvement in performance when we use the two ROIs fusion. The tests were performed with the results obtained with an RBF kernel.

	Accuracy	Sensitivity	specificity
p-value (AD vs NC)	$3.597^{-7} < 0.001$	$3.152^{-7} < 0.001$	$7.468^{-9} < 0.001$
p-value (MCI vs NC)	$3.211e^{-12} < 0.001$	$3.828^{-14} < 0.001$	$0.0002879 < 0.001$
p-value (AD vs MCI)	$1.326e^{-9} < 0.001$	$1.749e^{-9} < 0.001$	$1.111e^{-15} < 0.001$

Table 5.5: Statistical significance (paired-student t test) between the classification results obtained from using only hippocampal features and fusion of features from hippocampus and PCC respectively.

We found that $p - value < 0.001$ for all binary classification tasks (AD vs NC, NC vs MCI and AD vs MCI) (see Table 5.5). This means that we can confidently reject the null hypothesis and declare that adding the PCC features has shown a statistically significant improvement in the experiment compared to the use of hippocampus features alone. This suggests that integrating structural features from both hippocampus and PCC offers optimal results for AD subjects classification.

5.5 Discussion

In this chapter, we proposed a visual feature-based methods to provide clinical researchers with semantic similarity and to assist in the diagnostic AD process. We used visual similarity between baseline MRI to recognize three groups of subjects (AD, NC and MCI). An exact comparison with previous works is complicated since most of the proposed works in this subjects have used different statistical methods and several image analysis methods on different datasets. In addition, the differences demographic and clinical information of the subjects, the size of used data, severity of disease, duration of disease might account for the discrepancy between the current work and previous works. Furthermore, since the ADNI study is still ongoing, several subjects labeled as MCI will progress in the future to the AD group. In the following, we start by comparing our proposed method with a volumetric method proposed in (Yang et al., 2012).

5.5.1 Comparison with a sate-of-the-art volumetric method

Although the images are not exactly the same, we used the same data partition with a closed demographic characteristic as in (Yang et al., 2012). The authors in (Yang et al., 2012) use the hippocampal volume to distinguish MCI and AD from NC as well as AD from MCI. Our CHFs description of hippocampus preforms well in separating AD vs NC. In fact we obtained 80.4% accuracy, 74.2% specificity and 82.2% sensitivity compared to respectively 65.5%, 73.3% and 57.8% reported in (Yang et al., 2012). For MCI vs NC, we obtained better accuracy and specificity but lower sensitivity. In addition, for the most challenging classification task (AD vs MCI) we obtained much better results with 74.2% accuracy and higher sensitivity and specificity. It should be noted that the hippocampus ROI is extracted in (Yang et al., 2012) using the Freesurfer software which is time-consuming and depends on preliminary segmentation guided by expert knowledge of the location of the ROI. In this work, we used an automatic atlas-based parcellisation method and we obtained highly efficient classification results compared to the time-consuming segmentation executed by human experts, or by a specific software. However, volumetric analysis only assesses global changes of the ROI. On the other hand, content-based analysis methods can unveil local

atrophy of the ROI and then give more information about the disease.

5.5.2 Descriptor selection

Each individual subject's scan is represented as a collection of discrete features on two characteristic ROIs: Hippocampus and PCC. This information was used to discriminate the MCI and AD subjects from normal controls, as well as between the MCI and AD patients. To position our contribution with regard to other feature-based approaches, we would cite the work (Toews et al., 2010). Here, the authors proposed a features-based morphometry method to analyze the structural local changes of the brain. The method is based on learning a probabilistic model of local SIFT descriptors that reflect group-related anatomical characteristics. Only classification results for AD versus NC were provided in their paper. It was performed on the OASIS dataset. Indeed, SIFT or their approximated version SURF features, are not optimal for MRI with the lack of pronounced high frequency texture and clear structural models.

We used image descriptors better adapted to the MRI in the content-based approach: the CHF features. As shown, the results of CBVIR by similarity-search approach outperformed conventional SIFT descriptors on both ADNI and **"Bordeaux-3City"** datasets. That is why we choose to use them with a learning approach based on the SVM classifiers to classify patients. CHFs have a good property of capturing smooth contrasts which are characteristic of the structural brain MRI. Furthermore, these features are computed on patches inside the ROI or selected on the whole brain. They convey local structural information of image signals.

5.5.3 Specific attention to MCI category and ROI selection

All combinations for patients classification were considered on ADNI database: AD vs NC, NC vs MCI and AD vs MCI. The MCI category is the most difficult to recognize, as the structural changes in the characteristic brain regions are very unequal. Nevertheless, AD research has shifted to MCI in recent years, in the hope of tracking AD progression and resisting it, before individual progress to AD. We showed that the use of two characteristic

regions (Hippocampus and PCC) systematically outperforms the classification results obtained when only the Hippocampus is used. According to Table 5.3, the BAC quality metric is increased by at least 5% when classifying groups with MCI. The similarity between MCI and AD categories was supported by the complementary description of PCC.

Table 5.6 presents classification results of a selection of very cited works in the field of classification AD subjects. Here, compared to other works that used the Hippocampus ROI only (Colliot et al., 2008), where the authors proposed an individual classification based on the Hippocampus volume, our method performs better. Indeed, (Colliot et al., 2008) achieved a 69% of correct classification rate between MCI patients and AD, while we achieved 76.5% accuracy for this case. Even if two ROIs were used in previous research, such as Hippocampus and entorhinal cortex (Fan et al., 2008), our approach performs better in the case of MCI versus AD classification. The most likely reason for this is that the Hippocampus region is less spatially correlated with PCC than the entorhinal cortex, which makes highest discriminative patterns for AD diagnostics. Indeed, in (Fan et al., 2008), the cross validation accuracy of voxel-based approach for the classification of AD vs MCI is 74.3% (and 58%when using the ROI volumetry). In our case applied to two ROIs together, it is 76.5% on the ADNI dataset.

If we compare our approach with two ROIs: Hippocampus and PCC, with the approach of (Zhang et al., 2011), which uses the gray matter maps, we can state the following. In the latter, authors extract volumetric features from the 93 ROIs in the gray matter maps and classify them using SVM (as this is the case of our classification framework). The accuracies of the proposed methods on classifying NC vs MCI are 72% along with 78.5% sensitivity and 59.5% specificity. Our figures on ADNI dataset are (see Table 5.3) 66.7% accuracy, 68.3% specificity and 62% sensitivity respectively. Therefore, based on this analysis, we can conclude that the choice of Hippocampus and PCC is better for the classification problem we have addressed.

To compare with a voxel based approach we select the work of (Klöppel et al., 2008). In this work, the authors used temporal lobe and Hippocampus regions features analysis. For MCI versus NC classification, the authors obtained lower accuracies than us (63% for the whole brain and 71% for ROI), compared to 66.7% achieved by our proposed approach. Furthermore, the ROI approach requires a segmentation step which is time-consuming and

Works	Subjects	Results	AD vs NC	MCI vs NC	MCI vs AD
(Colliot et al., 2008)	25 AD+ 25 NC +24 MCI	Acc	84%	73%	69%
		Sens	84%	75%	67%
		Spe	84%	70%	71%
(Fan et al., 2008)	56 AD+ 66 NC +88 MCI	Acc	94.3%/82%	81.8%/76%	74.3%/58.3%
		Sens	-	-	-
		Spe	-	-	-
(Zhang et al., 2011)	51 AD+ 52 NC +99 MCI	Acc	86.2%	72%	-
		Sens	86 %	78.5%	-
		Spe	86.3%	59.6%	-
(Klöppel et al., 2008) Whole brain	23 AD+ 25 NC +23 MCI	Acc	90%	63%	-
		Sens	-	-	-
		Spe	-	-	-
(Klöppel et al., 2008) ROIs	23 AD+ 25 NC +23 MCI	Acc	86%	71%	-
		Sens	-	-	-
		Spe	-	-	-
(Cuingnet et al., 2011)	162 NC + 137 AD + 76 MCI	Acc	88.6%	81.17%	-
		Sens	95%	85%	-
		Spe	81%	73%	-
(Wee et al., 2013) (hippocampus volume)	198 AD+ 200 NC + 200 MCI	Acc	81.54%	72.78%	63.43%
		Sens	76.92%	67.55%	65.66%
		Spe	86.15%	78%	61.26%
(Yang et al., 2012)	35 AD+ 72 NC + 111 MCI	Acc	85.4%	72%	60.9%
		Sens	88.8%	70.1%	80.4%
		Spe	82%	73.9%	41.4%
The proposed early fusion Chapter 5	35 AD+ 72 NC +111 MCI	Acc	83.7%	66.7%	76.5%
		Sens	85.7%	62%	78.9%
		Spe	78.8%	68.3%	52.8%
The proposed late fusion Chapter 4	35 AD+ 72 NC +111 MCI	Acc	87%	78.22%	72.23%
		Sens	75.5%	70.73%	75%
		Spe	100%	83.34%	70%

Table 5.6: Classification results of Normal control (NC) Alzheimer disease (AD) and Mil cognitive impairment (MCI) patients reported by some woks in the literature compared to our proposed methods

for practical diagnostics we need a system that gives a quick decision. (Klöppel et al., 2008) proposed another method based on the whole brain. In this case, features were extracted from several brain areas and classified by SVM. They reached an accuracy of 90% which is higher than ours. The whole brain approach gives better results but with much more information. Furthermore, finer classification performances (specificity, sensitivity) are not available in their paper. However, the AD group used in the latter are with 16.7 mean MMSE (more severe Alzheimer's) which is more easy to detect. Finally, a thorough comparison between our methods and others proposed works in the literature is hard to do because different data were used. Nevertheless, on the basis of reported correct classification rates and MMSE

values, it can be concluded that the method proposed in the current research is comparable to volumetric/voxel-based methods and even better in same cases.

5.5.4 Atlas-based approach vs accurate segmentation

Generally, methods based on manual hippocampal delimitation reported classification rates be- tween 80% and 95% (Xu et al., 2000; Jack et al., 1992). However, the discriminating power of the hippocampus volume was lower in the MCI case. Classification methods that used a manual segmentation of the hippocampus reported classification rates of raging between 60% and 74% (Convit et al., 1997; Pennanen et al., 2004; Xu et al., 2000) for MCI patients. Hence, our results obtained using an atlas-based method are promising and even better compared to the results obtained with the time-consuming and user-depend manuel segmentation method.

The advantage of our approach which performs on ROIs consists in the fact, that feature-based description compensates inaccuracies of selection of the ROIs with an atlas based approach. It does not require any segmentation of ROI, but only a rough selection as ensured by AAL. The AAL can model different structures with similar intensity values. In contrast, accurate manual segmentation techniques are time-consuming and present delimitation imprecision. Other proposed techniques are computationally expensive (run-time of hours to days) (Chupin et al., 2009a) or require expert neuroanatomical knowledge (Cuingnet et al., 2011). Therefore, they are not always practical in a clinical setting. Using a simple atlas based method, we built a fast framework to classify AD subjects. Although AAL was not designed for studying patients with AD, through the use of local CHF descriptors, we can adequately capture the pathological structure (e.g. shrunken Hippocampus) vs a normal one thanks to different signal types captured by CHFs inside the ROI. The main advantage of our method is its ability to capture atrophy patterns of progressive neurological disorders and then overcome the drawbacks of the Atlas based segmentation methods.

5.5.5 Time efficiency

Our platform is implemented in C/C++. The Average diagnosis time per scan (including the preprocessing step done with matlab) is about 6.3 minutes. Tests are done using an

Intel processor with 4 GO memory. It is to note that computational time depends on the number of scans, software and used hardware. In our experiments it is an average spread for one query as: 2.5 minutes for preprocessing, 0.7 minutes for features computation and 3.1 minutes for classification.Indeed, the results are obtained with a lower number of features. Also, the proposed framework is able to classify new subjects based on a single time point contrary to longitudinal studies.

5.6 Conclusion

In this chapter, we introduced a new approach to discriminate subjects in epidemiological studies of AD using structural MRI. The approach does not require a precise segmentation of ROIs, and belongs to the feature-based family of methods. The features we used, Circular Harmonics Functions, convey 2D information in each scan. This information was used to effectively discriminate the MCI and AD patients from normal controls, as well as between the MCI and AD patients. Compared to our previous works, the method used two characteristic ROIs: Hippocampus area and Posterior Cingulate Cortex. Despite difficulties in visual inspection of the latter in the diagnosis process, the fusion of features from both regions improves classification results.

Unlike the method requiring precise segmentation of ROIs our approach is less time-consuming, computer-based and does not require the intervention of an expert. Results are promising and indicate that the combination of Hippocampus and PCC atrophy captured by specific CHF features gives a good indicator to the diagnostics.Structural MRI have demonstrated effectiveness in detecting brain macrostructural atrophy. However, they failed in detecting microstructural alterations. In the next chapter, we will consider the use of other MRI modalities: the Tensor Diffusion Imaging for AD subject retrieval and classification at the microscopic level.

Chapter 6

Features-based approach for Alzheimer disease diagnosis using visual pattern of water diffusion in MD maps

Contents

6.1 Introduction

Structural Magnetic Resonance Imaging (sMRI) have long time been the most used modality to detect regional neurodegeneration in AD studies. Most investigations using structural MRI have focus on measuring atrophy of some Regions of Interest known to be affected by AD such as the hippocampus and the entorhinal cortex. Despite effectiveness of structural MRI in detecting macro structural loss for AD diagnosis, micro-structural changes remain not visible in anatomical scans but can be clearly delineated in other MRI modalities such as Diffusion Tensor Imaging (DTI).

DTI is a recent MRI technique based on motion of water molecules in brain tissues(Bihan, 2003). The principle of DTI is to interpret the water diffusion in the brain as MR signal loss. A neurodegeneration is accompanied by a loss of barriers that restrict motion of water molecules. In case of Alzheimer's disease the DTI-derived maps can quantify in vivo the neurodegeneration and the structural alteration of the hippocamups (den Heijer et al., 2012; Müller et al., 2007) which is the most affected region by AD. In fact, elevated MD and reduced FA in hippocampal areas might be highly indicative of hippocampal atrophy (Mielke et al., 2009). In (Müller et al., 2007), the authors showed that values of MD and FA maps in the hippocampus were more sensitive than the hippocampal volume to discriminate AD subjects.

In Chapter 4 and Chapter 5, we showed the effectiveness of content-based structural MRI description for AD diagnosis. However, visual features extraction from DTI-derived maps could be a challenging problem since this modality does not contain any anatomical information about the brain structure. Thus, in this chapter we aim to test the ability of using visual features to highlight anatomical structure in DTI. To our best knowledge, there is no previous work trying to investigate visual feature extraction techniques to capture structural information within DTI for AD diagnosis. Hence, we apply the content-based image retrieval/ classification approaches developed for sMRI in previous chapters in order to distinguish between subjects with and without AD from DTI-derived map (MD). Features are extracted from the most involved area in the disease : hippocampus.

6.2 Visual interpretation of DTI-derived maps : AD-related signature

Mean Diffusivity (MD) and Fractional Anisotropy (FA) maps are quantitative gray-scale images that provide information about pathways and the integrity of brain structure. Both of those maps encode each pixel by an intensity value (See Chapter 1). Here, image intensities are related to the motion and direction of water molecules in brain tissue. Figure 6.1 shows an example of the MD and the FA maps respectively of healthy and AD individuals. In general, as it is shown in Figure 6.1 (a), image intensity represents the quantitative value of the diffusion coefficient of the brain tissue at each point in the image plane. Due to the free motion of water molecules, the diffusion in ventricles is faster and the MD map is brighter. In white and grey matter regions, diffusion is slower and the MD pixels are darker. In the FA map (see Figure 6.1 (b)), white pixels correspond to high values of fractional anisotropy (FA) and dark pixels correspond to low values of FA.

Referring to the domain knowledge: when a brain is affected by Alzheimer's disease, hippocampus ROI undergoes a cells degeneration and then water molecules become less hindered because of loss of barriers for diffusion motion. In this case we hypothesize that the fast diffusion of water on the hippocampal area results in brighter pixels on the MD maps. Hence, from MD maps, it is possible to extract features and build specific signature to distinguish between an affected or a healthy hippocampus for AD diagnosis problem.

6.3 Data

Three groups of subjects are used to evaluated the current research: We first selected two groups of Diffusion Tensor Imaging and their corresponding structural MRI from the **Alzheimer's Disease Neuroimaging Initiative (ADNI)** database. In this work, we use only the MD maps. **Group 4** contains 25 AD and 32 Normal Control (NC) subjects and **Group 5** contains 25 NC, 24 AD and 21 MCI. Then, we also evaluated our method on the **"Bordeaux-3City"** (Catheline et al., 2010) dataset **(Group 6)**. We have only 7 DTI scans of AD and 21 NC subjects. Demographic description of those three groups are given

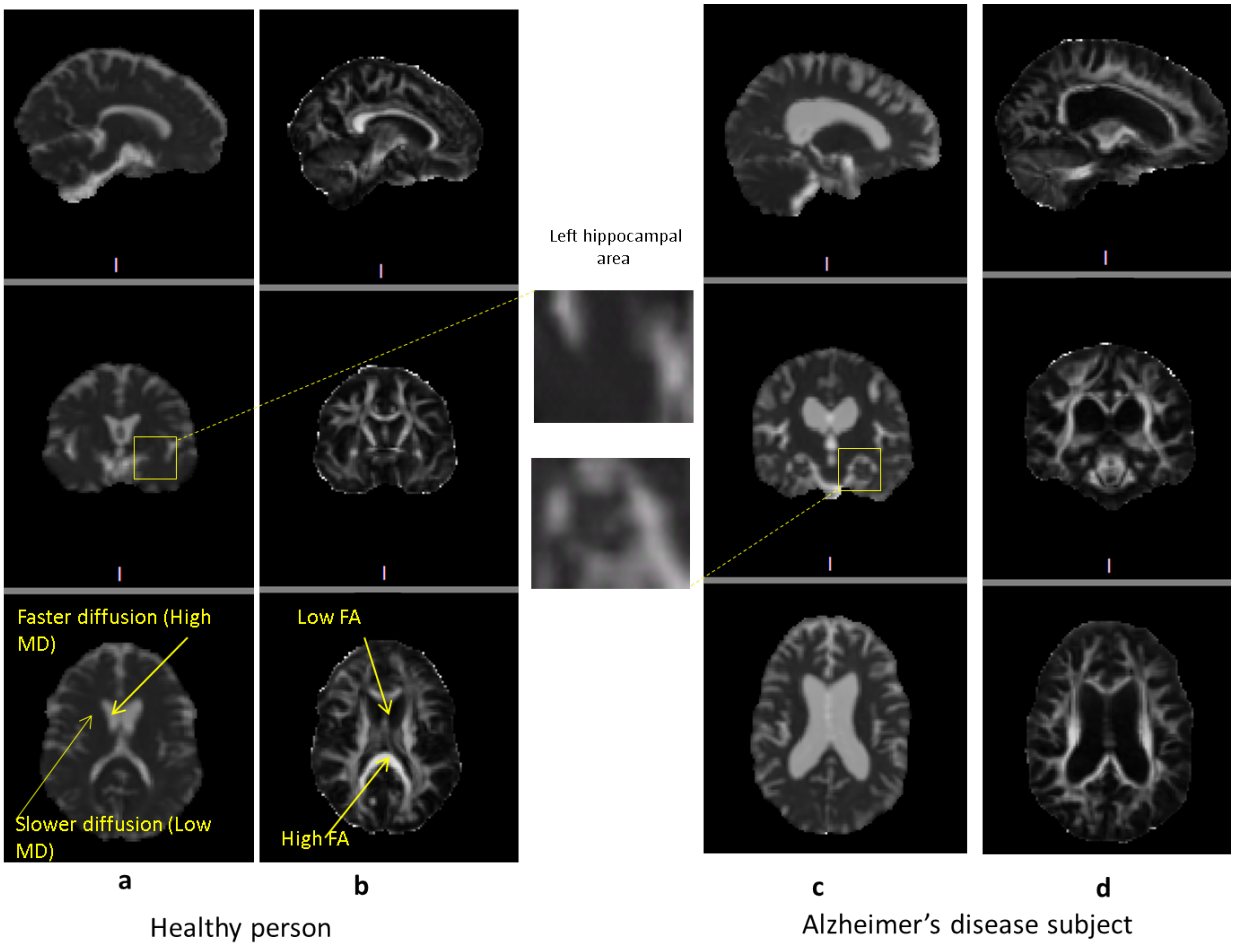

Figure 6.1: Example Mean Diffusivity (a,c) and Fractional Anisotropy (b,d) maps of (from left to right) a healthy and AD persons. Image are taken from the ADNI dataset.

in Section 3.4.

6.4 MD maps preprocessing

Since in this work, we aim to extract visual features related to the hippocampus alterations from the MD map, we need to locate this ROI on the MD maps. Thus, we perform a co-registration of MD maps to anatomical images (sMRI).

We follow here (Cherubini et al., 2010; Mesrob et al., 2012) where co-registation was used to extract regional values of DTI parameters in some specific areas. Moreover, because of the strong variability between individual scans and brain anatomies, before features extraction step, DTI data have to be normalized. It is to note that all performed transformations are

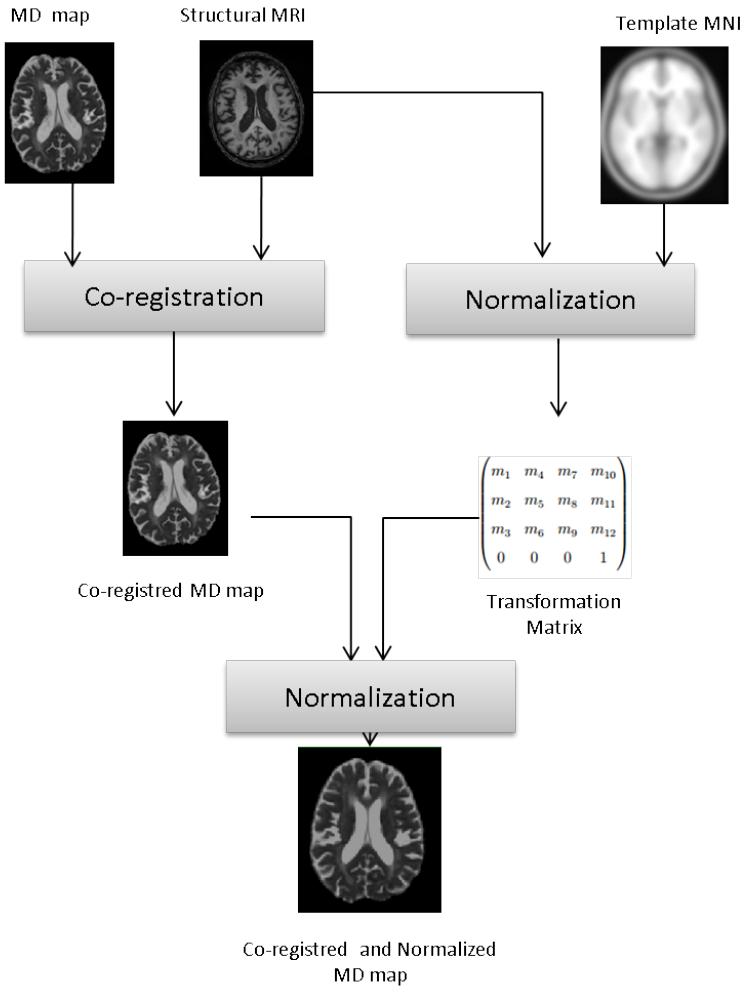

Figure 6.2: Block diagram of the preprocessing pipeline

affine in order to not deform the pattern of the features. For each subject, preprocessing of DTI included corrections for eddy currents and head motion, skull stripping with the Brain Extraction Tool (BET) and fitting of diffusion tensors to the data with DTIfit module of the Software Library FSL [1]. Fitting step allows the generation of the MD and FA maps.

In the current research, we retain only the MD maps. The diagram of the preprocessing pipeline is presented in Figure 6.2. All MD image preprocessing steps were performed using Statistical Parametric Mapping (SPM8, Welcome Department of Imaging Neuroscience, London, UK;)[2] running on MATLAB (MathWorks, Sherborn,MA, USA). After MD images alignment whose purpose is to adjust movement between slices of DTI-derived maps. Mean

[1] http://www.fmrib.ox.ac.uk/fsl
[2] http://www.fil.ion.ucl.ac.uk/spm

diffusivity images were affinely co-registered to the corresponding anatomical scans using the default parameters of SPM. Indeed, Anatomical scans were normalized onto the T1 template in Montreal Neurological Institute (MNI) brain template using the VBM8 toolbox [3] implemented in SPM8, (See Chapter 3) and the resulting transformation parameters were applied to the subjects corresponding co-registered MD maps. Finally, the spatially normalized MD maps were smoothed with a Gaussian filter to improve signal to noise ratio using the smoothing module of SPM. Figures 6.3 show screen-shots of MD-maps co-registration result with the SPM software.

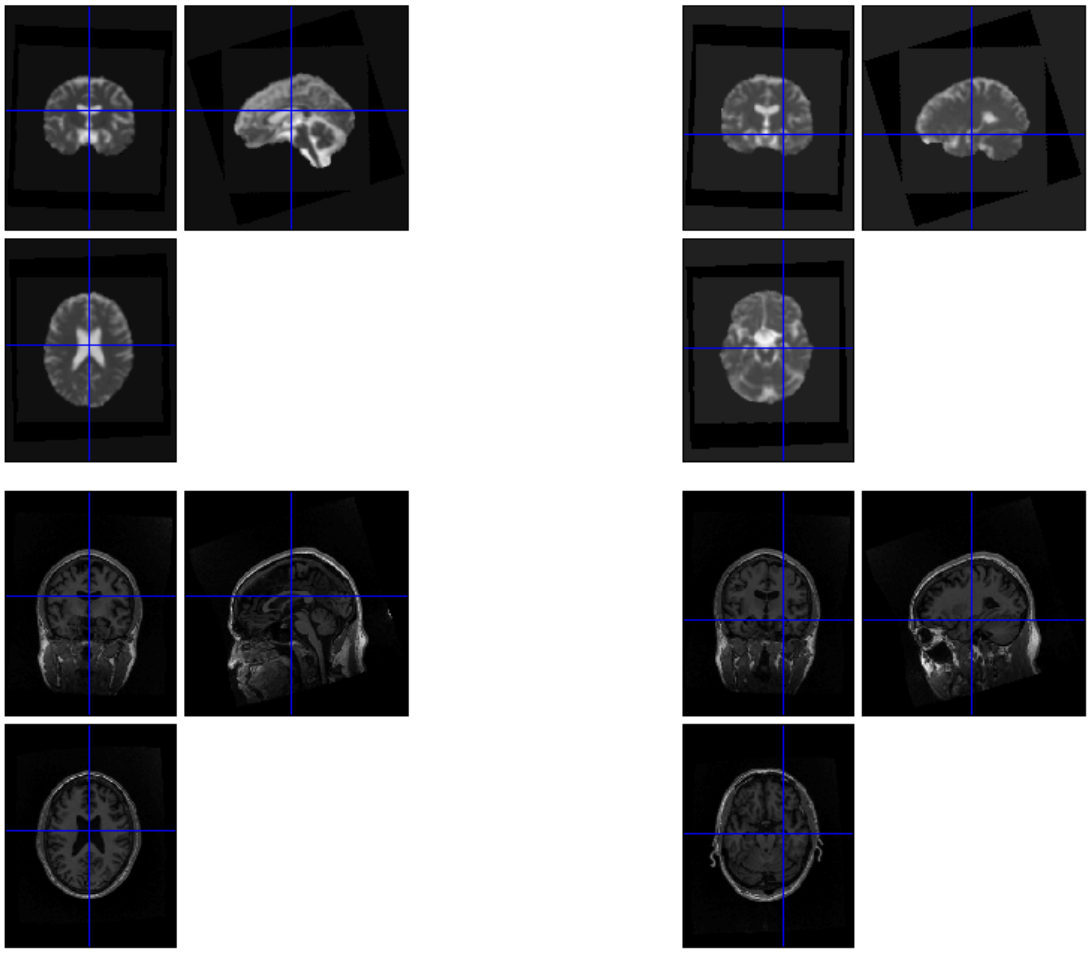

Figure 6.3: Screenshot of the MD map/sMRI coregistration (using Check-Reg function in SPM software)

[3] http://dbm.neuro.uni-jena.de/vbm8/

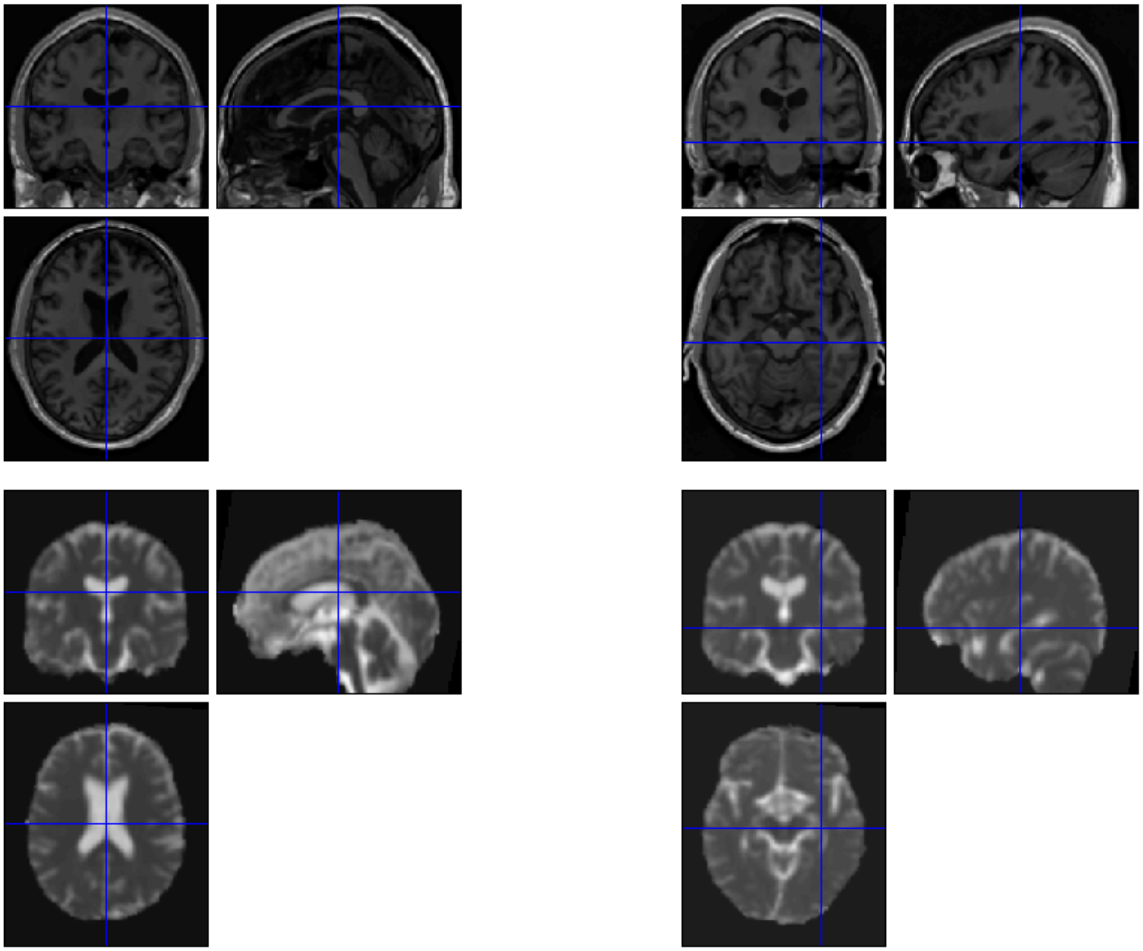

Figure 6.4: Screenshot of the MD map/sMRI After co-registration and Normalization (using Check-Reg function of the SPM software)

In our work, co-registration consists in superimposing DTI-derived maps (MD images) on the subject's corresponding anatomical scan. We use the registration method of SPM8 with a "normalized mutual information" approach. Co-registration maximizes the mutual information between two images. This helps to overlay MD values onto an individual's own anatomy and to check MD values overlaying on structural space as it is show in Figure 6.3. Indeed, The method maximizes the mutual information in the 2D histogram in a limited number of iterations. Because there is a limited number of iterations, it is important in that prior to co-registration, the images are in approximately the same location. The correspondence between obtained Normalized-Coregistred MD maps and their normalized

corresponding anatomical scans is shown in Figure 6.4.

Mutual Information similarity measure Mutual information (MI) is a similarity measure introduced by (Maes et al., 1997) to do co-registration between two images of different modality (West et al., 1996; Fitzpatrick et al., 1998) (such as the structural MRI and the MD map in our case). MI consists in measuring the entropy of the joint histogram of the two images.

According to information theory, entropy is the amount of information that contains an image. The entropy of an image A is defined as:

$$H(A) = \sum_i p(i) \log p(i) \tag{6.1}$$

where i is the intensity values in A and $p(i)$ is the marginal probability distribution function (PDF) of i. The amount of combined information of two images is measured by their joint entropy.

For two images A and B, their joint entropy is defined as:

$$H(A, B) = \sum_{i,j} p(i, j) \log p(i, j) \tag{6.2}$$

where i is the PDF of A and j is the PDF of B. Hence, the MI of A and B is given by:

$$MI(A, B) = H(A) + H(B) - H(A, B) \tag{6.3}$$

Where $H(A)$ and $H(B)$ are the individual image's entropy and $H(A, B)$ is the joint entropy.

However, Studholme and colleagues proved that MI measure is sensitive to changes overlap and proposed the Normalized mutual information (NMI) measures as an alternative to overcome this problem (Studholme et al., 2006). The NMI is defined as:

$$NMI(A, b) = \frac{H(A) + H(B)}{H(A, B)} \tag{6.4}$$

6.5 Content-Based MD maps Retrieval framework

The Diffusion Tensor Imaging (DTI) is a relatively recent technique and CBIR approaches have not yet been developed on it. The proposed Content-Based MD maps Retrieval Framework as illustrated in Figure 6.5 consists of three main steps : Image preprocessing (explained in section 6.4), visual features extraction and finally image retrieval.

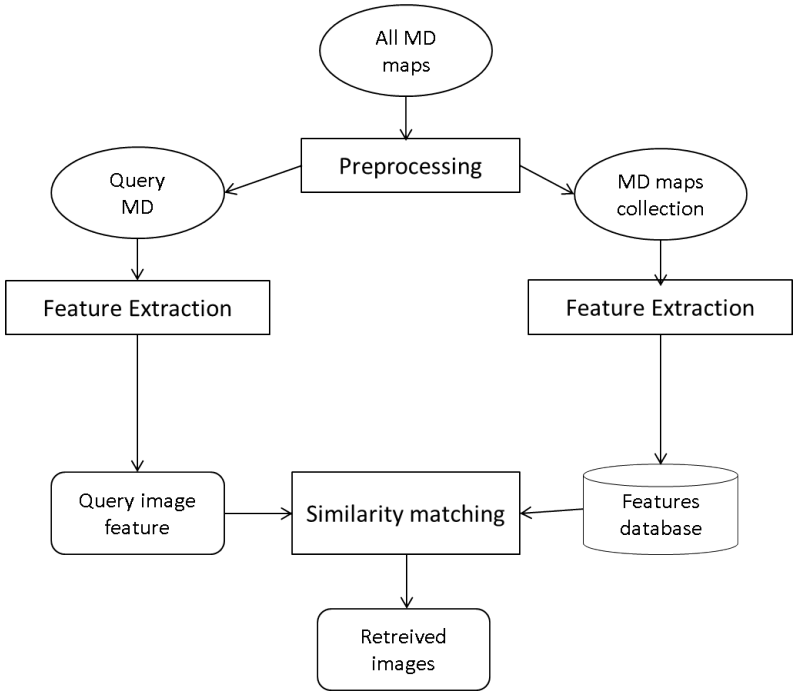

Figure 6.5: Diagram of the proposed content-based MD maps retrieval framework

6.5.1 Features Extraction

The hippocampus ROI was extracted from an anatomical scan using the AAL template. A binary mask of the hippocampus was thus obtained in each anatomical scan. The hippocampal region of interest in MD map was obtained by superimposing the binary hippocampus masks from anatomical scans to MD image. Then, hippocampus features were computed on MD map by the development of the MD image signal on the basis of Circular Harmonic Functions (CHFs). Although AAL was not designed for studying patients with AD, CHF coefficients extracted from the areas overlapping with the mask are different and depend on the signal presented in the ROI (atrophy or not) which can adequately capture the patholog-

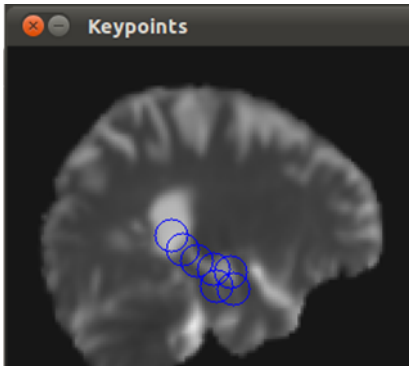

Figure 6.6: CHF features detection

ical structure. The CHF decomposition of a signal is performed on a 2D patch. We used a "Dense Sampling" strategy to detect features. Thus the final feature vector consists of CHF coefficients computed on the hippocampal ROI on MD map. Figure 6.6 shows an example of features detection on a coronal projection from a MD map of an ADNI subject.

Now, to justify the choice of the signal decomposition basis we briefly remind the definition of CHF functions. The advantages of these features are such that they capture both the direction and smooth variations of image signal. Note that MD images are even more blurry than anatomical scans for which the CHF features showed good results in our previous work. They allow for capturing slow signal variations. Their draw back is in a rather slow convergence, hence a sufficient number of coefficients has to be retained for image description. The number of coefficients retained define the dimensionality of the descriptor. The reasonable dimensionality of 150 coefficients was used in the present work. Hence the dimension of the descriptor is comparable with that one of conventional SIFT.

MD maps Retrieval

Brain scans are aligned and can be compared slice by slice since the features are extracted in a 2D space. The retrieval consists in comparing hippocampal ROIs in MD maps. Similar regions are expected to have similar features. Since the images are aligned, we used a one-to-one region similarity computation scheme, scans are compared slice by slice. As features were computed using the dense sampling strategy (dense placement of features), the number of features and their coordinates are the same for all images. We compare them by using the

simple distance metric as described in Equation 6.5.

$$d_n = \sqrt{\sum_{s=1}^{S} \sum_{i=1}^{I^s} \left\| f_i^{*s} - f_{n,i}^{s} \right\|^2} \tag{6.5}$$

Here n is the index of a MD map in the database, $f_{n,i}^{s}$ are features inside a given slice s, (we denote the features of the query scan by f_i^{*s}), S is the total number of slices containing the 3D ROI in query image, I^s is the number of features in a slice s The similarity of a query MD map to n^{th} map is $Sim_1(n) = 1/(d_n + 1)$. Lower distance means better similarity.

In a second experiment, we tested the matching method proposed in Lowe (2004). The approach consists in finding for every feature f_i^* from one image the best matching feature from other image $f_{n,i}^{s}$. We used, as similarity measure, the formula given in Equation 6.6 to measure similarities across images. This presents the number of matching descriptors, Indeed, the descriptors are matching when the distance between descriptors $f_i^*, f_{n,i}^{s}$ is lower than a threshold T. The threshold was found experimentally and its value for these experiments was fixed as 0.4. Note that in our previous work, we used quantized features accordingly to a visual dictionary in a Bag-of-Visual-Words Paradigm (see Chapter 3). Nevertheless before we can use this paradigm, it is necessary to asses the performance of our description in th original space, what we have done in the present work.

$$Sim_2(n) = \sum_{s=1}^{S} \sum_{i=1}^{I^{s*}} \begin{cases} 1, & \min_{j=1\ldots I^s} \left\| f_i^* - f_{n,j}^{s} \right\| < T \\ 0, & otherwise \end{cases} \tag{6.6}$$

6.5.2 MD maps retrieval Results

In our testing procedure, we assess the performance of the method in terms of the "precision at N" metric used in information retrieval. Here the proportion of correct matches of classes between the query image and the N returned images is computed. Then a mean precision at N is computed for all query trials.

- Precision at N^{th} = Number of images correctly classified/N

The retrieval approach has been tested on the MD images. Using this test we analyze the raw performance of the proposed descriptor-based technique. In Figure 6.7 and Figure 6.8, the percent of correct classes in N most relevant images is shown both with Sim_1 and Sim_2 corresponding respectively to the "1-to-1" matching and the (Lowe, 2004) matching algorithm p proposed for the "BoF".

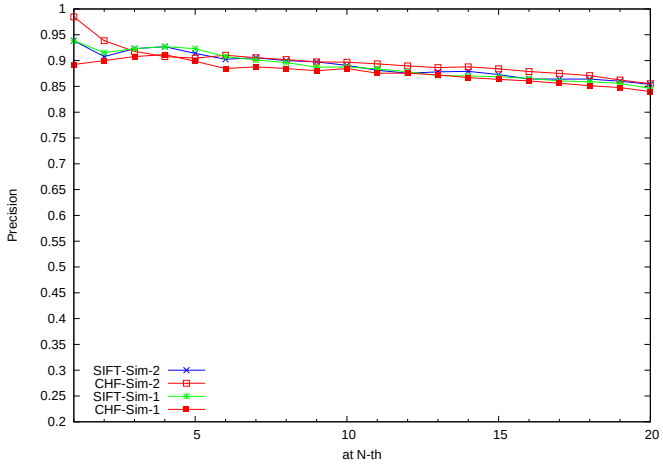

Figure 6.7: Retrieval results for CHF and SIFT descriptors: **ADNI subset (Group 4)**

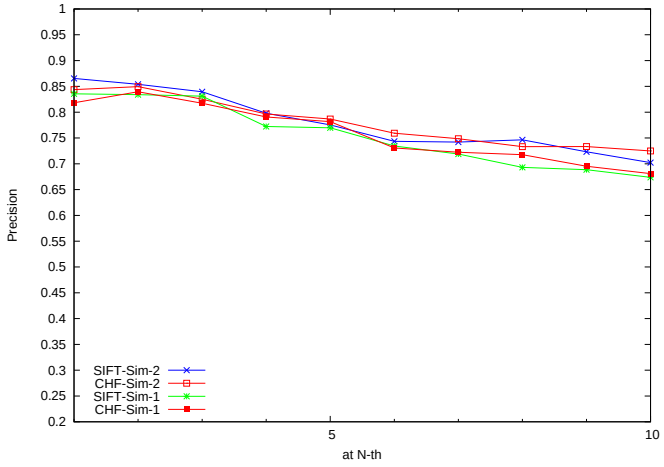

Figure 6.8: Retrieval results for CHF and SIFT descriptors: **"Bordeaux-3City" (Group 6)**

The precision at N^{th} of CHF descriptor using the Sim_1 scheme is in the worst case of 89.69% as ilustrated in Figure 6.7. No significant difference is identified between the two matching modes except the precision at 1. One can see that the precision at 1 is the best with the Sim_2 of CHFs compared to conventional SIFT features.

The Figure 6.8 illustrates the result on **"Bordeaux-3City"**. For example, the precision value at 4^{th} for CHFs descriptor with Sim_1 base retrieval approach is about 83%. We can see from Figure 6.7 and Figure 6.8 that both CHF and SIFT descriptors give high retrieval results. These descriptors thus prove to be suitable for capturing the DTI image content.

Hence, in this section we proposed CBIR approach on the DTI MD maps to evaluate the performance of these classical scheme on the recent MRI modality. Despite the tests were conducted on a small (for cohort population reasons) test set, the results obtained are

promising. Alone this modality shows rather high scores in a realistic situation of a small cohort. In The next section we will design a classification framework of MD maps.

6.6 MD maps classification

6.6.1 Disease-related signature generation using the Bag-of-Words approach

In this section, we apply the same features extraction approach we have proposed in chapter 4. The same schemes are applied to the preprocessed MD maps (See section 6.4). Finally, we obtain an histogram of visual words of the hippocampus ROI extracted from MD maps using the CHFs features. The obtained signature is then reduced using the PCA technique.

6.6.2 Classification framework

SVMs are used to classify subjects, we are interested in the binary classification (AD versus NC), (NC versus MCI) and the (AD versus MCI). We use 10-fold cross validations to evaluate classification performance. We repeated the 10 fold cross-validation 10 times for a more general performance estimation of the classifier. Each time the 10 randomly selected folds were generated and the final result is the average accuracy, sensitivity and specificity of the 10 experiments. The BAC metric values are reported also. All those metrics of evaluation are presented in (Section 4.5.1).

6.6.3 Experiments and results

Signature dimensionality reduction To reduce signatures dimensionality, we consider percentages of total energy which is obtained from cumulative energy vector. As the percentage of energy is reduced, the number of coefficients required also dramatically reduces, and according the candidate feature vector size is reduced for classification. Figure 6.9 shows the average cumulative sum of the eigenvalues, obtained from PCA. It is depicted against the number of eigenvalues. For instance, the **ADNI** group signature's size is equal to 600 =200 x 3 with 200 is the codebook. Whereas the size of signature for the **"Bordeaux-3City"**

data is 450=150 x 3 with 150 is the codebook size. Therefore, using PCA the signatures sizes were reduced by keeping 95% of energy (Figure 6.9).

Codebook size Variation In a second part of experiments, we plot the variation of classification accuracy (AD vs NC, NC vs MCI and MCI vs AD) function to the codebook size changes (Figure 6.10). In most cases, the accuracy can be improved with a larger codebook size, but it can also decrease in certain cases. In general, the accuracy does not change significantly with codebook size. A similar trend has been observed for The **"Bordeaux-3City"** data. Hence, we set the codebook sizes to 200 and 150 respectively for **Group 5 (ADNI)** and the "Bordeaux-3City" group.

SVM parameters optimizations For classification, SVM is used with an RBF kernel. In our experiments an SVM classifier is trained with value of regularization parameter C and the scaling parameters *gamma* by using grid search on the log ratio of the parameters associated with 5 fold cross validation. Then, value pairs (C, γ) are assessed using cross validation and then the pair with highest accuracy is chosen. The value of C and γ are exponentially varied ($C = 2e^{-6}, 2e^{3}, ..., 2e^{14}$; $\gamma = 2e^{-15}, ..., 2e^{10}$). Thus, the grid search has built dozens of SVM models with various parameter settings, and optimal parameters relatively to the training data were selected.

Table 6.1 and Table 6.2 present the classification results in terms of sensitivity, specificity, accuracy and BAC metrics for respectively the **Group 5 (ADNI)** and **"Bordeaux-3City"** data.

	AD versus NC	NC versus MCI	AD versus MCI
Accuracy %[95% CI]	86.73 [86.10 87.37]	77.39 [75.67 79.12]	73.11[71.32 74.90]
Specificity %[95% CI]	98 [96.76 99.24]	89.20 [86.97 91.43]	77.92[76.26 79.57]
Sensitivity %[95% CI]	75[74 75]	63.33 [60.68 65.99]	67.62[63.7 71. 53]
BAC (%)	86.5	76.27	72.77

Table 6.1: Classification results: AD, versus NC, Nc versus MCI and AD versus MCI **(Group2)**

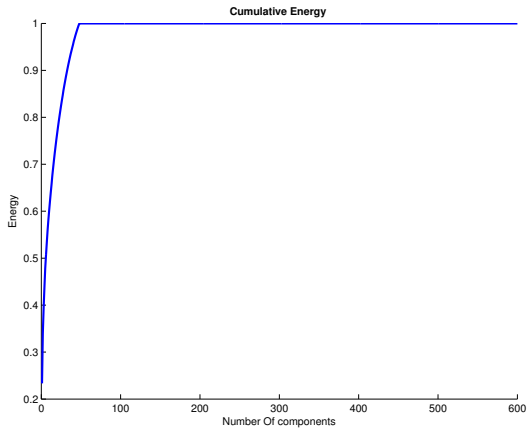

Figure 6.9: Cumulative energy as a function of the number of components (ADNI group)

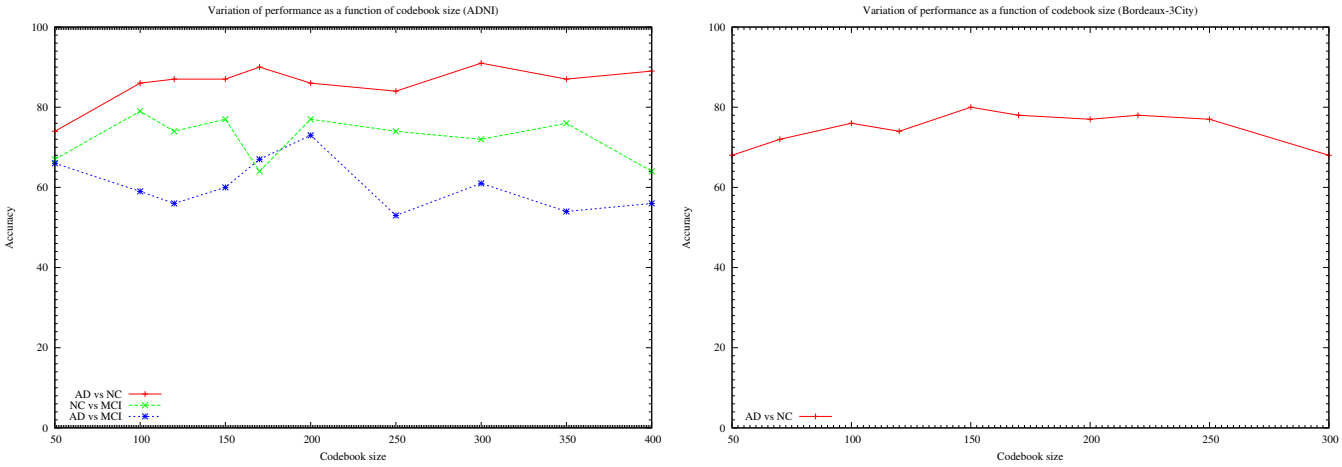

Figure 6.10: Codebook variation for the **ADNI** dataset **(Group 5)** and **"Bordeaux-3City "**group

	AD versus NC
Accuracy %[95% CI]	80.34 [77.47 83.22]
Specificity %[95% CI]	90.91 [88.09 93.73]
Sensitivity %[95% CI]	47.14 [43.09 51.20]
BAC (%)	69.03

Table 6.2: Classification results: AD versus NC (Bordeaux-3City)

Classification results for (NC vs AD)

In this section, we present the classification results obtained in the first experiment, which consisted on the classification of AD versus NC . Our method achieved classification accura-

cies of 86.73% and 80.34% respectively for the **Group 5 (ADNI)** and **"Bordeaux-3City"** data **(Group 6)**. We reported for the **ADNI** subset **(group 5)** a specificity 98% of and a sensitivity of 75%. Indeed, for **"Bordeaux-3City"** data, we reported a hight specificity (90.91%) but lower sensitivity this could be caused by the small number of AD subjects compared to the number of Normal control used in this experiment.

Classification results for (NC vs MCI)

A hight specificity is obtained for the NC versus MCI classification (89.20%). In addition, an accuracy of 77.39% and a sensitivity of 63.33% were reported.

Classification results for (AD vs MCI)

The most challenging classification task concerning the **Group 5 (ADNI)** is to distinguish AD from MCI patients. We obtained an accuracy of 73.11%, a specificity of 77.92% and a sensitivity of 67.62%. This is presumably due to the fact that MCI is a transitory heterogeneous stage between NC and AD.

The obtained results show how the Laguerre Gauss CHFs seems to provide a robust representation of the hippocampus atrophy from the MD maps. The BoVW method proved to be effective in explaining the visual richness of MD images and relations between visual patterns and their semantic meaning.

Alone, the MD maps show rather high scores in a realistic situation of a small cohort. Furthermore, our approach, do not require a precise segmentation of ROI, performs well not only on sMRI, what we showed in our previous work (Chapter 5), but also on more challenging modality such as MD maps. Combining DTI data with structural findings should further increase its diagnostic performance. However, without the aid of an sMRI, the anatomical information of the Hippocampus acquired by MD maps is difficult to interpret due to the lack of anatomical information in this modality.

6.7 Conclusion

In the current chapter, we introduced a new approach of visual-related signature of hippocampus ROI on MD maps of DTI modality. This information was used to effectively discriminate the MCI and AD patients from normal controls, as well as between the MCI and AD patients. Besides, it achieves good values of accuracy, sensitivity and specificity. The present research is the first attempt (in our best knowledge) to apply features-based approaches on this modality for AD diagnosis. The proposed method is based on the comparison of visual features extracted from the hippocampal area. We use the Circular Harmonic Functions (CHFs) to extract content from the Diffusion Tensor-derived map: Mean Diffusivity (MD). The obtained results are encouraging and open interesting perspectives. In the perspective of this work we will proceed with fusion of different modalities in a global classification framework.

Chapter 7

Main Conclusion and perspectives

7.1 Conclusion

MRI is an integral part of the clinical assessment to detect and to follow the evolution of brain atrophy. Due to the variability of subjects, features-based methods have become popular for AD diagnosis thanks to their statistical redundancy and selectivity of salient image areas. Thus, in the current PhD research we proposed CAD approaches for AD detection using classical tools of content-based image indexing, retrieval and classification . These approaches consist of features extraction, image signature generation, similarity matching and supervised learning. We adopted them for two MRI modalities (Structural MRI and DTI-derived map). Our goal throughout this thesis has been to show the effectiveness of such approaches combined with domain knowledge in supporting AD diagnosis.

The first main contribution has been the construction of distinctive local patterns of AD-related atrophy using an atlas-based approach without the need of a tedious ROI segmentation. This help capturing different signals from a number of different tissues inside the ROI itself. Here, we used domain knowledge of the MRI and Alzheimer's disease characteristics to extract the appropriate features from ROIs known to be affected by AD namely the hippocamps and the PCC. Thus, the extracted patterns are leveraged to distinguish normal from abnormal ROIs/Brains.

Considering sMRI modality, we showed that our approach which requires only rough selection of the ROI is comparable and even outperforms traditional volumetric methods

which require a tedious and interactive ROI segmentation.

We have also proposed Early and Late fusion schemes to take advantages to the domain knowledge namely fusion of features from two characteristics regions (hippocampus and PCC) and fusion of output's classifiers on CSF and structural changes in the Hippocampus. Both MRI modalities: Structural MRI and Diffusion Tensor Imaging (DTI) are used in this thesis. We also used supplementary biomarker such as the the augmentation of CSF amount in brain.

As sMRI and DTI modalities are characterized by smooth contrast, we used as descriptors the coefficients of projection of MRI signalon Circular Harmonic Functions basis. We showed that CHFs descriptors outperform conventional SIFT and SURF both in similarity matching and classification. They are therefore interesting to be used on MR Images. In addition, we addressed the most challenging task of recognition of MCI subjects which is not very often addressed in the literature due to the heterogeneity of this category.

The obtained results demonstrate promising classification performance and simplicity compared to the state-of-the-art volumetric AD diagnosis methods. The strength of the proposed work consists in the flowing:

- The main advantage of our methods is its capability to capture atrophy patterns of progressive neurological disorders and also overcome the limits of fine segmentation methods.
- Our approach is automatic, less time consuming than segmentation-based methodology and does not require the intervention of the clinician during the disease diagnosis.
- It is extensible to other diseases that can be diagnosed by brain MRI such as Schizophrenia and brain tumors.
- The method uses 2D slices that allows the use of well studied mathematical models of features

Limitations occur in the normalization process which may produce the loss of some local information in the images. Also the atlas-based approach may generate a small amount of

Region of Interest localization error. Finally, the DTI-derived maps suffer from noise and an denoising step is needed to ensure more efficients classification results.

Additional work may be needed to improve work. Future work will include considering other ROIs which may be more discriminative together for diagnosis. We intend to further evaluate our approach performance in other datasets in the aim of predicting subject conversion to AD rather than recognizing subject's category. Furthermore, we think that application of Convolutional Neural Networks (CNN) with deep learning may be interesting for AD diagnosis using several modalities. It is also interesting to generalize this approach for the 3D case using 3D SIFT to compare it with its 2D version. We have used classical hard coding of quantified features and it will be interesting also to apply soft coding. moreover, Numerous DTI studies for Alzheimer's disease demonstrated that the use of DTI voxel values together with stuctural MRI voxel values improves classification accuracies. In the perspective of this PhD research, we will proceed with fusion of sMRI and DTI modalities in a global classification framework using Multiple kernel leaning technique for instance. Finally, a graphical user interface could be developed to Computer-aided diagnosis.

Appendix A

.1 SIFT

There are four specific steps SIFT follows to figure out robust image features. These are 1) Scale-space extrema detection 2) Key-point localization 3) Orientation assignment and 4) Key-point descriptor

Scale space extrema detection The scale space of an image is presented by $L(x, y, \sigma)$ that is obtained from a convolution of a variable scale Gaussian $G(x, y, \sigma)$, with an image $I(x, y)$:

$$L(x, y, \sigma) = G(x, y, \sigma) * I(x, y) \tag{1}$$

Where $G(x, y, \sigma) = \frac{1}{2\Pi\sigma^2} e^{-(x^2+y^2)/2\sigma^2}$

Accordingly to (Lowe, 2004), a Keypoint corresponds to the local extrema in the Difference Of Gaussian (DoG) function convolved with the image, $D(x, y, \sigma)$ given by:

$$\begin{aligned} D(x, y, \sigma) &= (G(x, y, k\sigma) - G(x, y, \sigma)) * I(x, y) \\ &= L(x, y, k\sigma) - L(x, y, \sigma) \end{aligned} \tag{2}$$

Which is just the difference of the Gaussian-blurred images at scales σ and $k\sigma$. This process is done for different octaves of the image in Gaussian Pyramid. It is illustrated in

Figure 1:

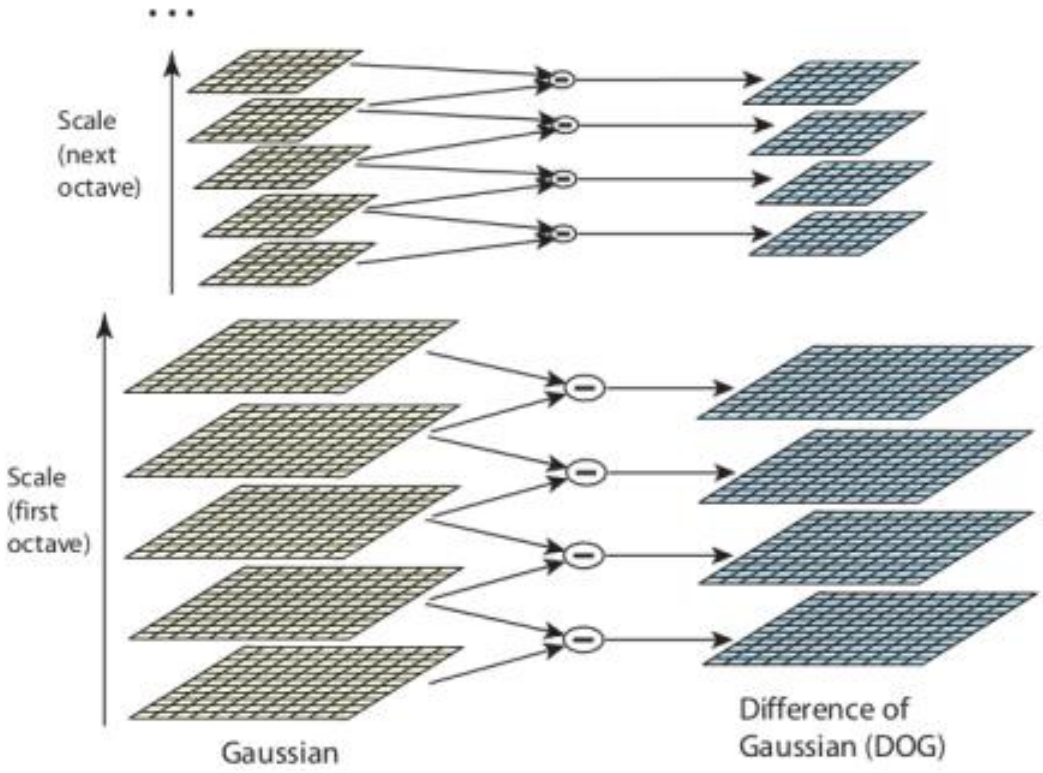

Figure 1: Diagram illustrating the blurred images at different scales, and the Difference of Gaussian computation (Lowe, 2004)

Once this DoG are functions are computed across neighboring scales, images are looked for local extrema over scale and space. Each pixel in the DoG image is compared with its 8 neighbours at the same scale as well as 9 pixels at neighbouring scales. If the pixel is a local extrema, it is selected as candidate keypoint (see Figure 2).

Keypoint localization The next step consists in eliminating low-contrast and edge keypoints. Only the strong interest points are conserved, exhibiting signal particularities, where signal changes in two directions.

Taylor series expansion of scale space is used to get more accurate location of extrema.

$$D(x) = D + \frac{\partial D^T}{\partial x}x + \frac{1}{2}x^T\frac{\partial^2 D}{\partial x^2}x \tag{3}$$

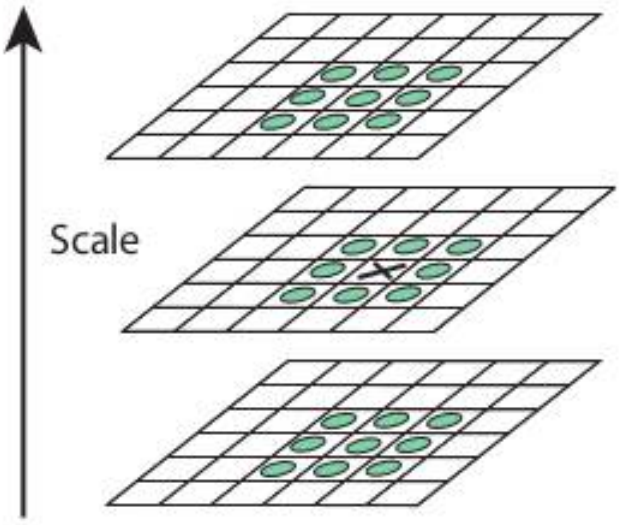

Figure 2: Local extrema detection(Lowe, 2004)

To obtain the extremum point, the derivate should be equal to zero:

$$\hat{x} = -(\frac{\partial^2 D^{-1}}{\partial x^2})^{-1}\frac{\partial D}{\partial x} \tag{4}$$
$$D(\hat{x}) = D + \frac{1}{2}\frac{\partial D^T}{\partial x}\hat{x}$$

if the intensity of this extremum is less than a threshold value fixed to 0.03 ($if D(\hat{x}) <= 0.03$) in (Lowe, 2004)) it is rejected.

The detector first computes the Harris matrix H for each pixel in an image and then computes its eigenvalues which indicate the principal curvature of H.

$H = \begin{pmatrix} D_{xx} & D_{xy} \\ D_{xy} & D_{yy} \end{pmatrix}$ $\frac{(D_{xx}+D_{yy})^2}{D_{xx}D_{yy}-D_{xy}^2} < \frac{(r+1)^2}{r}$ where $r = \frac{Largest\ eigenvalue}{smallest\ eigenvalue}$

Hessian matrix was used to compute the principal curvatures and to eliminate the low contrast points. Lowe assume r=10. Thus, keypoints having a ratio between the principal curvatures greater than 10 are eliminated

Orientation Assignment To determine key-point dominant orientation, histogram is formed from the gradient orientations of sample points within a region around the keypoint.

This step achieve invariance to image rotation since he keypoint descriptor can be represented relatively to this orientation. The scale is used to select the Gaussian smoothed image $L(x, y)$. The gradient magnitude $m(x, y)$ and the orientation $\theta(x, y)$ are computed using the pixels differences as follows:

$$m(x,y) = \sqrt{(L(x+1,y) - (x-1,y))^2 + (L(x,y+1) - L(x,y-1))^2} \tag{5}$$

$$\theta(x,y) = arctang(\frac{L(x,y+1) - L(x,y-1)}{L(x+1,y) - L(x-1,y)}) \tag{6}$$

Keypoint descriptor The descriptor comprises histograms of image gradient amplitudes, using 8 orientation bins on a $4x4$ grid around each keypoint, as shown in Figure 3. The SIFT feature vector consists of 128 elements ($4x4x8$). This feature vector is normalized to enhance invariance to changes in illumination. An image with n keypoints contains $nx128$ features.

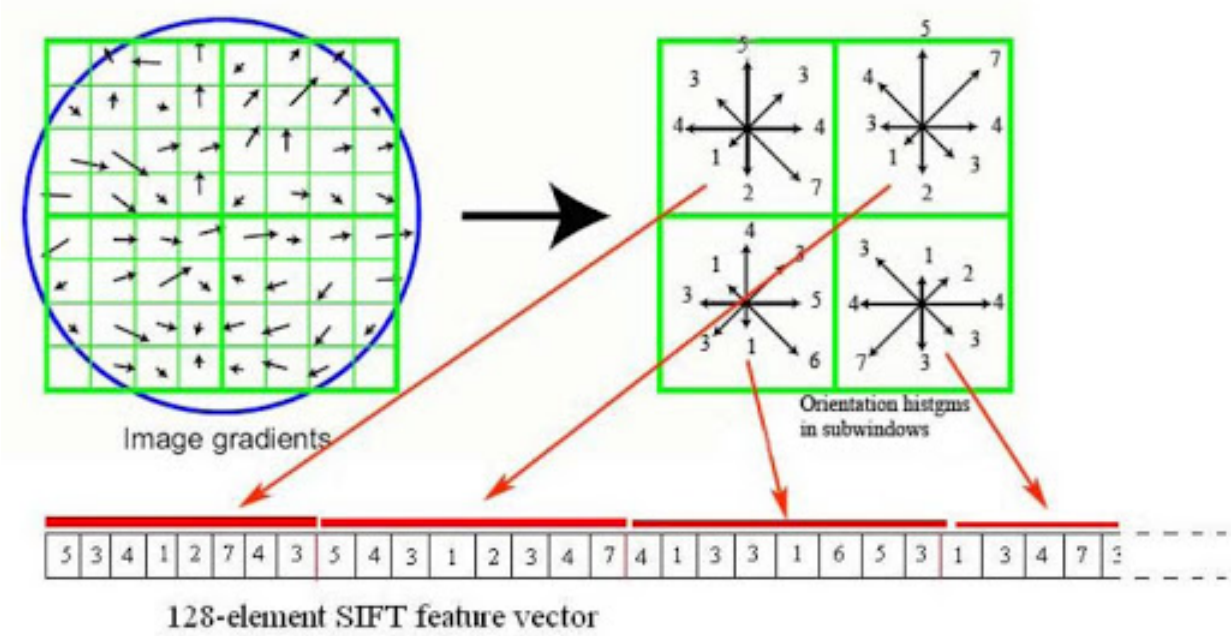

Figure 3: An orientation histogram in the SIFT method.

The SIFT descriptor in particular provides "robustness against localization errors and small geometric distortions".

.2 SURF

Keypoint detection While SIFT is based on scale space theory and the feature detector is based on Hessian matrix. SURF (Speed Up Robust Features) (Bay et al., 2008) descriptor is based on similar properties as SIFT. Indeed, the SURF detector finds interest points (scale and location) as extrema of the determinant of the Hessian matrix in scale space, $det(H(x, y, \sigma))$. Given a point $X = (x, y)$ in an image I, the Hessian matrix $H(x, y, \sigma)$ in X at scale σ is defined as follows:

$$H(x, \sigma) = \begin{pmatrix} L_{xx}(x, \sigma) & L_{xy}(x, \sigma) \\ L_{xy}(x, \sigma) & L_{yy}(x, \sigma) \end{pmatrix} \tag{7}$$

here

$$L_{xx}(x, \sigma) = I(x) * \frac{\partial^2}{\partial x^2} g(\sigma) \tag{8}$$

$$L_{xy}(x, \sigma) = I(x) * \frac{\partial^2}{\partial xy} g(\sigma) \tag{9}$$

$L_{xx}(x, \sigma)$, $L_{yy}(x, \sigma)$ and $L_{xy}(x, \sigma)$ denote the convolution of the image with a second order Gaussian derivative$\frac{\partial^2}{\partial x^2}, \frac{\partial^2}{\partial y^2}$ and $\frac{\partial^2}{\partial xy}$ respectively. This convolution is very costly and it is approximated and speeded-up with the use of integral image [1]. These derivatives are known as Laplacian of Gaussians.

They are approximated by box filters and are defined as D_{xx} , D_{xy} and D_{yy} . From those term, the Hessian determinant is computed as follows:

$$det(H_{approx}) = D_{xx}D_{yy} - (0.9D_{xy})^2 \tag{10}$$

[1]Every entry of an integral image is the sum of all pixels values contained in the rectangle between the origin and the current position

The Hessian matrix is calculated for various filter sizes, where the filter size corresponds to the region around which the matrix determinant is calculated, with different scale factors. This is repeated for several octaves. After computing the Hessian matrix at different scale factors, the interest points are selected by calculating the local maxima (in a 3 x 3 x 3 neighborhood) in scale and image space.

Figure 4 shows an illustration of such an approximation. The advantage of this approximation is that, convolution with box filter can be easily calculated using the integral images and it can be done in parallel for different scales.

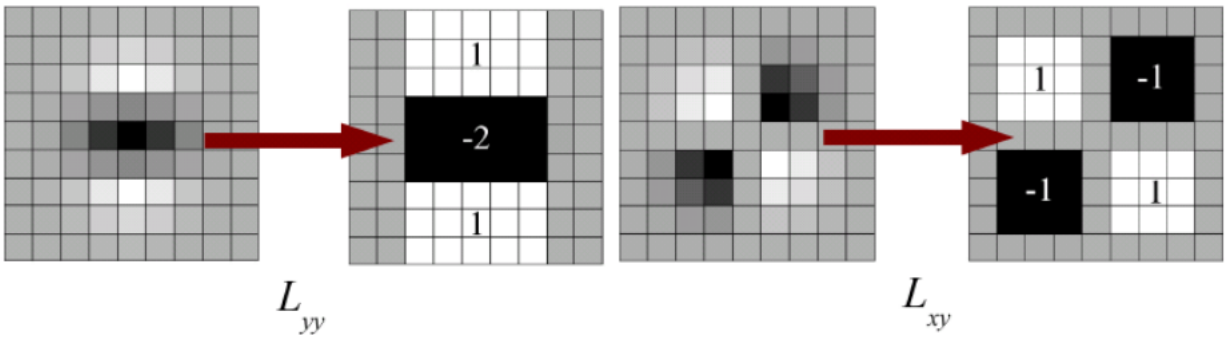

Figure 4: Laplacian of Gaussian Approximation

SURF descriptor To describe each feature, SURF summarizes the pixel information within a local neighborhood. The first step consists of defining a reproducible orientation based on information from a circular region around the point of interest. And second constructs a square region aligned with the selected orientation, and extract the SURF descriptor from it.

Similarly to SIFT, SURF identifies a reproachable "orientation" of a keypoint but with different computation manner. For that purpose, SURF uses responses of Haar wavelet in horizontal and vertical direction for a neighborhood of size 6s around the interest point, with s the scale at which the interest point was detected. The responses of the Haar wavelets are weighted with a Gaussian ($\sigma = 2.5s$) centered at the point. Then, the horizontal and vertical wavelet responses are summed within a sliding orientation window covering an angle of $\Pi/3$ in the wavelet response space (see Figure 5) in order to estimate the dominant orientation.

The resulting maximum is then chosen to represent the orientation of the interest point descriptor.

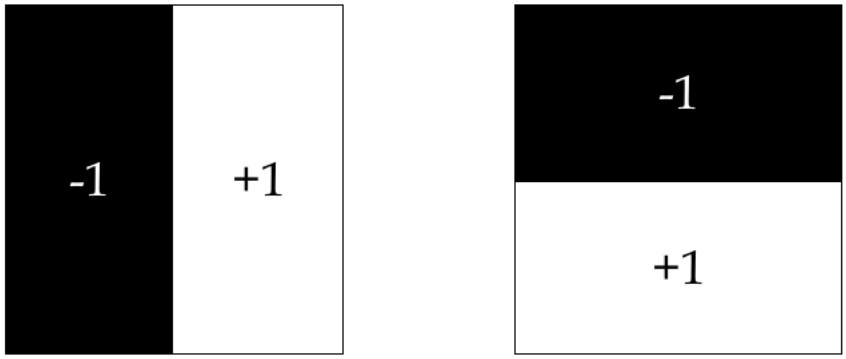

Figure 5: Horizontal and vertical Haar wavelet filter

The SURF descriptor describes an interest area with size 20s where s is the scale . This region of interest is divided into 4x4 sub-regions. For each sub-region, horizontal and vertical wavelet responses are taken and a vector is formed like this, $v = (\sum d_x \sum d_y, \sum |d_x|, \sum |d_y|)$ where d_x and d_y refer respectively to the horizontal and the vertical wavelets responses. This when represented as a vector gives SURF feature descriptor with total 64 dimensions (see Figure 6). Lower is the dimension, higher is the speed of computation and matching, but provide better distinctiveness of features.

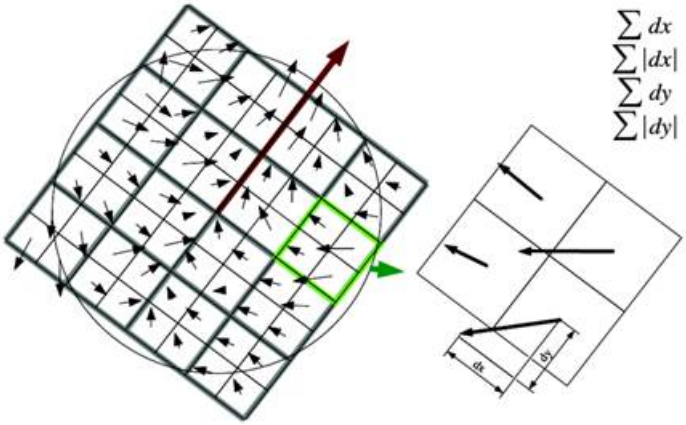

Figure 6: SURF descriptor Computation

.3 LBP

LBP comprises a binary code that is obtained by thresholding a neighborhood according to the grey value of its center. Given a center pixel in the image, the LBP value is computed by comparing its gray value with its neighbors.

$$\sum_{p=1}^{P} 2^{(p-1)} S(g_p - g_c) \tag{11}$$

$$S(x) = \left\{ \begin{array}{ll} 1, & x >= 0 \\ 0, & otherwise \end{array} \right\} \tag{12}$$

Where g_c is the gray value of the center pixel, g_p is the gray value of its neighbors, P is the number of neighbors, and R is the radius of the neighborhood:

$$g_p = I(x_p, y_p)\, for\, p = 0...P$$
$$x_p = x + R\cos(\tfrac{2\Pi p}{P})\, and\; y_p = y + R\sin(\tfrac{2\Pi p}{P})$$

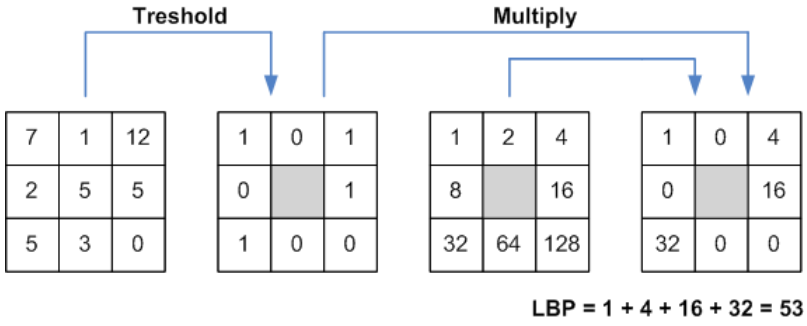

Figure 7: Example of LBP computation

The simple LBP operator labels the pixels of an image by thresholding a 3 x 3 neighborhood of each pixel with the center value and considering the results as an 8-bit binary number or an LBP label for that pixel and than converting the resulting binary into a decimal. Figure 7 shows step by step example of computing LBP. From left to right; the first panel shows

a pixel along with its spatial neighborhood. The second panel shows the same pixel after sub-tracting intensity of the inner pixel from all intensities. The third panel shows the same pixel after applying the step function, note that the value of inner pixel is omitted as it is no longer needed. The fourth panel shows the multipliers for corresponding neighborhood pixels. The resulting pattern is $1 + 4 + 16 + 32 = 53$.

Appendix B

Otsu's method (Otsu, 1979) is a simple and automatic thresholding technique. The algorithm assumes that the image to be thresholded contains two classes of pixels (e.g. foreground and background) then calculates the optimum threshold separating those two classes.

Fundamentals

Given an image $I(x, y)$ and N is the number of its pixels. The gray-values of the image range in $[0..L]$ where $L = 255$. The number of pixels at level i is denoted by h_i. The $N = h_0 + h_1 + ...h_{L-1}$. The occurrence probability of gray level i, in $I(x, y)$ is given by:

$$p_i = \frac{h_i}{N}, p_i >= 0, \sum_{i=0}^{L-1} p_i = 1 \tag{13}$$

If an Image is segmented into two clusters C_0 and C_1. C_0 denotes the pixels level $[1, ..., k]$ and C_1 denotes pixels level $[k + 1, ..., L]$. The probability of class occurrence and the class mean levels, respectively, are given by:

$$\omega_o = P(C_0) = \sum_{i=1}^{k} p_i = \omega(k) \tag{14}$$

$$\omega_1 = P(C_1) = \sum_{i=k+1}^{L} p_i = 1 - \omega(k) \tag{15}$$

where of course $\omega_o + \omega_1 = 0$ and The class m The class mean levels are given by:

$$\mu_0 = \sum_{i=1}^{k} iP(i|C_0) = \sum_{i=1}^{k} ip_i|\omega_0 = \mu(k)/\omega(k) \tag{16}$$

$$\mu_0 1 \sum_{k+1=1}^{L} iP(i|C_1) = \sum_{i=k+1}^{L} ip_i|\omega_1 = \frac{\mu_T - \mu(k)}{1 - \omega(k)} \tag{17}$$

For any choice of k we have:

$$\omega_o\mu_0 + \omega_1\mu_1 = \mu_T \tag{18}$$

where

$$\omega(k) = \sum_{i=1}^{k} p_i \tag{19}$$

and

$$\mu(k) = \sum_{i=1}^{k} ip_i \tag{20}$$

Hence, the class variance are given by:

$$\sigma_0^2 = \sum_{i=1}^{k}(i - \mu_0)P(i|C_0) = \sum_{i=1}^{k}(i - \mu_0)^2 p_i/\omega_0 \tag{21}$$

$$\sigma_1^2 = \sum_{i=k+1}^{L}(i - \mu_1)P(i|C_1) = \sum_{i=k+1}^{L}(i - \mu_1)^2 p_i/\omega_1 \tag{22}$$

Hence, the optimal class threshold can be determined by maximizing the between-class variance:

$$\sigma_B^2(k) = (i - \mu_1)^2 p_i \tag{23}$$

total class variance is given by

$$\sigma_T^2 = \sum i = 1^L (i - \mu_T)^2 p_i \tag{24}$$

the optimal threshold k^* can be determined by maximizing the following equation:

$$\sigma_B^2(k)/\sigma_T^2 \tag{25}$$

Bibliography

Agarwal, M., Mostafa, J., 2010. Image retrieval for Alzheimer disease detection, in: Proceedings of the First MICCAI international conference on Medical Content-Based Retrieval for Clinical Decision Support, Springer-Verlag, Berlin, Heidelberg. pp. 49–60.

Aisen, A.M., Broderick, L.S., Winer-Muram, H., Brodley, C.E., Kak, A.C., Pavlopoulou, C., Dy, J., Shyu, C.R., Marchiori, A., 2003. Automated storage and retrieval of thin-section ct images to assist diagnosis: System description and preliminary assessment. Radiology 228, 265–270.

Akgul, C.B., Unay, D., Ekin, A., 2009. Automated diagnosis of Alzheimer's disease using image similarity and user feedback, in: Proceedings of the ACM International Conference on Image and Video Retrieval.

Andreas, F., Igor, Y., 2011. Diffusion tensor imaging of the hippocampus in MCI and early Alzheimer's disease. Journal of Alzheimer's Disease 26, 257262.

Apostolova, L.G, T.P.M., 2008. Mapping progressive brain structural changes in early Alzheimers disease and mild cognitive impairment. Neuropsychologia 46, 15971612.

Arakeri, M.e.a., 2013. An intelligent content-based image retrieval system for clinical decision support in brain tumor diagnosis. International Journal of Multimedia Information Retrieval 2, 175–188.

Arnold, S.E., Hyman, B.T., Flory, J., Damasio, A.R., Van Hoesen, G.W., . The topographical

and neuroanatomical distribution of neurofibrillary tangles and neuritic plaques in the cerebral cortex of patients with Alzheimer's disease. Cerebral Cortex .

Arsenault, H.H., Sheng, Y., 1986. Properties of the circular harmonic expansion for rotation-invariant pattern recognition. Appl. Opt. 25, 3225–3229.

Ashburner, J., Friston, K.J., 1999. Nonlinear spatial normalization using basis functions. Human Brain Mapping 7, 254–266.

Ashburner, J., Friston, K.J., 2000. Voxel-Based Morphometrythe methods. Neuroimage 11, 805–821.

Ashburner, J., Neelin, P., Collins, D., Evans, A., Friston, K., 1997. Incorporating prior knowledge into image registration. Neuroimage 6, 344–352.

Alzheimer's Association, A., 2014. Alzheimer's, disease facts and figures 2014. Alzheimer's and Dementia 10, e47 – e92.

Ayache, S., Quénot, G., Gensel, J., 2007. Classifier fusion for svm-based multimedia semantic indexing, in: Proceedings of the 29th European conference on IR research, pp. 494–504.

B. Parente, D., Gasparetto, E.L., Cruz Jr, L.C.H.d., Domingues, R.C., Baptista, A.C., Carvalho, A.C.P., Domingues, R.C., 2008. Potential role of diffusion tensor MRI in the differential diagnosis of mild cognitive impairment and Alzheimer's disease. American Journal of Roentgenology 190, 1369–1374.

Balmashnova, E., Platel, B., Florack, L., ter Haar Romeny, B., 2007. Content-based image retrieval by means of scale-space top-points and differential invariants, in: Proceedings of the MICCAI Workshop on Medical Content-Based Image Retrieval for Biomedical Image Archives: Achievements, Problems, and Prospects Brisbane, Australia, pp. 83–92.

Basser, P.J., Pierpaoli, C., 1996. Microstructural and physiological features of tissues elucidated by quantitative-diffusion-tensor {MRI}. Journal of Magnetic Resonance 213, 560 – 570.

Bay, H., Ess, A., Tuytelaars, T., Van Gool, L., 2008. Speeded-Up Robust Features (SURF). Comput. Vis. Image Underst. 110, 346–359.

Beg, M.F., Raamana, P.R., Barbieri, S., Wang, L., 2013. Comparison of four shape features for detecting hippocampal shape changes in early Alzheimer's. Statistical Methods in Medical Research 22, 439–462.

Berry, D.A., 2004. Bayesian statistics and the efficiency and ethics of clinical trials. Statistical Science , 175–187.

Bicacro, E., Silveira, M., Marques, J.S., Costa, D.C., 2012. 3d brain image-based diagnosis of Alzheimer's disease: Bringing medical vision into feature selection, in: ISBI'12, pp. 134–137.

Bihan, D.L., 2003. Looking into the functional architecture of the brain with diffusion MRI. Nature Reviews. Neuroscience 4, 469–80.

Blennow, K., Hampel, H., Weiner, M., Zetterberg, H., 2010. Cerebrospinal fluid and plasma biomarkers in Alzheimer disease. Nature Reviews Neurology 6, 131–144.

Boser, B.E., Guyon, I.M., Vapnik, V.N., 1992. A training algorithm for optimal margin classifiers, in: the fifth annual workshop on Computational learning theory, ACM. p. 144152.

Bozzali, M., Falini, A., Franceschi, M., Cercignani, M., Zuffi, M., Scotti, G., Comi, G., Filippi, M., 2002. White matter damage in Alzheimer's disease assessed in vivo using diffusion tensor magnetic resonance imaging. Journal of Neurology, Neurosurgery & Psychiatry 72, 742–746.

Braak, H., Braak, E., 1998. Evolution of neuronal changes in the course of Alzheimer's disease. Neurology 53, 127–140.

Bradley, K.M., Bydder, G.M., Budge, M.M., Hajnal, J.V., White, S.J., Ripley, B.D., Smith, A.D., 2002. Serial brain mri at 3-6 month intervals as a surrogate marker for Alzheimer's disease. The British Journal of Radiology 75, 506–513.

Brun, A., Gustafson, L., 1976. Distribution of cerebral degeneration in Alzheimer's disease. Archiv fur Psychiatrie und Nervenkrankheiten 223, 15–33.

Busatto, G.F., Garrido, G.E., Almeida, O.P., Castro, C.C., Camargo, C.H., Cid, C.G., Buchpiguel, C.A., Furuie, S., Bottino, C.M., 2003. A voxel-based morphometry study of temporal lobe gray matter reductions in Alzheimers disease. Neurobiology of Aging 24, 221 – 231.

C Nestor, P.J., Fryer, T.D., Ikeda, M., Hodges, J.R., 2003. Bretrosplenial cortex (ba 29/30) hypometabolism in mild cognitive impairment (prodromal Alzheimer's disease). European Journal of Neuroscience 18, 2663 – 2667.

Callen, D.J., Black, S.E., Gao, F., Caldwell, C.B., Szalai, J.P., 2001. Beyond the hippocampus: Mri volumetry confirms widespread limbic atrophy in ad. Neurology 57, 1669–74.

Castellani, U., Rossato, E., Murino, V., Bellani, M., Rambaldelli, G., Perlini, C., Tomelleri, L., Tansella, M., Brambilla, P., 2012. Classification of schizophrenia using feature-based morphometry. Journal of Neural Transmission 119, 395–404.

Castellani, U., Rossato, E., Murino, V., Bellani, M., Rambaldelli, G., Tansella, M., Brambilla, P., 2009. Local kernel for brains classification in schizophrenia, in: Serra, R., Cucchiara, R. (Eds.), AI*IA 2009: Emergent Perspectives in Artificial Intelligence. Springer Berlin Heidelberg. volume 5883 of *Lecture Notes in Computer Science*, pp. 112–121.

Catheline, G., Periot, O., et al, 2010. Distinctive alterations of the cingulum bundle during aging and Alzheimers disease. Neurobiology of Aging 31, 1582 – 1592.

Chang, C.W., Ho, C.C., Chen, J.H., 2012. ADHD classification by a texture analysis of anatomical brain MRI data. Frontiers in Systems Neuroscience 6.

Chen, D.R., Huang, Y.L., Lin, S.H., 2011. Computer-aided diagnosis with textural features for breast lesions in sonograms. Computerized Medical Imaging and Graphics 35, 220 – 226.

Chen, H.L., Yang, B., Wang, G., Wang, S.J., Liu, J., Liu, D.Y., 2012. Support vector machine based diagnostic system for breast cancer using swarm intelligence. Journal of Medical Systems 36, 2505–2519.

Chen, Y., Storrs, J., Tan, L., Mazlack, L.J., Lee, J.H., Lu, L.J., 2014. Detecting brain structural changes as biomarker from magnetic resonance images using a local feature based SVM approach. Journal of Neuroscience Methods 221, 22 – 31.

Cherubini, A., Péran, P., Spoletini, I., Paola, M.D., Iulio, F.D., al, 2010. Combined volumetry and DTI in subcortical structures of mild cognitive impairment and Alzheimer's disease patients. Journal of Alzheimer's Disease 19, 47 – 55.

Chetelat, G., Baron, J.C., 2003. Early diagnosis of Alzheimers disease: contribution of structural neuroimaging. NeuroImage 18, 525 – 541.

Choo, I.H., Lee, D.Y., Oh, J.S., Lee, J.S., Lee, D.S., Song, I.C., Youn, J.C., Kim, S.G., Kim, K.W., Jhoo, J.H., Woo, J.I., 2010. Posterior cingulate cortex atrophy and regional cingulum disruption in mild cognitive impairment and Alzheimer's disease. Neurobiology of Aging 31, 772 – 779.

Christos, D., Yong, F., Xiaoying, W., Dinggang Shen, and Susan, M.R., 2008. Detection of prodromal Alzheimer's disease via pattern classification of magnetic resonance imaging. Neurobiology of Aging 29, 514 – 523.

Chupin, M., Gérardin, E., Cuingnet, R., et al, 2009a. Fully automatic hippocampus segmentation and classification in Alzheimer's disease and mild cognitive impairment applied on data from ADNI. Hippocampus 19, 579–587.

Chupin, M., Hammers, A., Liu, R.S.N., et al, 2009b. Automatic segmentation of the hippocampus and the amygdala driven by hybrid constraints: Method and validation. NeuroImage 46, 749–761.

Clerx, L., Visser, P.J., Verhey, F., Aalten, P., 2011. New MRI markers for Alzheimer's disease: A meta-analysis of diffusion tensor imaging and a comparison with medial temporal lobe measurements. Journal of Alzheimer's Disease 29, 405429.

Colliot, O., Chételat, G., Chupin, M., et al, 2008. Discrimination between Alzheimer disease, mild cognitive impairment, and normal aging by using automated segmentation of the hippocampus. Radiology 248, 194–201.

Convit, A., de Asis, J., de Leon, M., Tarshish, C., Santi, S.D., Rusinek, H., 2000. Atrophy of the medial occipitotemporal, inferior, and middle temporal gyri in non-demented elderly predict decline to Alzheimers disease. Neurobiology of Aging 21, 19 – 26.

Convit, A., Leon, M.D., Tarshish, C., Santi, S.D., Tsui, W., Rusinek, H., George, A., 1997. Specific hippocampal volume reductions in individuals at risk for Alzheimers disease. Neurobiology of Aging 18, 131 – 138.

Coupé, P., Eskildsen, Simon, F., Manjón, José, V., Fonov, V., Pruessner, Jens, C., Allard, M., Collins, L., 2012. SNIPE: A New Method to Identify Imaging Biomarker for Early Detection of Alzheimer's Disease, in: MICCAI 2012 Workshop on Novel Biomarkers for Alzheimer's Disease and Related Disorders, Nice, France. pp. 41–51.

Csurka, G., Dance, C.R., Fan, L., et al, 2004. Visual categorization with bags of keypoints, in: Workshop on Statistical Learning in Computer Vision, ECCV, pp. 1–22.

Cuingnet, R.e., Gerardin, E., Tessieras, J.e., et al, 2011. Automatic classification of patients with Alzheimer's disease from structural MRI: A comparison of ten methods using the ADNI database. NeuroImage 56, 766–781.

Daliri, M.R., 2012. Automated Diagnosis of Alzheimer disease using the Scale-Invariant Feature Transforms in Magnetic Resonance Images. J. Med. Syst. 36, 995–1000.

Damoiseaux, J.S., Smith, S.M., Witter, M.P., Sanz-Arigita, E.J., Barkhof, F., Scheltens, P., Stam, C.J., Zarei, M., Rombouts, S.A., 2009. White matter tract integrity in aging and Alzheimer's disease. Human brain mapping 30, 1051–1059.

DeKosky, S.T., Marek, K., 2003. Looking backward to move forward: Early detection of neurodegenerative disorders. Science , 830–834.

Dickerson, B., Goncharova, I., Sullivan, M., Forchetti, C., Wilson, R., Bennett, D., Beckett, L., deToledo Morrell, L., 2001. Mri-derived entorhinal and hippocampal atrophy in incipient and very mild Alzheimers disease. Neurobiology of Aging 22, 747 – 754.

Duchesne, S., Bocti, C., Sousa, K.D., Frisoni, G.B., Chertkow, H., Collins, D.L., 2010. Amnestic MCI future clinical status prediction using baseline MRI features. Neurobiology of Aging 31, 1606–1617.

Dy, J., Brodley, C., Kak, A., Broderick, L., Aisen, A., 2003. Unsupervised feature selection applied to content-based retrieval of lung images. IEEE Transactions on Pattern Analysis and Machine Intelligence 25, 373–378.

Dyrba, M., Ewers, M., Wegrzyn, M., Kilimann, I., Plant, C., al, 2012. Combining DTI and MRI for the automated detection of Alzheimer's disease using a large european multicenter dataset, in: Multimodal Brain Image Analysis, Springer Berlin / Heidelberg, Nice, France. pp. 18–28.

E. Mark Haacke, Robert W. Brown, M.R.T.e.e., 1999. Magnetic resonance imaging : physical principles and sequence design. J. Wiley & Sons, New York, Chicester, Weinheim.

El-Dahshan, E.A., Mohsen, H.M., Revett, K., Salem, A.M., 2014. Computer-aided diagnosis of human brain tumor through MRI: A survey and a new algorithm. Expert Syst. Appl. 41, 5526–5545.

Fan, Y., Batmanghelich, N., Clark, C.M., Davatzikos, C., 2008. Spatial patterns of brain atrophy in mci patients, identified via high-dimensional pattern classification, predict subsequent cognitive decline. NeuroImage 39, 1731 – 1743.

Fan, Y., Shen, D., Gur, R.C., Gur, R.E., Davatzikos, C., 2007. Compare: classification of morphological patterns using adaptive regional elements. Medical Imaging, IEEE Transactions on 26, 93–105.

Farhan, S., Fahiem, M.A., Tauseef, H., 2014. An ensemble-of-classifiers based approach for early diagnosis of Alzheimer's disease: Classification using structural features of brain images. Computational and Mathematical Methods in Medicine 2014, 1–11.

Felipe, J.C., Traina, A.J.M., Traina, Jr., C., 2003. Retrieval by content of medical images using texture for tissue identification , 175–180.

Fitzpatrick, J.M., Hill, D.L., Shyr, Y., West, J., Studholme, C., Maurer, C.R., 1998. Visual assessment of the accuracy of retrospective registration of mr and ct images of the brain. Medical Imaging, IEEE Transactions on 17, 571–585.

Fletcher, R., 1987a. Practical methods of optimization. A Wiley Interscience Publication, John Wiley & Sons, Chichester, New York, Brisbane. Autre tirage : 1989 (rel.).

Fletcher, R., 1987b. Practical methods of optimization. A Wiley Interscience Publication, John Wiley & Sons, Chichester, New York, Brisbane. Autre tirage : 1989 (rel.).

Frisoni, G.B., Testa, C., Sabattoli, F., Beltramello, A., Soininen, H., Laakso, M.P., 2005. Structural correlates of early and late onset Alzheimers disease: voxel based morphometric study. Journal of Neurology, Neurosurgery and Psychiatry 76, 112–114.

Fung, G., Stoeckel, J., 2007. Svm feature selection for classification of spect images of Alzheimer's disease using spatial information. Knowledge and Information Systems 11, 243–258.

Gaser, C., Nenadic, I., Buchsbaum, B.R., Hazlett, E.A., Buchsbaum, M.S., 2001. Deformation-based morphometry and its relation to conventional volumetry of brain lateral ventricles in {MRI}. NeuroImage 13, 1140 – 1145.

Gerardin, E., Chételat, G., Chupin, M., et al, 2009. Multidimensional classification of hippocampal shape features discriminates Alzheimer's disease and mild cognitive impairment from normal aging. NeuroImage 47, 1476–86.

Geva, T., 2006. Magnetic resonance imaging: Historical perspective. Journal of Cardiovascular Magnetic Resonance, 8, 573–580.

Ghosh, P., Antani, S., Long, L.R., Thoma, G.R., 2011. Review of medical image retrieval systems and future directions, in: Proceedings of the 2011 24th International Symposium on Computer-Based Medical Systems, pp. 1–6.

Greenfield, J.G., Graham, D.I., Lantos, P.L., 1997. Greenfield's neuropathology. Arnold.

tebbins GT, Smith CA, B.R.e.a., 2007. Hiv-associated alterations in normal-appearing white matter: a voxel-wise diffusion tensor imaging study. J Acquir Immune Defic Syndr 46, 564–573.

Gutman, B., Morra, Y.W.J., Toga, A., Thompson, P., 2009. Disease classification with hippocampal shape invariants. Hippocampus 19, 572–578.

Haller, S., Lovblad, K.O., Giannakopoulos, P., 2011. Principles of classification analyses in mild cognitive impairment (MCI) and Alzheimer disease. Journal of Alzheimer's Disease 26, 389–394.

Haller, S., Nguyen, D., Rodriguez, C., Emch, J., Gold, G., Bartsch, A., Lovblad, K., Giannakopoulos, P., 2010. Individual prediction of cognitive decline in mild cognitive impairment using support vector machine-based analysis of diffusion tensor imaging data. Journal of Alzheimer's Disease 22, 315–327.

Hani, A., Nugroho, H., Nugroho, H., 2010. Gaussian bayes classifier for medical diagnosis and grading: Application to diabetic retinopathy, in: Biomedical Engineering and Sciences (IECBES), 2010 IEEE EMBS Conference on, pp. 52–56.

Hebert, L.E., Weuve, J., Scherr, P.A., Evans, D.A., 2013. Alzheimer disease in the united states (2010–2050) estimated using the 2010 census. Neurology 80, 1778–1783.

Heggie, J., 2001. Magnetic resonance imaging: Principles, methods and techniques by perry sprawls. Australasian Physics & Engineering Sciences in Medicine 24, 57–57.

den Heijer, T., van der Lijn, F., al, 2012. Structural and diffusion mri measures of the hippocampus and memory performance. NeuroImage 63, 1782–1789.

Hinrichs, C., Singh, V., Mukherjee, L., Xu, G., Chung, M.K., Johnson, S.C., 2009. Spatially augmented lpboosting for ad classification with evaluations on the adni dataset. NeuroImage 48, 138–149.

Huang, C., Wahlund, L.O., Svensson, L., Winblad, B., Julin, P., 2002. Cingulate cortex hypoperfusion predicts Alzheimer's disease in mild cognitive impairment. BMC Neurology 2, 1–6.

Huang, M., Yang, W., Wu, Y., Jiang, J., Gao, Y., Chen, Y., Feng, Q., Chen, W., Lu, Z., 2014. Content-based image retrieval using spatial layout information in brain tumor t1-weighted contrast-enhanced mr images. PLoS ONE 9, e102754.

Huang, M., Yang, W., Yu, M., Lu, Z., Feng, Q., Chen, W., 2012. Retrieval of brain tumors with region-specific bag-of-visual-words representations in contrast-enhanced MRI images. Comp. Math. Methods in Medicine 2012.

Illán, I., Górriz, J., López, M., Ramórez, J., Salas-Gonzalez, D., Segovia, F., Chaves, R., Puntonet, C., 2011. Computer aided diagnosis of Alzheimers disease using component based SVM. Applied Soft Computing 11, 2376 – 2382.

Jack, C.R., Petersen, R.C., O'Brien, P.C., Tangalos, E.G., 1992. Mr-based hippocampal volumetry in the diagnosis of Alzheimer's disease. Neurology 42, 183–183.

Jain, A.K., Murty, M.N., Flynn, P.J., 1999. Data clustering: A review. ACM Comput. Surv. 31, 264–323.

Jiang, M., Zhang, S., Liu, J., Shen, T., Metaxas, D.N., 2014. Computer-aided diagnosis of mammographic masses using vocabulary tree-based image retrieval, in: Biomedical Imaging (ISBI), 2014 IEEE 11th International Symposium on, pp. 1123–1126.

Jolliffe, I.T., 2002. Principal Component Analysis. Springer. second edition.

Jones, B.F., Barnes, J., Uylings, H.B.M., Fox, N.C., Frost, C., Witter, M.P., Scheltens, P., 2006. Differential regional atrophy of the cingulate gyrus in Alzheimer disease: a volumetric mri study. Cereb Cortex 16, 1701–8.

Kale, R.A., Gupta, R.K., Saraswat, V.A., Hasan, K.M., Trivedi, R., Mishra, A.M., Ranjan, P., Pandey, C.M., Narayana, P.A., 2006. Demonstration of interstitial cerebral edema with diffusion tensor mr imaging in type c hepatic encephalopathy. Hepatology 43, 698–706.

Kantarci K, Petersen RC, B.B.e.a., 2005. Dwi predicts future progression to Alzheimer disease in amnestic mild cognitive impairment. Neurology 64, 902904.

Kemp, P.M., Holmes, C., Hoffmann, S.M.A., Bolt, L., Holmes, R., Rowden, J., Fleming, J.S., 2003. Alzheimer's disease: differences in technetium-99m hmpao spect scan findings between early onset and late onset dementia. Journal of Neurology, Neurosurgery and Psychiatry 74, 715–719.

Keysers, D., Dahmen, J., Ney, H., Wein, B., Lehmann, T., 2002. A statistical framework for model-based image retrieval in medical applications.

Kim, J., Cai, W., Feng, D., Wu, H., 2006. A new way for multidimensional medical data management: Volume of interest (voi)-based retrieval of medical images with visual and functional features. Trans. Info. Tech. Biomed. 10, 598–607.

Kinoshita, S.e., de Azevedo-Marques, P., Pereira, RobertoRodrigues, J., Rodrigues, J., Rangayyan, R., 2007. Content-based retrieval of mammograms using visual features related to breast density patterns. Journal of Digital Imaging 20, 172–190.

Klöppel, S., Stonnington, C.M., Chu, et al, 2008. Automatic classification of MR scans in Alzheimer's disease. Brain 131, 681–9.

van der Kouwe, A.J., Benner, T., Salat, D.H., Fischl, B., 2008. Brain morphometry with multiecho mprage. NeuroImage 40, 559–569.

Kumar, A., Kim, J., Cai, W., Fulham, M., Feng, D., 2013. Content-based medical image retrieval: A survey of applications to multidimensional and multimodality data. Journal of Digital Imaging , 1–15.

Lao, Z., Shen, D., Xue, Z., Karacali, B., Resnick, S.M., Davatzikos, C., 2004. Morphological classification of brains via high-dimensional shape transformations and machine learning methods. Neuroimage 21, 46–57.

Lebihan, D., Breton, E., 1985. Imagerie de Diffusion In Vivo par Résonance Magnétique Nucléaire. XXX CR Académie des Sciences de Paris 301, 1109–1112.

Lecron, F., Benjelloun, M., Mahmoudi, S., 2012. Descriptive image feature for object detection in medical images, in: Campilho, A.e., Kamel, M. (Eds.), Image Analysis and Recognition. Springer Berlin Heidelberg. volume 7325 of *Lecture Notes in Computer Science*, pp. 331–338.

Lee, W., Park, B., Han, K., 2013. Classification of diffusion tensor images for the early detection of Alzheimer's disease. Computers in Biology and Medicine 43, 1313 – 1320.

Lehericy, S., M.M.M.L.S.M.K.S., 2007. Magnetic resonance imaging of Alzheimers disease. European Radiology 17, 347–362.

Lehmann, T.M., Gold, M., Thies, C., Fischer, B., Spitzer, K., Keysers, D., Ney, H., Kohnen, M., Schubert, H., Wein, B.B., 2004. Content-based image retrieval in medical applications. Methods of Information in Medicine 43, 354–361.

Li-jia, Z., Shao-min, Z., Da-zhe, Z., Zhao, H., Shu-kuan, L., 2009. Medical image retrieval using sift feature, in: Image and Signal Processing, 2009. CISP '09. 2nd International Congress on, pp. 1–4.

Li M1, Oishi K2, H.X.Q.Y.G.F.M.S.A.D.N.I., 2014. Toews. 9, e105563.

Liu, J., Yin, C., Xia, S., Jia, L., Guo, Y., Zhao, Z., Li, X., Han, Y., Jia, J., 2013. White matter changes in patients with amnestic mild cognitive impairment detected by diffusion tensor imaging. PLoS ONE 8, e59440.

Liu, Y., Paajanen, T., Zhang, Y., Westman, E., et al, 2009. Combination analysis of neuropsychological tests and structural MRI measures in differentiating AD, MCI and control groups-the addneuromed study. Neurobiol Aging .

Liu, Y., Spulber, G., Lehtimäki, K.K., Könönen, M., Hallikainen, I., Gröhn, H., Kivipelto, M., Hallikainen, M., Vanninen, R., Soininen, H., 2011. Diffusion tensor imaging and tract-based spatial statistics in Alzheimer's disease and mild cognitive impairment. Neurobiology of aging 32, 1558–1571.

Long, F., Zhang, H., Feng, D., 2003. Fundamentals of content-based image retrieval, in: Feng, D., Siu, W.C., Zhang, H.J. (Eds.), Multimedia Information Retrieval and Management. Springer Berlin Heidelberg. Signals and Communication Technology, pp. 1–26.

Lopes Simoes, A.R., Slump, C.H., van Cappellen van Walsum, A.M., 2012. Using local texture maps of brain mr images to detect mild cognitive impairment, in: 21st International Conference on Pattern Recognition (ICPR 2012), Tsukuba, Japan, IEEE Computer Society. pp. 153–156.

Lowe, D.G., 2004. Distinctive Image Features from Scale-Invariant Keypoints. Int. J. Comput. Vision 60, 91–110.

Madden, D.J., Bennett, I.J., Burzynska, A., Potter, G.G., kuei Chen, N., Song, A.W., 2012. Diffusion tensor imaging of cerebral white matter integrity in cognitive aging. Biochimica et Biophysica Acta (BBA) - Molecular Basis of Disease 1822, 386–400. Imaging Brain Aging and Neurodegenerative Disease.

Maes, F., Collignon, A., Vandermeulen, D., Marchal, G., Suetens, P., 1997. Multimodality image registration by maximization of mutual information. Medical Imaging, IEEE Transactions on 16, 187–198.

Magnin, B., Mesrob, L., Kinkingn éhun, S., P él égrini Issac, M.e., Colliot, O., Sarazin, M., Dubois, B., Leh éricy, S.e., Benali, H., 2009. Support vector machine-based classification of Alzheimers disease from whole-brain anatomical mri. Neuroradiology 51, 73–83.

Mangin, J.F., Rivière, D., Cachia, A., Papadopoulos-Orfanos, D., et al, 2003. Object-based strategy for morphometry of the cerebral cortex, in: IPMI, Ambleside, UK, LNCS-2732, SpringerVerlag, UK, SpringerVerlag. pp. 160–171.

Mechelli, A., Price, C.J., Friston, K.J., Ashburner, J., 2005. Voxel-based morphometry of the human brain: Methods and applications. Current Medical Imaging Reviews 1, 105–113.

Medina, D., deToledo Morrell, L., Urresta, F., Gabrieli, J.D., Moseley, M., Fleischman, D., Bennett, D.A., Leurgans, S., Turner, D.A., Stebbins, G.T., 2006. White matter changes

in mild cognitive impairment and ad: A diffusion tensor imaging study. Neurobiology of aging 27, 663–672.

Meijuan Yang, Yuan Yuan, X.L., Yan, P., 2011. Medical image segmentation using descriptive image features, in: Proceedings of the British Machine Vision Conference, BMVA Press. pp. 94.1–94.11.

Mesrob, L., Sarazin, M., Hahn-Barma, V., al, 2012. DTI and structural MRI classification in Alzheimer's disease. Advances in Molecular Imaging 2, 12 – 20.

Mielke, M., Kozauer, N., Chan, K., George, M., al, 2009. Regionally-specific diffusion tensor imaging in mild cognitive impairment and Alzheimer's disease. NeuroImage 46, 47 – 55.

Minoshima, S., Giordani, B., Berent, S., Frey, K.A., Foster, N.L., Kuhl, D.E., 1997. Metabolic reduction in the posterior cingulate cortex in very early Alzheimer's disease. Annals of neurology 42, 85–94.

Misra, C., Fan, Y., Davatzikos, C., 2009. Baseline and longitudinal patterns of brain atrophy in mci patients, and their use in prediction of short-term conversion to ad: Results from adni. NeuroImage 44, 1415–1422.

Mizotin, M., Benois-Pineau, J., Allard, M., Catheline, G., 2012. Feature-based brain MRI retrieval for Alzheimer disease diagnosis, in: 19th IEEE International Conference on Image Processing (ICIP), pp. 1241–1244.

Montagne, C., Kodewitz, A., Vigneron, V., Giraud, V., Lelandais, S., 2013. 3d local binary pattern for PET image classification by SVM - application to early Alzheimer disease diagnosis, in: BIOSIGNALS 2013 - Proceedings of the International Conference on Bio-inspired Systems and Signal Processing, Barcelona, Spain, 11-14 February, 2013., pp. 145–150.

Mortensen, E.N., Barrett, W.A., 1995. Intelligent scissors for image composition, in: Proceedings of the 22nd annual conference on Computer graphics and interactive techniques, ACM. pp. 191–198.

Mukherjee, P., Berman, J., Chung, S., Hess, C., Henry, R., 2008. Diffusion tensor mr imaging and fiber tractography: theoretic underpinnings. American journal of neuroradiology 29, 632–641.

Müller, H., Deserno, T.M., 2011. Content-based medical image retrieval, in: Biomedical Image Processing - Methods and Applications. Springer.

Müller, H., Michoux, N., Bandon, D., Geissbuhler, A., 2004. A review of content-based image retrieval systems in medical applicationsclinical benefits and future directions. International Journal of Medical Informatics 73, 1– 23.

Müller, M.J., Greverus, D., Weibrich, C., Dellani, P.R., Scheurich, A., Stoeter, P., Andreas, 2007. Diagnostic utility of hippocampal size and mean diffusivity in amnestic mci. Neurobiology of Aging 28, 398 –403.

Naggara, O., Oppenheim, C., Rieu, D., Raoux, N., Rodrigo, S., Dalla Barba, G., Meder, J.F., 2006. Psychiatry Research: Neuroimaging 146, 243–249.

Nanni, L., Lumini, A., Brahnam, S., 2010. Local binary patterns variants as texture descriptors for medical image analysis. Artificial Intelligence in Medicine 49, 117–125.

Nazari, M.R., Fatemizadeh, E., 2010. Article:a cbir system for human brain magnetic resonance image indexing. International Journal of Computer Applications 7, 33–37. Published By Foundation of Computer Science.

Nestor, S.M., Rupsingh, R., Borrie, M., Smith, M., Accomazzi, V., Wells, J.L., Fogarty, J., Bartha, R., et al., 2008. Brain 131, 2443–2454.

Nir, T.M., Jahanshad, N., Villalon-Reina, J.E., Toga, A.W., Jack, C.R., Weiner, M.W., Thompson, P.M., 2013. Effectiveness of regional dti measures in distinguishing Alzheimer's disease, mci, and normal aging. NeuroImage: Clinical 3, 180–195.

Nissan, A., Protic, M., Bilchik, A., Eberhardt, J., Peoples, G.E., Stojadinovic, A., 2010. Predictive model of outcome of targeted nodal assessment in colorectal cancer. Annals of surgery 251, 265–274.

Nowak, E., Jurie, F., Triggs, B., 2006. Sampling strategies for bag-of-features image classification, in: Computer Vision–ECCV 2006. Springer, pp. 490–503.

Nyúl, L.G., Udupa, J.K., Zhang, X., 2000. New variants of a method of mri scale standardization. IEEE Trans. Med. Imaging 19, 143–150.

O'Dwyer, L., Lamberton, F., Bokde, A.L.W., Ewers, M., Faluyi, Y.O., Tanner, C., Mazoyer, B., O'Neill, D., Bartley, M.e., Collins, D.R., Coughlan, T., Prvulovic, D., Hampel, H., 2012. Using support vector machines with multiple indices of diffusion for automated classification of mild cognitive impairment. PLoS ONE 7, e32441.

Ojala, T., Pietikäinen, M., Mäenpää, T., 2002. Multiresolution gray-scale and rotation invariant texture classification with local binary patterns. IEEE Trans. Pattern Anal. Mach. Intell. 24, 971–987.

Oliver, A., LladO; X., Freixenet, J., MartI; J., 2007. False positive reduction in mammographic mass detection using local binary patterns, in: Ayache, N., Ourselin, S.e., Maeder, A. (Eds.), Medical Image Computing and Computer-Assisted Intervention MICCAI 2007. Springer Berlin Heidelberg. volume 4791 of *Lecture Notes in Computer Science*, pp. 286–293.

Oppedal, K., Engan, K., Aarsland, D., Beyer, M., Tysnes, O.B., Eftestol, T., 2012. Using local binary pattern to classify dementia in MRI, in: Biomedical Imaging (ISBI), 2012 9th IEEE International Symposium on, pp. 594–597.

Ortiz, A., Górriz, J.M., Ramírez, J., Martínez-Murcia, F., 2013. Lvq-svm basedcad tool applied to structural mri for the diagnosis of the Alzheimers disease. Pattern Recognition Letters 34, 1725 – 1733. Innovative Knowledge Based Techniques in Pattern Recognition.

Otsu, N., 1979. A Threshold Selection Method from Gray-level Histograms. IEEE Transactions on Systems, Man and Cybernetics 9, 62–66.

Patil, R.B., Piyush, R., Ramakrishnan, S., 2013. Identification of brain white matter regions for diagnosis of Alzheimer using diffusion tensor imaging. Conf Proc IEEE Eng Med Biol Soc , 6535–6538.

Patil, R.B., Ramakrishnan, S., 2014. Analysis of sub-anatomic diffusion tensor imaging indices in white matter regions of Alzheimer with mmse score. Computer Methods and Programs in Biomedicine 117, 13 – 19.

Pelletier, A., Periot, O., Dilharreguy, B., Hiba, B., Bordessoules, M., Pérès, K., Amieva, H., Dartigues, J.F., Allard, M., Catheline, G., 2013. Structural hippocampal network alterations during healthy aging: a multi-modal mri study. Frontiers in aging neuroscience 5.

Pengas, G., Hodges, J., Watson, P., Nestor, P., 2010. Focal posterior cingulate atrophy in incipient Alzheimer's disease. Neurobiol Aging 31, 25–33.

Pennanen, C., Kivipelto, M., Tuomainen, S., Hartikainen, P., Hänninen, T., Laakso, M.P., Hallikainen, M., Vanhanen, M., Nissinen, A., Helkala, E.L., et al., 2004. Hippocampus and entorhinal cortex in mild cognitive impairment and early ad. Neurobiology of aging 25, 303–310.

Platt, J.C., 1999. Probabilistic outputs for support vector machines and comparisons to regularized likelihood methods, in: Advances in large margin and classifiers, MIT Press. pp. 61–74.

Van de Pol, L., van Der Flier, W., Korf, E., Fox, N., Barkhof, F., Scheltens, P., 2007. Baseline predictors of rates of hippocampal atrophy in mild cognitive impairment. Neurology 69, 1491–1497.

Qin, Y.Y., Hsu, J.T., Yoshida, S., Faria, A.V., Oishi, K., Unschuld, P.G., Redgrave, G.W., Ying, S.H., Ross, C.A., van Zijl, P.C., Hillis, A.E., Albert, M.S., Lyketsos, C.G., Miller, M.I., Mori, S., Oishi, K., 2013. Gross feature recognition of anatomical images based on atlas grid (gaia): Incorporating the local discrepancy between an atlas and a target image to capture the features of anatomic brain MRI. NeuroImage: Clinical 3, 202–211.

Quellec, G., Lamard, M., Cazuguel, G., Roux, C., Cochener, B., 2010. Wavelet optimization for content-based image retrieval in medical databases. Medical Image Analysis 14, 227 – 241.

Quellec, G., Lamard, M., Cazuguel, G., Roux, C., Cochener, B., 2011. Case retrieval in medical databases by fusing heterogeneous information. Medical Imaging, IEEE Transactions on 30, 108–118.

Querbes, O., Aubry, F., Pariente, J., Lotterie, J.A., Deacute;monet, J.F., Duret, V., Puel, M., Berry, I., Fort, J.C., Celsis, P., , 2009. Early diagnosis of Alzheimers disease using cortical thickness: impact of cognitive reserve. Brain 132, 2036–47.

Radanovic, M., Pereira, F.R.S., Stella, F., Aprahamian, I., Ferreira, L.K., Forlenza, O.V., Busatto, G.F., 2013. White matter abnormalities associated with Alzheimers disease and mild cognitive impairment: a critical review of mri studies. Expert Review of Neurotherapeutics 13, 483–493.

Ramirez, J., Gorriz, J., Salas-Gonzalez, D., Romero, A., pez, M.L.., Ívarez, I.A., Gomez-Rió, M., 2013. Computer-aided diagnosis of Alzheimers type dementia combining support vector machines and discriminant set of features. Information Sciences 237, 59 – 72.

Ridha, B.H., Barnes, J., Bartlett, J.W., Godbolt, A., Pepple, T., Rossor, M.N., Fox, N.C., 2006. Tracking atrophy progression in familial Alzheimer's disease: a serial mri study. The Lancet Neurology 5, 828 – 834.

Ridha, B.H., Barnes, J., Van de Pol, L.A., et al, 2007. Application of automated medial temporal lobe atrophy scale to Alzheimer disease. Archives of Neurology 64, 849–854.

Rodgers, A.B., on Aging., N.I., 2002. Alzheimer's disease [electronic resource] : unraveling the mystery. National Institute on Aging, National Institutes of Health [Bethesda, Md.].

Rose, S.E., Janke PhD, A.L., Chalk, J.B., 2008. Gray and white matter changes in Alzheimer's disease: A diffusion tensor imaging study. Journal of Magnetic Resonance Imaging 27, 20–26.

Rovira, A., Swanton, J., Tintore, M., et al, 2009. A single, early magnetic resonance imaging study in the diagnosis of multiple sclerosis. Archives of Neurology 66, 587–592.

Rueda, A., Arevalo, J.E., Cruz-Roa, A., Romero, E., González, F.A., 2012. Bag of features for automatic classification of Alzheimer's disease in Magnetic Resonance Images, in: CIARP, pp. 559–566.

Salmond, C., Ashburner, J., Vargha-Khadem, F., Connelly, A., andK.J. Friston, D.G.G., 2002. The precision of anatomical normalisation in the medial temporal lobe using spatial basis functions. NeuroImage 17, 507–512.

Sargent, D., Chen, C.I., Tsai, C.M., Wang, Y.F., Koppel, D., 2009. Feature detector and descriptor for medical images. Proc. SPIE 7259, 72592Z–72592Z–8.

Scher, A., Xu, Y., Korf, E., White, L., Scheltens, P., Toga, A., Thompson, P., Hartley, S., Witter, M., Valentino, D., Launer, L., 2007. Hippocampal shape analysis in Alzheimers disease: A population-based study. NeuroImage 36, 8 – 18.

Schott, J.M., Price, S.L., Frost, C., Whitwell, J.L., Rossor, M.N., Fox, N.C., 2005. Measuring atrophy in Alzheimer disease: A serial mri study over 6 and 12 months. Neurology 65, 119–124.

Schuff, N., Woerner, N., Boreta, L., Kornfield, T., Shaw, L., Trojanowski, J., Thompson, P., Jack, C., Weiner, M., et al., 2009. MRI of hippocampal volume loss in early alzheimer's disease in relation to apoe genotype and biomarkers. Brain 132, 1067–1077.

Serra, L., Cercignani, M., Lenzi, D., Perri, R., Fadda, L., Caltagirone, C., Macaluso, E., Bozzali, M., 2010. Grey and white matter changes at different stages of Alzheimer's disease. Journal of Alzheimer's Disease 19, 147 – 159.

Shaw, L.M., Vanderstichele, H., Knapik-Czajka, M., et al, 2009. Cerebrospinal fluid biomarker signature in Alzheimer's disease neuroimaging initiative subjects. Annals of Neurology 65, 403–413.

Shen, K., Bourgeat, P., Fripp, J., Meriaudeau, F., Salvado, O., 2011. Detecting hippocampal shape changes in Alzheimer's disease using statistical shape models , 796243–796243–7.

Shen, K.K., Fripp, J., Meriaudeau, F., Chetelat, G.e., Salvado, O., Bourgeat, P., 2012. Detecting global and local hippocampal shape changes in Alzheimer's disease using statistical shape models. NeuroImage 59, 2155–2166.

Shiino, A., Watanabe, T., Maeda, K., Kotani, E., Akiguchi, I., Matsuda, M., 2006. Four subgroups of Alzheimer's disease based on patterns of atrophy using vbm and a unique pattern for early onset disease. NeuroImage 33, 17 – 26.

Shyu, C.R., Brodley, C.E., Kak, A.C., Kosaka, A., Aisen, A.M., Broderick, L.S., 1999. Assert: A physician-in-the-loop content-based retrieval system for hrct image databases. Computer Vision and Image Understanding 75, 111–132.

Sivic, J., Zisserman, A., 2009. Efficient visual search of videos cast as text retrieval. IEEE Trans. Pattern Anal. Mach. Intell. 31, 591–606.

Smeulders, A.W.M., Worring, M., Santini, S., Gupta, A., Jain, R., 2000. Content-based image retrieval at the end of the early years. IEEE Trans. Pattern Anal. Mach. Intell. 22, 1349–1380.

Smith, S.M., Jenkinson, M., Johansen-Berg, H., Rueckert, D., Nichols, T.E., Mackay, C.E., Watkins, K.E., Ciccarelli, O., Cader, M.Z., Matthews, P.M., Behrens, T.E., 2006. Tract-based spatial statistics: Voxelwise analysis of multi-subject diffusion data. NeuroImage 31, 1487 – 1505.

Sorgi, L., Cimminiello, N., Neri, A., 2006. Keypoints Selection in the Gauss Laguerre Transformed Domain., in: BMVC, British Machine Vision Association. pp. 539–547.

Sorokin, D.V., Mizotin, M.., Krylov, A.S., 2011. Gauss-laguerre keypoints extraction using fast hermite projection method, in: Proceedings of the 8th international conference on Image analysis and recognition - Volume Part I, Springer-Verlag, Berlin, Heidelberg. pp. 284–293.

Stahl, R., Dietrich, O., Teipel, S.J., Hampel, H., Reiser, M.F., Schoenberg, S.O., 2007. White matter damage in Alzheimer disease and mild cognitive impairment: Assessment with diffusion-tensor mr imaging and parallel imaging techniques 1. Radiology 243, 483–492.

Stefan, J., Teipel, Christine, B., Michael, E., Arun, L.B., Maximilian, F.R., Hans-J ürgen, M., Harald, H., 2007. Multivariate deformation-based analysis of brain atrophy to predict Alzheimer's disease in mild cognitive impairment. NeuroImage 38, 13 – 24.

Stoub TR, Bulgakova M, L.S.e.a., 2005. Mri predictors of risk of incident Alzheimer's disease: a longitudinal study. Neurology 64, 1520–1524.

Stricker NH, Schweinsburg BC, D.W.L.e.a., 2009. Decreased white matter integrity in late-myelinating fiber pathways in Alzheimer's disease supports retrogenesis. Neuroimage 45, 10–16.

Studholme, C., Drapaca, C., Iordanova, B., Cardenas, V., 2006. Deformation-based mapping of volume change from serial brain MRI in the presence of local tissue contrast change. Medical Imaging, IEEE Transactions on 25, 626–639.

Tabelow K, Polzehl J, S.V.e.a., 2008. Diffusion tensor imaging: structural adaptive smoothing. Neuroimage 39, 1763–1773.

Takahashi S, Yonezawa H, T.J.e.a., 2002. Selective reduction of diffusion anisotropy in white matter of Alzheimer's disease brains measured by 3.0 tesla magnetic resonance imaging. Neurosci Lett 332, 45–48.

Tamaki, T., Yoshimuta, J., Kawakami, M., Raytchev, B., Kaneda, K., Yoshida, S., Takemura, Y., Onji, K., Miyaki, R., Tanaka, S., 2013. Computer-aided colorectal tumor classification in NBI endoscopy using local features. Medical Image Analysis 17, 78 – 100.

Tao, D., Tang, X., Li, X., Wu, X., 2006. Asymmetric bagging and random subspace for support vector machines-based relevance feedback in image retrieval. Pattern Analysis and Machine Intelligence, IEEE Transactions on 28, 1088–1099.

Tapiola, T., Pennanen, C., Tapiola, M., Tervo, S., Kivipelto, M., änninen, T.H., äki, M.P., Laakso, M.P., Hallikainen, M., äm äl äinen, A.H., Vanhanen, M., Helkala, E.L., Vanninen, R., Nissinen, A., Rossi, R., Frisoni, G.B., Soininen, H., 2008. {MRI} of hippocampus and entorhinal cortex in mild cognitive impairment: A follow-up study. Neurobiology of Aging 29, 31–38.

Toews, M., Wells, W., Collins, D.L., Arbel, T., 2010. Feature-Based Morphometry: Discovering Group-related Anatomical Patterns. NeuroImage , 2318–2327.

Tzourio-Mazoyer, N., Landeau, B., Papathanassiou, D., et al, 2002. Automated Anatomical Labeling of Activations in SPM using a macroscopic anatomical parcellation of the MNI MRI single-subject brain. NeuroImage 15, 273 – 289.

Unay, D., 2010. Augmenting clinical observations with visual features from longitudinal mri data for improved dementia diagnosis, in: Proceedings of the International Conference on Multimedia Information Retrieval, ACM, New York, NY, USA. pp. 193–200.

Unay, D., Ekin, A., 2011. Dementia diagnosis using similar and dissimilar retrieval items, in: Biomedical Imaging: From Nano to Macro, 2011 IEEE International Symposium on, pp. 1889–1892.

Unay, D., Ekin, A., Jasinschi, R., 2008. Medical image search and retrieval using local binary patterns and klt feature points, in: Image Processing, 2008. ICIP 2008. 15th IEEE International Conference on, pp. 997–1000.

Unay, D., Ekin, A., Jasinschi, R.S., 2010. Local structure-based region-of-interest retrieval in brain MR images. IEEE Transactions on Information Technology in Biomedicine 14, 897–903.

Vasconcelos, L.d.G., Jackowski, A.P., Oliveira, M.O.d., Flor, Y.M.R., Bueno, O.F.A., Brucki, S.M.D., 2011. Voxel-based morphometry findings in Alzheimer's disease: neuropsychiatric symptoms and disability correlations-preliminary results. Clinics 66, 1045–1050.

Vemuri, P., Gunter, J.L., Senjem, M.L., Whitwell, J.L., Kantarci, K., Knopman, D.S., Boeve, B.F., Petersen, R.C., Jr, C.R.J., 2008. Alzheimer's disease diagnosis in individual subjects using structural mr images: Validation studies. NeuroImage 39, 1186 – 1197.

Villain, N., Desgranges, B., Viader, F., et al, 2008. Relationships between hippocampal atrophy, white matter disruption, and gray matter hypometabolism in Alzheimer's disease. The Journal of neuroscience : the official journal of the Society for Neuroscience 28, 6174–6181.

Wang, H., Ren, Y., Bai, L., Zhang, W., Tian, J., 2012. Morphometry based on effective and accurate correspondences of localized patterns (meacolp). PLoS ONE 7, e35745.

Wang, L., Swank, J.S., Glick, I.E., Gado, M.H., Miller, M.I., Morris, J.C., Csernansky, J.G., 2003. Changes in hippocampal volume and shape across time distinguish dementia of the Alzheimer type from healthy aging. NeuroImage 20, 667 – 682.

Wee, C., Yap, P., Shen, D., 2013. Prediction of Alzheimer's disease and mild cognitive impairment using cortical morphological patterns. Human Brain Mapping .

Weiner, M.W., Aisen, P.S., Jack Jr, C.R., Jagust, W.J., Trojanowski, J.Q., Shaw, L., Saykin, A.J., Morris, J.C., Cairns, N., Beckett, L.A., et al., 2010. The Alzheimer's disease neuroimaging initiative: progress report and future plans. Alzheimer's & Dementia 6, 202–211.

Welter, P., Fischer, B., Gunther, R.W., Deserno, T.M., 2012. Generic integration of content-based image retrieval in computer-aided diagnosis. Computer Methods and Programs in Biomedicine 108, 589 – 599.

West, J.B., Fitzpatrick, J.M., Wang, M.Y., Dawant, B.M., Maurer Jr, C.R., Kessler, R.M., Maciunas, R.J., Barillot, C., Lemoine, D., Collignon, A.M., et al., 1996. Comparison and evaluation of retrospective intermodality image registration techniques, in: Medical Imaging 1996, International Society for Optics and Photonics. pp. 332–347.

Xu, Y., Jack, C., Obrien, P., Kokmen, E., Smith, G., Ivnik, R., Boeve, B., Tangalos, R., Petersen, R., 2000. Usefulness of mri measures of entorhinal cortex versus hippocampus in ad. Neurology 54, 1760–1767.

Yakushev, I., üller, M.J.M., Lorscheider, M., Schermuly, I., Weibrich, C., Dellani, P.R., Hammers, A., Stoeter, P., Fellgiebel, A., 2010. Increased hippocampal head diffusivity predicts impaired episodic memory performance in early Alzheimer's disease. Neuropsychologia 48, 1447 – 1453.

Yang, S.T., Lee, J.D., Huang, C.H., Wang, J.J., Hsu, W.C., Wai, Y.Y., 2010. Computer-aided diagnosis of Alzheimer's disease using multiple features with artificial neural network., in: PRICAI, Springer. pp. 699–705.

Yang, X., Tan, M.Z., Qiu, A., 2012. CSF and brain structural imaging markers of the Alzheimer's pathological cascade. PLoS ONE 7, e47406.

Ye, J., Chen, K., Wu, T., Li, J., Zhao, Z., Patel, R., Bae, M., Janardan, R., Liu, H., Alexander, G., et al., 2008. Heterogeneous data fusion for Alzheimer's disease study.

Zacharaki, E., Wang, S., Chawla, S., Yoo, D.S., Wolf, R., Melhem, E., Davatzikos, C., 2009. MRI-based classification of brain tumor type and grade using SVM-RFE, in: Biomedical Imaging: From Nano to Macro, 2009. ISBI '09. IEEE International Symposium on, pp. 1035–1038.

Zhang, D., Wang, Y., Zhou, L., Yuan, H., Shen, D., 2011. Multimodal classification of Alzheimer's disease and mild cognitive impairment. NeuroImage 55, 856–867.

Zhang, Y., Schuff, N., Jahng, G.H., Bayne, W., Mori, S., Schad, L., Mueller, S., Du, A.T., Kramer, J., Yaffe, K., et al., 2007. Diffusion tensor imaging of cingulum fibers in mild cognitive impairment and Alzheimer disease. Neurology 68, 13–19.

Zhiqiang, L., Dinggang, S., Zhong, X., Bilge, K., Susan, Resnickb, M., Christos, D., 2004. Morphological classification of brains via high-dimensional shape transformations and machine learning methods. NeuroImage 21, 46 – 57.

Zhuang, L., Wen, W., Zhu, W., Trollor, J., Kochan, N., Crawford, J., Reppermund, S., Brodaty, H., Sachdev, P., 2010. White matter integrity in mild cognitive impairment: a tract-based spatial statistics study. Neuroimage 53, 16–25.

Titre : Classification des IRM par les descripteurs de contenu : Application au diagnostic précoce de la maladie d'Alzheimer

Résumé :
Les outils méthodologiques en indexation et classification des images par le contenu sont déjà assez matures et ce domaine s'ouvre vers les applications médicales. Dans cette thèse, nous nous intéressons à l'indexation visuelle, à la recherche et à la classification des images cérébrales IRM par le contenu pour l'aide au diagnostic de la maladie d'Alzheimer (MA). L'idée principale est de donner au clinicien des informations sur les images ayant des caractéristiques visuelles similaires. Trois catégories de sujets sont à distinguer: sujets sains (NC), sujets à troubles cognitifs légers (MCI) et sujets atteints par la maladie d'Alzheimer (AD). Nous représentons l'atrophie cérébrale comme une variation de signal dans des images IRM (IRM structurelle et IRM de Tenseur de Diffusion). Cette tâche n'est pas triviale, alors nous nous sommes concentrés uniquement sur l'extraction des caractéristiques à partir des régions impliquées dans la maladie d'Alzheimer et qui causent des changements particuliers dans la structure de cerveau : l'hippocampe le Cortex Cingulaire Postérieur. Les primitifs extrais sont quantifiés en utilisant l'approche sac de mots visuels. Cela permet de représenter l'atrophie cérébrale sous forme d'une signature visuelle spécifique à la MA. Plusieurs stratégies de fusion d'information sont appliquées pour renforcer les performances de système d'aide au diagnostic. La méthode proposée est automatique (sans l'intervention de clinicien), ne nécessite pas une étape de segmentation grâce à l'utilisation d'un Atlas normalisé. Les résultats obtenus apportent une amélioration par rapport aux méthodes de l'état de l'art en termes de précision de classification et de temps de traitement.

Mots clés : Alzheimer, indexation des images par le contenu, classification, IRM, ITD, aide au diagnostic

---

Title: Features-based MRI brain classification with domain knowledge: Application to Alzheimer's disease diagnosis

Abstract:
Content-Based Visual Information Retrieval and Classification on Magnetic Resonance Imaging (MRI) is penetrating the universe of IT tools supporting clinical decision making. A clinician can take profit from retrieving subject's scans with similar patterns. In this thesis, we use the visual indexing framework and pattern recognition analysis based on structural MRI and Tensor Diffusion Imaging (DTI) data to discriminate three categories of subjects: Normal Controls (NC), Mild Cognitive Impairment (MCI) and Alzheimer's Disease (AD). The approach extracts visual features from the most involved areas in the disease: Hippocampus and Posterior Cingulate Cortex. Hence, we represent signal variations (atrophy) inside the Region of Interest anatomy by a set of local features and we build a disease-related signature using an atlas based parcellation of the brain scan. The extracted features are quantized using the Bag-of-Visual-Words approach to build one signature by brain/ROI (subject). This yields a transformation of a full MRI brain into a compact disease-related signature. Several schemes of information fusion are applied to enhance the diagnosis performance. The proposed approach is less time-consuming compared to the state of the arts methods, computer-based and does not require the intervention of an expert during the classification/retrieval phase.

Keywords : Alzheimer, MRI, DTI, CBVIR, classification, Computer-aided diagnosis

---

Laboratoire Bordelais de Recherche en informatique, UMR 5800, Talence, Bordeaux